Tactile probing strategies for soft tissue examination

Konstantinova, Jelizaveta

Awarding institution:
King's College London

KING'S College LONDON

Tactile probing strategies for soft tissue examination

by Jelizaveta Konstantinova

A thesis submitted in partial fulfilment of the requirements for the degree of
Doctor of Philosophy in Robotics

to

King's College London
School of Natural and Mathematical Sciences
Department of Informatics
Centre for Robotics Research

July 2015

This thesis is dedicated to my beloved parents

and to the memory of my sister Anna

Acknowledgements

I would like to sincerely thank those who helped me in the various stages of this journey. Foremost, I would like to express my gratitude to my supervisor Dr. Thrishantha Nanayakkara for his guidance and support, inspiration and priceless scientific discussions, great research atmosphere and development opportunities. I am sincerely thankful to my second supervisor Professor Kaspar Althoefer for his support, excellent comments and scientific advice. I am grateful to him for providing me with the opportunity to embark on my doctoral studies and for his encouragement. I also thank my third supervisor Professor Prokar Dasgupta for his support.

I am thankful to my friends and colleagues Anuradha Ranansinge, Dr. Min Li, Dr. Sina Sareh, Dr. Allen Jang, Angela Faragasso, Dr. Vahid Aminzadeh, Dr. Helge Wurdemann, and Dr. Yohan Noh for their support, valuable suggestions and discussions. Also I thank all my other colleagues at the Centre for Robotics Research, King's College London for the time spent together during the last four years.

Also I acknowledge and thank all the people who have contributed to my experimental studies. Most of my work and results would not have been possible without their time

and contributions.

The work carried out in this thesis would not have been possible without the financial support of Guy's and St. Thomas' Charity Trust in collaboration with the Centre for Robotics Research at King's College London.

Finally, no words can express my deepest gratitude to my parents for their endless support, love and belief in my strength. I am grateful to my husband and friend Giuseppe Cotugno for his moral support, patience, understanding, and priceless scientific discussions and advice. Also I would like to thank all the people who have been supporting me during these years.

Abstract

This thesis investigates the ways how behavioural examination strategies are used to enhance tactile perception during examination of soft viscoelastic environments.

During the last few decades, Robot-assisted Minimally Invasive Surgery (RMIS) has become increasingly popular and has been employed in various medical procedures with proven benefits for the patient. However, direct tactile feedback which greatly improves surgical outcomes is not present in RMIS.

Artificial probing performed on ex-vivo and phantom tissues shows high variability in the obtained data. Variability is caused by non-homogeneous tissue stiffness and the resulting nonlinear temporal dynamics of tool indentation. Performed numerical simulations indicate that probing speed for fixed indentation influences the variability of tissue viscoelastic parameter estimation. To reduce variability in artificial tactile examination, suitable probing behaviour should be implemented. Three techniques of manual palpation are studied to understand the behavioural patterns of soft tissue tactile examination, namely, modulation of the applied force, localised, and global examination.

Humans use force modulation strategies to enhance their perception of harder areas in non-homogeneous environments. A second-order reactive autoregressive model has been found to describe this type of technique. Robotic palpation showed how this technique enhances the perceived inhomogeneous stiffness of the environment.

The study of unidirectional localised manual palpation, has shown that combinations of force-velocity strategies can be used to enhance the perception of hard formations in viscoelastic environments. To validate the obtained probing strategies, finite element simulations and tele-manipulated palpation were used. It was found that kinaesthetic and/or force feedback are used by humans to detect hard formations.

Finally, a remote palpation procedure on a silicone phantom utilizing a tele-manipulation setup was performed to study the behaviour of remote global palpation. The results demonstrate the effectiveness of global palpation pattern used during manual soft tissue examination as well as in tele-manipulated palpation.

Contents

List of Figures

List of Tables

Chapter 1

Introduction

1.1 Motivation of the Thesis

Minimally invasive laparoscopic surgery was first performed in 1987 [13] and soon became popular due to the benefits it offered to both patient and surgeon. Shorter recovery time, reduced pain and trauma, and less post-operative medication needed are the frequently referred to positive aspects of laparoscopy and RMIS. From the point of view of the surgeon RMIS compensates for natural hand tremor and reduces muscle fatigue. These are the key reasons for the worldwide popularity and continuous development of minimally invasive techniques [14]. Studies have shown that RMIS is effective in hysterectomy, prostatectomy, and thyroid surgery [15, 16].

The development of RMIS brought with it new technological challenges, as RMIS is accompanied with restricted access to the organs and loss of tactile information, there is a need for the development of tactile feedback sensors that provide haptic perception equal to that provided by manual palpation during surgery. Tactile feedback provides

the information about properties of an object being examined, such as hardness or softness, surface properties, temperature or wetness. Haptic perception, in its turn, enables the ability to perceive the environment and its properties through touch. Namely, in this case the ability to feel an organ's mechanical properties can help the surgeon to detect tumours and lumps in the organ, as well as to understand the margin of the abnormality so as to perform a successful dissection. However, the main feedback RMIS users receive is through vision, and in order to understand tool-tissue interaction forces, specialised training and extensive experience on the robot is required [17]. Visualization during surgery can only partially compensate for the lack of tactile feedback, as vision only provides information about the outer surface of an organ; and abnormalities are often concealed by layers of healthy tissue. Therefore, the thorough assessment of an organ's mechanical properties should be realized with the help of force sensing devices. Force feedback transmits the forces occurring from the interaction of the sensing device and the organ's tissue. Harder tissue abnormalities provide stronger force magnitude compared to healthy and softer areas, enabling the possibility to use force feedback to provide haptic perception.

During open surgery, practitioners use their hands to palpate organs in order to assess the mechanical properties of soft tissue, to locate a tumour, for instance. Thanks both to the advanced human perceptive system and and employment of certain palpation strategies, surgeons are able to distinguish between healthy soft tissues and inhomogeneous areas. Medical manual palpation has a set of pre-defined strategies that are used to obtain the shape, size, location and the structure of the hard formation. In addition to this, humans have the natural ability to explore and identify objects relying on the obtained tactile sensation. Therefore, it is possible to assume that artificial palpation can benefit from defined behavioural patterns and improve the perception using current

tactile devices.

The human sensory perceptive system has numerous receptors that react to environmental challenges and perceive multimodal feedback from thousands of stimuli. Manual examination of any given object is usually performed with the fingertips that contain the largest concentration of mechanoreceptors. The perception of sensory information and interaction behaviour during manual palpation are intrinsically coupled. However, if a surgeon performs palpation with a simple tactile sensing probe, such as probing with a spherical indenter and a force sensor, perception is significantly reduced. To improve the tactile information an advanced sensor with high technological capabilities, such as high accuracy, sensitivity and sensing range, needs to be developed. In addition, the mechanism whereby enhanced perception of the environment is achieved needs to be fully understood. Therefore, this thesis poses the question as to given the simplest probing tool, to what extent can the sensing capabilities of sensing tools be improved? Does the palpation behaviour play a major role in haptic perception?

1.1.1 Aim and Objectives of the Thesis

The aim of the thesis is *to study how behavioural examination strategies are used to enhance tactile perception during examination of soft viscoelastic environments.* The objectives of the thesis are:

1. to explore the current state-of-the-art in medical tactile sensing and the main challenges associated with this area, - and further on to understand the effect of variability of tactile data and the need of probing behaviour during examination of viscoelatic environment, such as soft biological tissues;

2. to outline the set of behavioural strategies that can be used to enhance the perception of stiffness during tactile examination;

3. to validate the obtained palpation strategies for implementation in robotic-assisted surgery and artificial palpation.

1.2 Contributions

The contributions of the thesis can be summarised as follows:

1. This thesis contributes to the knowledge of the field of palpation and probing devices for RMIS. Biologically inspired design guidelines are given based on human tactile perception mechanism, manual palpation, as well as practical requirements of RMIS (Chapter 2).

2. Variability of artificial tactile palpation depends on the distribution of tissue properties and the resulting temporal response of the indentation of the probe. This thesis shows, using basic hardware experiments that the speed of traversing for a given indentation depth can influence the variability of estimating the viscoelastic parameters of the tissue (Chapter 3).

3. Humans possess a natural ability to perform tactile exploration and examination of a given object in an efficient and productive way to obtain the details of the mechanical structure or to detect an embedded hard formation, such as a tumour in a soft tissue. In this thesis, human tactile demonstrations were used to define an autoregressive model of the modulation of the applied force during single point palpation. The obtained mathematical model was successfully tested for

the autonomous robotic palpation that can be used to enhance tactile perception (Chapter 4).

4. An important behavioural feature of artificial or manual tactile examination is the exploration of the given area during scanning in continuous path. Variability of the applied velocity and force is used to enhance the perception and to improve the results of examination. In this thesis, behavioural characteristics of localized manual palpation are studied. It was found and validated that in order to detect a hard formation inside a soft environment the control behaviour of the tactile probe can follow two strategies: 1) keep the indentation constant, therefore perceiving variability of feedback force; or 2) keep the applied force constant, relying just on the kinaesthetic feedback (Chapter 5).

5. Tele-operation of surgical tools is a conventional approach used in RMIS. In this thesis tele-operated artificial palpation is explored in order to understand its effectiveness in robotic surgery. The palpation pattern for tele-manipulated artificial palpation, built on top of global manual palpation strategies, is defined. It is shown that this approach can be used to enhance perception and to increase the efficiency of the examination (Chapter 6).

1.2.1 Contributed Papers

The contributions of the thesis led to the following publications:

Journal Papers

1. J. Konstantinova, M. Li, G. Mehra, P. Dasgupta, K. Althoefer, T. Nanayakkara, "Behavioral characteristics of manual palpation to localize hard nodules in soft

tissues," *IEEE Transactions on Biomedical Engineering*, vol.61, no.6, pp.1651-1659, June 2014

2. J. Konstantinova, A. Jiang, K. Althoefer, P. Dasgupta, T. Nanayakkara, "Implementation of tactile sensing for palpation in robot-assisted minimally invasive surgery," *IEEE Sensors, Journal*, vol. 14(8), pp. 2490-2501, 2014

3. J. Konstantinova, G. Cotugno, K. Althoefer, P. Dasgupta, T. Nanayakkara, "Palpation force modulation strategies to identify non-homogeneous regions in soft tissue organs" - *IEEE Transactions on Haptics*, under review

Conference Papers

1. J. Konstantinova, M. Li, V. Aminzadeh, P. Dasgupta, K. Althoefer, and T. Nanayakkara, "Force-Velocity modulation strategies for soft tissue examination" in *IEEE International conference on Intelligent Robots and Systems*, 2013

2. J. Konstantinova, M. Li, V. Aminzadeh, K. Althoefer, P. Dasgupta, and T. Nanayakkara, "Evaluating manual palpation trajectory patterns in tele-manipulation for soft tissue examination", in *IEEE Systems Men and Cybernetics*, 2013.

3. J. Konstantinova, K. Althoefer, P. Dasgupta, and T. Nanayakkara, "Salient features of soft tissue examination velocity during manual palpation," in *Hamlyn Symposium* 2013, pp.41-42.

4. J. Konstantinova, L. Min, K. Althoefer, P. Dasgupta, T. Nanayakkara, "Palpation strategies for artificial soft tissue examination," in *3rd Joint Workshop on New Technologies for Computer/Robot Assisted Surgery*, 11-13 Sept. 2013

5. J. Zirjakova (Konstantinova), K. Althoefer, P. Dasgupta, T. Nanayakkara, "Prob-

ing behaviour for soft tissue stiffness measurement", in *2012 World Congress of Endourology*, Sept. 2012

Co-authored Papers

1. M. Li, *J. Konstantinova*, E. L. Secco, A. Jiang, H. Liu, T. Nanayakkara, L.D. Senevirante, P. Dasgupta, K. Althoefer, H. A. Wurdemann, "Using visual cues to enhance haptic feedback for palpation on virtual model of soft tissue," *Medical & Biological Engineering & Computing*, May 2015

2. M. Li, A. Faragasso, *J. Konstantinova* , L. D. Seneviratne, V. Aminzadeh, P. Dasgupta, K. Althoefer, "A novel tumor localization method using haptic palpation based on soft tissue probing data," in *2014 IEEE International Conference on Robotics & Automation (ICRA)*, pp. 4188 - 4193,May 31 - June 7, 2014

3. G. Cotugno, *J. Konstantinova* , K. Althoefer, T. Nanayakkara, "On the dexterity of robotic manipulation: are robotic hands ill designed?", in the *6th International Conference on Cognitive Science*, June, 2014

4. N. Sornkarn, *J. Konstantinova*, P. Dasgupta, K. Althoefer, T. Nanayakkara, "Palpation with controllable stiffness for robot-assisted minimally invasive surgery," in *International Conference on Robotics and Automation (ICRA)* 2014, Hong Kong 30 June - 5 May, 2014

5. M. Li, *J. Konstantinova*, V. Aminzadeh, L. D. Seneviratne, P. Dasgupta, and K. Althoefer, "Real-time visual stiffness feedback for soft tissue palpation in a telemanipulation environment," in *Hamlyn Simposium 2013*, pp. 77-78.

6. M. Li, *J. Zirjakova (Konstantinova)*, W. Yao, K. Althoefer, P. Dasgupta, L.D.

Seneviratne, "Passive robotic platform for three-dimensional scanning of ex-vivo soft tissue", *Advances in Reconfigurable Mechanisms and Robots I. Berlin: Springer-Verlag*, 2012. pp. 477-487.

7. J. Li, H. Liu, *J. Zirjakova (Konstantinova)*, B. Challacombe, P. Dasgupta, L.D. Seneviratne, K. Althoefer, "Clinical study of prostate tumour identification using a rolling indenter robot", *Hamlyn Symposium on Medical Robotics*, 1-2 July, 2012, pp.85-86

8. F. Bianchi, G. Bartoli, K. Shoar, M.R. Armas Fernandez V. Pereno, *J. Zirjakova (Konstantinova)*, A. Jiang, T. Nanayakkara, "Adaptive internal impedance control for stable walking on uncertain visco-elastic terrains", in *2012 IEEE/RSJ International Conference on Intelligent Robots and Systems*, 2012, pp. 2465 - 2470

1.3 Thesis Structure

The work done in this thesis is presented in five main chapters.

Chapter 2 discusses major challenges of tactile sensing for surgical applications and addresses the implementation of tactile sensing technologies in real-life surgery.

Chapter 3 presents the challenges of tactile examination in the context of the variability of viscoelastic environment. Hardware simulation studies of tool and environment are presented and the importance of probing behaviour is demonstrated.

Chapter 4 presents the first set of studies on manual palpation in order to explore and analyse the principles of probing behaviour during artificial tactile examination. This

chapter outlines the mathematical model of the modulation of the applied forces during palpation. The findings are validated using autonomous robotic palpation.

Chapter 5 discusses the second set of studies that are based on manual palpation for localised examination. The obtained probing strategies are tested using finite element modelling and tele-manipulated palpation.

Chapter 6 presents the analysis of the global palpation approach and the evaluation of its performance during tele-manipulated palpation.

1.3.1 Schematic Thesis Structure

The structure of the thesis is schematically shown on Fig. 1.1.

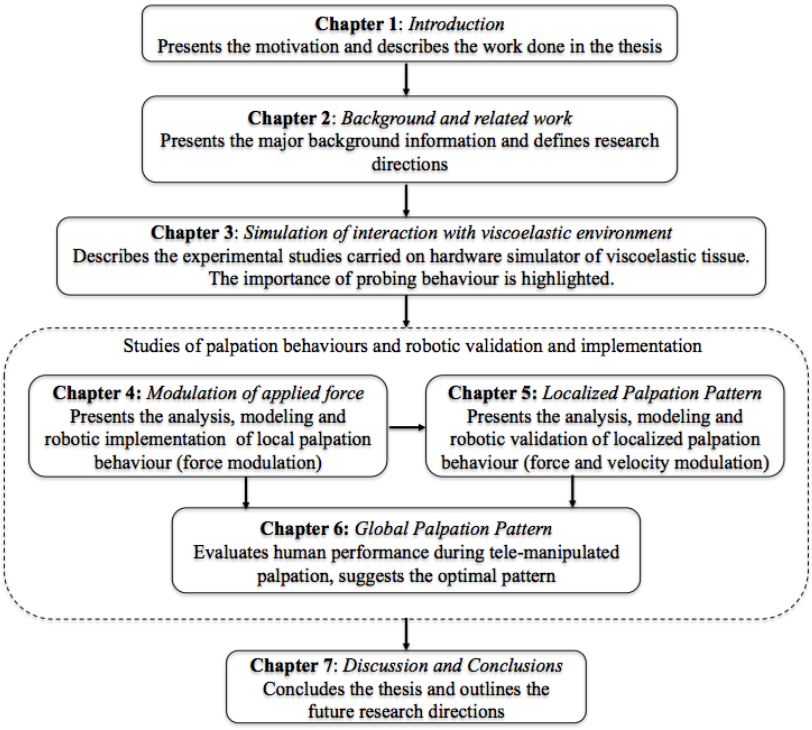

Figure 1.1: Schematic structure of thesis

Chapter 2

Background and Related Work

2.1 Introduction

The sense of touch is an essential component for our perception of the world. It helps humans to navigate in the dark and gives them the possibility to detect the presence of an object, its shape, size, temperature and mechanical surface properties. The somatosensory system that is distributed throughout the human body and sends a complex set of signals to the brain originating from a multitude of receptors and nerve endings. These are located in muscles, joints, mucosa, and the surface of the skin and respond to various inputs, including touch, pressure, temperature, pain, and body orientation in space.

Human beings' ability to explore the tactile properties of an object is subjective and changes with experience [18]. Therefore, in order to recreate a realistic sense of touch in robotic applications, multiple sensing devices and a complex control system for the behavioural control are needed to perceive and interpret different types of stimuli.

Nowadays, no sensor system exists that is capable of measuring the full complexity of tactile cues as accurately as the human tactile receptive system does. The development of such a system presents an important scientific challenge.

Despite its short history, medical tactile sensing has been researched extensively. A good overview of earlier medically-applied tactile sensor research is presented in [19–21] work. In [22] the main focus is on recent research exploring the mechanisms of human tactile sensing, which is believed to be an ideal model for artificial touch sensors. A general overview of tactile technologies is presented in [23,24]. This chapter surveys the RMIS tactile devices and discusses the main challenges and possible directions of the development of surgical tactile sensors. It explores how biology can be used as an inspiration for the development of tactile sensors. It also discusses the important issue of the interaction between soft tissue and medical tools and its impact on tactile sensor requirements, specifically using tissue manual palpation as an example to understand the desired design characteristics of sensing devices.

The mechanical properties of healthy soft tissues differ from those of cancerous ones, that is, the elastic modulus of tumours is approximately higher by a factor of ten [25, 26]. The knowledge of the exact tumour location allows surgeons to perform a more accurate resection and to preserve healthy tissue as much as possible. Thus, the trauma from surgery can be reduced. Tactile feedback during surgery, along with the visualization of an operation site, can enhance the dexterity and controllability of a surgical instrument, which in turn can improve the quality of tool and tissue interaction and help to reduce trauma [27, 28]. Conversely, the lack of tactile feedback during RMIS can result in serious complications while performing difficult manipulations, such as coronary artery bypass grafting [29].

2.2 Biological Background of Tactile Sensing

The process of touching and examining an object can be divided into three main stages: evaluation of environment, exploratory action and correction of the action to enhance perception. The evaluation stage includes visual assessment of the geometrical parameters of an object - its size, shape and curvature. Based on prior knowledge and vision information the general mechanical properties of the surface, such as friction, roughness of the surface are estimated. Walker and Tan [30] report that among all perceptive systems visual information is dominant in the perception of objects. However, many assumptions about mechanical properties like force and stiffness can be estimated mainly by means of tactile contact. Subjects evaluated stiffness by combining visual information about displacement and force cues, but spatial position information was largely ignored by the subjects. The second stage of object examination is touching action, when the examiner receives correct information about the mechanical properties of an object. Then, based on the perceived information, the movement is corrected, and certain probing dynamics can be applied, in order to enhance the perceived sensation.

Research on tactile technologies and on human tactile perception is on the rise [31]. The simultaneous development of these two areas is not a coincidence as human tactile sensing is the standard artificial tactile technology strives to reach. Therefore, to create an artificial tactile sensing device, it is essential to explore the biological tactile sensing, in particular the distribution and functionality of mechanoreceptors. These sensing elements are spatially distributed in the soft tissue between the skin, the finger bone and the nail in a strategic way, possibly to take advantage of different tissue dynamics under different probing behaviours.

Humans possess several types of mechanoreceptors [32,33], which respond to different

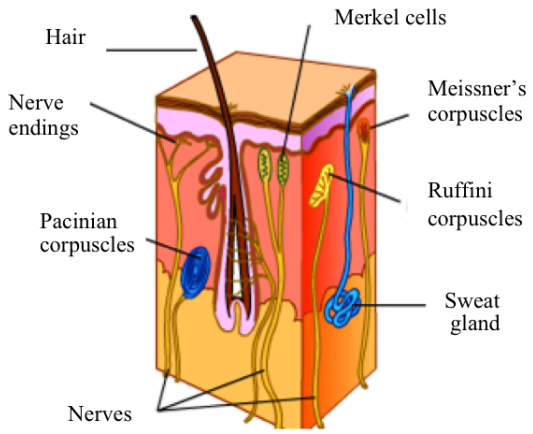

Figure 2.1: Cross section of human skin. Picture adapted from [1]

types of mechanical stimuli (Fig. 2.1). Receptors called Merkel cells are densely located in the top layer of the skin, and respond to light touch and static stimuli. These cells have a small receptive area, high sensitivity to small vibrations (less than 5 Hz) [34], fine spatial discontinuities (about 0.5 mm) [35], edges, and the orientation of the examined surface [36, 37]. Ruffini corpuscles are located deeper in the dermis and respond to stretching in the joining tissue. They mostly react to sustained pressure and are used in kinaesthetic sense. Meissner's corpuscles respond to vibrations ranging from 5 to 50 Hz [34] and are located close to the skin surface. These are the most dense mechanoreceptors, with the single receptors spaced 3 - 5 mm apart. Moreover, Meissner's corpuscles are responsible for slip detection between an object and the skin [38]. The receptors located most deeply in the skin (Pacinian corpuscles) respond to high-frequency vibrations and high pressure [39,40]. These receptors quickly adapt to the stimulus and do not respond to static exposure. The density of these receptors is not very high and the size of the cell is relatively large. According to [41] there is an average of 300 Pacinian corpuscles in human hands. In addition, Pacinian corpuscles

produce a response when the tactile stimulus is applied on the array of these cells on the wider area of the skin [42]. The human tactile system perceives distinct stimuli, such as different vibration frequencies, light and moderate touch and deep pressure with the help of mechanoreceptors, strategically located in the finger. Thus, the tactile perception of an object is formed from the combination of received stimuli.

The external stimuli on mechanoreceptors from the contact gets translated into different vibration patterns across the depth of the dermis. Varied spatial organization of mechanoreceptors suggests that they make use of the mechanical properties of the dermis to capture different mechanical features of an external perturbation. This means that the perception of a hard formation in soft tissue is associated with the finger-tissue interaction and the way the mechanoreceptors perceive the states of the interaction dynamics. Therefore, this thesis studies the way soft tissue is palpated using manual examination techniques.

2.3 Requirements of Robot-assisted Minimally Invasive Surgery

In this section it is important to understand the desirable requirements and constraints for the development of devices for RMIS. The lack of tactile feedback is an important drawback of RMIS, tactile sensation is not yet widely implemented in real surgical applications, as described in [20]. One of the main reasons for that is the strict certification requirements specified for medical devices. It is essential that medical devices provide accurate and stable and measurements. For example, if the sensor used to detect the presence and location of an abnormality provides incorrect tactile information, this may lead to false tumour detection or missing the abnormality altogether. Such variability of results will influence the clinical outcome of the examination and sub-

sequent treatment. Many natural factors and processes can also cause variability of tactile data. For instance, a patient's natural breathing causes a displacement of the internal organs, while blood and other fluids which can be excessive during surgery affect the surface properties of an organ. Thus, the sensing signal can be influenced by changes in friction between the sensing tool and tissue. These variability factors for tactile sensing should be taken into account when developing devices for RMIS. Fig. 2.2 demonstrates the high difference in stiffness distribution obtained during two separate measurements of the same ex-vivo prostate organ [43]. The red areas indicate the location of high stiffness areas measured during palpation with a hand-held probing device. This example demonstrates how changes in probing dynamics influence the process of tactile examination.

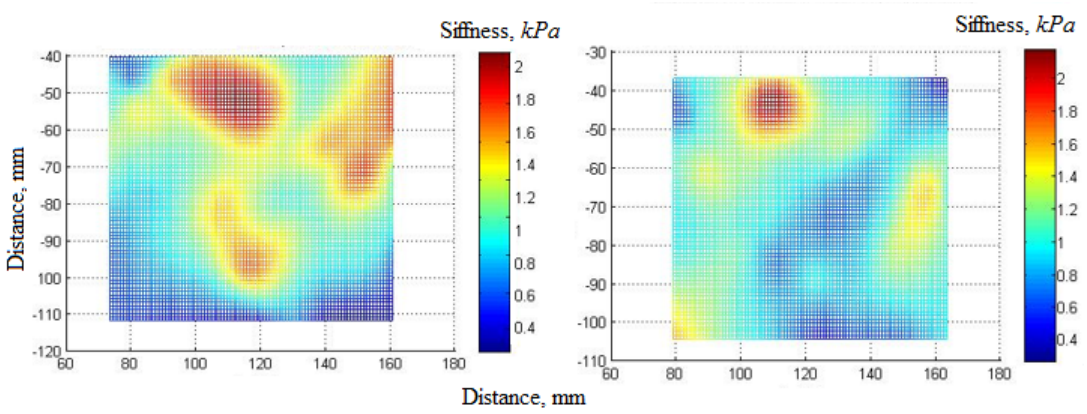

Figure 2.2: Two measurements of stiffness distribution for the same ex-vivo prostate, red areas indicate the location of the possible hard formation - tumour.

Keeping surgical procedures as short as possible is important as any additional surgery time can can increase the likelihood of complications for the patient and will increase the cost of the procedure. Time constraints mean that the surgeon cannot afford to perform multiple tactile scans of an organ to confirm the presence or location of a tumour within an organ. A probe for tactile data detection can allow the surgeon to measure

soft tissue properties within a short period of time, i.e. operate at fast traversing speeds.

RMIS is performed through small incisions, or trocar ports, whose diameters vary from 5 to 12 mm [44]. Therefore, all surgical devices should be miniaturized to fit through a trocar port. In addition, tactile sensing instruments should be either sterilizable or disposable. The latter case could be practically realized if low cost components are used. For sterilization it is necessary to take into account that it can be performed in a steam autoclave using high pressure vapour and high temperature [45], in a chemiclave with low humidity and chemical solution [46], or using gas sterilization [47]. The simplicity of the whole design of tactile device is another desirable feature leading to low cost and affordability.

In some cases, RMIS is performed using a magnetic resonance imaging (MRI) [48]. MRI is used when real time observation of the position of an instrument position in relation to an internal organ and other areas of interest is needed. MRI is enhancing the contrast of soft tissues and can be used for multi-planar spatial visualization [49, 50]. In contrast to X-ray, computer tomography and fluoroscopy, MRI is not subject to ionizing radiation and does not require the use of contrast agents. However, due to the applied magnetic field, only instruments made from non-magnetic materials can be used in combination with MRI [31, 51] to avoid interference with images.

The design requirements of a tactile sensing device depend on the type of application it will be used for in RMIS. Information about mechanical properties of soft tissue could be used in two ways: either to sense the pressure applied by an instrument in order to avoid injuring the tissue and blood vessels during manipulation, or to enable soft tissue palpation during RMIS to detect sites of abnormalities. In the first case, sensors are mainly used for the design of surgical instruments for specific manipulation task, such

as grippers, forceps, cutters and tips for catheters. In the second case, palpation probes are designed in order to evaluate the mechanical structure of tissue and to detect the presence of abnormalities.

2.4 Palpation Devices for Robot-Assisted Minimally Invasive Surgery

In this section an overview of the structural design and sensing principles of medical tactile sensors for RMIS is presented. The section reviews tactile devices developed for use in RMIS and other related surgical applications during the recent decade. Considering the fact that tactile devices are directly interacting with soft tissue, their design is one of the factors that can influence the surgical outcome. Table 2.1 classifies tactile sensing devices designed for surgical applications.

Table 2.1: Classification of Tactile Sensors for Surgical Applications

Construction principle	*Application type*
Indentation devices	Tactile probes for artificial palpation
Aspiration or Absorption devices	Tactile probes
Catheter tip with sensing element	Catheters
Layered structure	Grippers, Forceps, Cutters, Tactile probes
Arrayed structure	Various applications
Non-contact methods	Tactile probes
Combination of several design principles	Various applications

2.4.1 Contact Devices Based on the Indentation Principle

Common Design Principles of Indentation Devices

The most popular tactile device design for surgical applications is the contact probe, which is akin to the human finger and which measures indentation during probing. This design is usually employed for probing devices, which directly serve the purpose of artificial tactile probing or palpation. The typical application of such a device is the detection and localization of tissue abnormalities, such as malignant or benign formations. A certain amount of force is applied on the target tissue, which results in changes of stress and strain values. Then a finger-like indentation sensing device measures the stiffness of a soft tissue.

The shape of the indenter, which is the main construction element, plays an important role in the results of examination. Theoretically, to get the most accurate measurements from in-homogeneous material, the contact area of measurement should be minimal. The shape of an indenter should be designed in such way so as not to damage tissue during surgery. Moreover, for a complete organ representation, the measurement should be performed continuously over the surface of an organ. In addition, the indenter's shape should be similar to human fingertip, which is actively used to detect tactile information during manual palpation, is similar to a sphere and provides good sliding options for interaction with viscoelastic environment. The diameter of the spherical tip of the indenter should be chosen according to the viscoelastic properties of the tissue - a very large diameter requires higher loads and more effort during measurements, while too small, a diameter will not provide the desired dynamical properties for the measurement. It has been proven that depth and stress of indentation is inversely re-

lated to the diameter of the indenter, but this relationship is non-linear [52]. Hayes in 1972 [53] has derived a relationship which connects geometry of a spherical indenter, applied load and resulting indentation (Fig. 2.3).

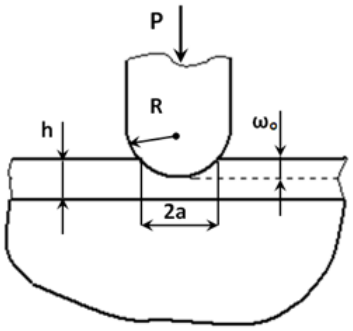

Figure 2.3: The contact of spherical indenter and target material, geometrical parameters: h - thickness of the material, ω_0 - indentation depth, R - the radius of an indenter, P - applied load, $2a$ - the diameter of indented material.

The relationship between the indentation depth ω_0 and radius of contact area is described by λ in Eq. 2.1.

$$\lambda = \frac{a^2}{\omega_0 R} \tag{2.1}$$

Thus, the relationship between displacement ω_0 and the applied load P can be formulated using non-dimensional coefficient k:

$$k = \frac{P(1-\nu)}{4aG\omega_0} \int_0^1 \omega(\tau) d\tau \tag{2.2}$$

Load is inversely proportional to contact area and indentation depth. In equation 2.2 ν is Poisson's ratio and G is shear modulus. During the development of an indentation device one may consider these relationship in order to check the selected diameter of

the hemispherical tip. The acceptable values of coefficient k can be found in [53].

Transduction Principles

The tactile devices based on the indentation construction principle allow the use of different transduction principles, which are discussed below. Force feedback measurement is one of the most widespread methods for soft tissue mechanical property examination as it is simple, accurate and convenient for use during RMIS.

Commercially available sensors offer easy and accurate force data measuring but they can be of an unsuitable size, or made from MRI-incompatible material. The most popular commercial device, used for indentation is the three-dimensional force and torque sensor NANO 17 (ATI industrial automation), which provides good accuracy and sensitivity and is of miniature size (17 mm in diameter). Examples of indentation devices using this sensor can be found in [54, 55].

To achieve an efficient examination RMIS tactile device that combines accuracy, miniature size and affordability, specially developed transducers should be developed. For instance, one can use strain gauges to measure force feedback. Such a method would allow relative flexibility in construction and therefore the possibility to design multi-dimensional sensors. An example of an indentation probe based on strain gauges can be found in [2] (Fig. 2.4), where a three-dimensional force and torque sensor was developed for arthroscopic surgery: the hollow structure of the sensor in this design allows the placement of the sensor on the tip of the probe thus enabling the use of visual feedback necessary in this type of surgery. Strain gauges are relatively cheap which allows for the disposal of the probe after use. However, because of ferromagnetic elements, such sensors cannot be used inside an MRI scanner and are sensitive to temperature

changes. The same limitations apply to sensors using piezoelectric effect [56, 57].

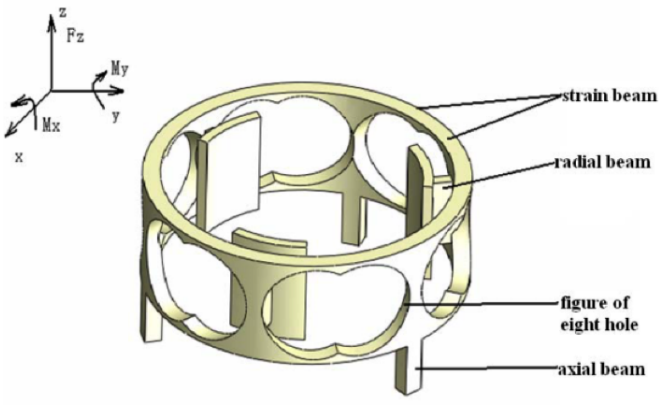

Figure 2.4: Design principle of sensing structure in [2].

Among tactile sensors, one can mention the indentation devices that work using the fibre optical principle, where the modulation of light intensity is used to represent the variable force feedback from the soft tissue [58–60]. They are compatible with MRI as the transducer is made of non-magnetic materials. In addition, fibre optic transducers can work with no wiring and are resistive to temperature variations. The construction principle of the fibre optic force sensor requires converting force feedback into displacement, which is usually achieved by means of deforming an elastic part of the sensor. The choice of elastic material becomes a very important issue in the sensor construction as the properties of the material define sensor accuracy parameters. The non-linear behaviour and response times of the elastic part are the important factors that should be considered during sensor calibration. The deformation of elastic tip of the sensor can also be used to measure tactile data using optical information. For instance, work in [61] describes the compliant optical tactile sensor where the shape change of the transparent elastomer is measured by a high speed image sensor.

An alternative albeit expensive sensing principle is based on Fibre Bragg Grating (FBG), which gives better accuracy of estimating stiffness parameters in addition to being a miniature solution. The specific feature of FBG is variation of the refractive index, and thus of the length of the wave, on the small section of the fibre. An example of such sensor can be found in [62]: the designed sensor is 2.4 $\times$ 2.4 mm^2 in size and shows good balance between sensitivity range and linearity. In this example FBG was embedded in the flexible silicone material and was found suitable for the force measurement in RMIS.

As the current state-of-the-art shows, the fibre-optical transduction principle allows building miniature multi-modal sensors. An example of a three-axis sensor can be found in [63] and of a six-axis in [64], where the size of the sensor is brought up to 11 $\times$ 10 $\times$ 6 mm^3 with the help of linear polarisers. However, if these sensors are employed in indentation devices, the performance and accuracy will be largely dependent on the design parameters of the probe. In addition, the structure of fibre-optical transducer can be relatively fragile and may be damaged due to excessive loads.

The indentation devices, which measure only force feedback from the target material, are suitable for static one-point measurements. Most of force feedback-based sensors measure just tissue response force while the indentation depth during measurement is assumed to be constant. This assumption leads to inaccuracy in the estimation of tissue mechanical properties. In order to estimate correct soft tissue parameters, the device should be able to measure both force feedback and indentation depth simultaneously. Alternatively, the indentation depth can be kept constant during measurement, but this approach can be hardly implemented for real surgical applications. The work described in [3] (Fig. 2.5) is based on the optical fibre force sensing, but its construction principle does not use deformable elastic material for the modulation of intensity.

Instead, a spherical indenter of the probe is pressed down to the target tissue by air flow and a non-contact position sphere is located on the fixed distance from the optical fibre. During measurements, variation in the tissue stiffness causes change in the distance between the sphere and the fibre. Thus, tissue stiffness is obtained by detecting indentation depth and force feedback. However, the relationship between airflow and non-linear soft tissue responses should be taken into consideration during sensor calibration. Another example of a sensor detecting two measurement variables simultaneously can be found in [65]. A third example of a stiffness sensor (Fig. 2.6), is based on the induction principle, where direction and amount of motion is measured along with force feedback [4]. This method is not MRI compatible and is not often used in the indentation devices, but the results show its good accuracy parameters.

Apart from force the sensing method, the resonance-frequency based method can be used for tactile examination. However, at the moment there is no indentation device, which is capable of measuring mechanical properties of soft tissue over a continuous path and provide reliable results. For example, work described in [66] uses the commercial resonance sensor Venutron®, where the static measurements of soft tissue phantoms are performed at controlled indentation depth. The indentation devices based on the combination of mass-spring model with LVDT (linear variable differential transducer) coils [5, 67], sample design principle are shown in Fig. 2.7. In that case the system is measuring a shift of resonance frequency during the indentation process. The main issues in the application of such devices are problems with the measurement repeatability and reliability, as well as dependence on the orientation of the probe. Such issues may lead to inaccuracies during the in-vivo application of the tactile device. However, the significant advantage of the resonant method is its capability to measure both elastic and viscose properties of soft tissues.

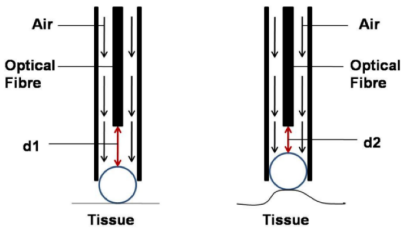

Figure 2.5: Sensing principle of stiffness sensor measuring based on optical fibre and air flow [3].

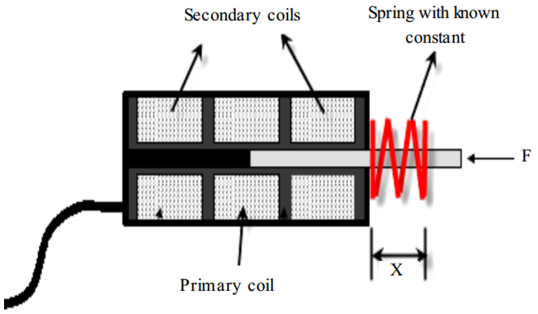

Figure 2.6: Measurement principle of tactile indenter which is based on the induction principle [4].

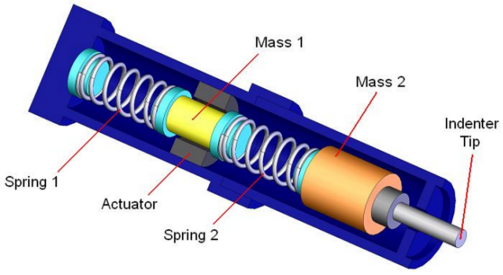

Figure 2.7: Design principle of an indentation device which measures soft tissue data based on the resonance-frequency method [5].

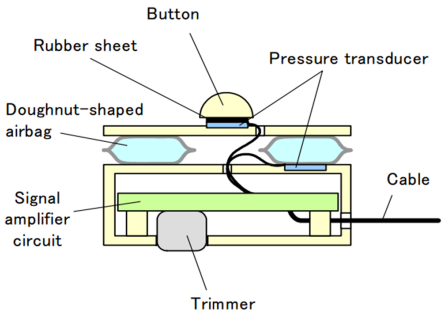

Figure 2.8: Schematic design and a prototype indentation device to measure liver stiffness [6].

In addition to the transduction principles presented above, there is a body of research on application-specific designed indentation devices. These device are developed for limited application or procedure with a construction principle that does not allow any modifications. An example of such an indentation device can be found in [6], (Fig. 2.8). A ring shaped airbag is used to detect contact force by measuring variable air pressure and to measure stiffness of liver. The employment of an air bag allows the measuring force feedback in arbitrary directions and minimizes the effect of variable indention.

In [68] the concept of wireless palpation was introduced. A magnetically actuated wireless probe measures stiffness using indentation in a vertical direction. The device does not require a separate trocar port, but is influenced by vibrations and uncertainties of the environment that can affect accuracy.

In summary, research into indentation devices for soft tissue probing or palpation continues along with the requirement for better technologies and designs, which would ensure accurate estimation of soft tissue parameters in a dynamical way.

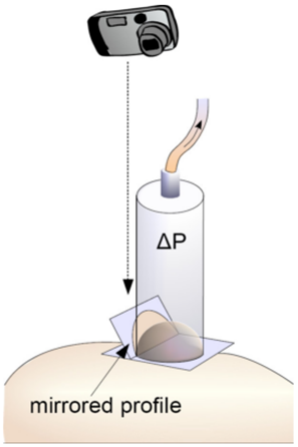

Figure 2.9: Measurement principle of an aspiration device: ΔP - aspiration pressure, mirrored profile of aspirated tissue area is captured by camera [7].

2.4.2 Aspiration Devices

A method that is not very well represented in the scientific literature for the purpose of soft tissue palpation, but which can be used for tactile examination of soft tissue, and particularly for stiffness estimation, is the aspiration or suction of the target tissue with a pipette device. This approach is used to perform biopsy for tumour and infection diagnosis [69]. Aspiration devices are MRI-compatible, sterilizable, and, more importantly, able to estimate the value of Young's modulus instead of the relative stiff-

ness parameter of the area. However, there are no examples of such tactile devices developed directly for RMIS. Interesting works describing this principle on soft tissue examination are presented in [7, 70, 71].

In order to measure stiffness the device should be in direct contact with the tissue as the air from the pipette is sucked out. There should be a mechanism to measure the aspirated level of soft tissue, that is assumed to be homogeneous and then analysed to estimate Young's modulus (Fig. 2.9). A drawback of this method is its inability to produce fast measurements over an organ areaas aspiration and release of the target area is time consuming. In addition, to create a full representation of an organ, a so-called stiffness distribution map, the positioning of the pipette should be very accurate in order to gather the information from the whole organ. The design of a pipette device is directly influencing the accuracy of the measurements. The diameter of an aspirated area and wall thicknesses of a pipette are important parameters. More information about this design can be found in [70].

2.4.3 Catheters with Tactile Elements

Catheters are widely used for minimally invasive cardiac surgeries, such as coronary artery bypass surgery, beating heart bypass, and mitral valve procedures [72]. During catheterization procedures, it might be desired to control the applied force during catheter insertion to avoid damage of the vessels or chambers as well as to distinguish between the stiffness of soft tissues by employing the tip of catheter with force sensor. It is worth mentioning that in these cases the tactile device is mostly used in order to evaluate the strength of the applied force or to detect the contact, without having to scan the soft tissue.

Catheterization procedures often require the use of MRI during surgery. Therefore, tactile sensors employed in catheters should not contain any metal parts. The analysis of the devices with fibre optic sensors, shows that this type of sensing is feasible for different applications in RMIS, including catheterization procedures. An example of a catheter based on this transduction principle can be found in [73] and in [74]. The sensor described in [75] uses expansion of the soft and flexible balloon with fluid for tactile information sensing. The pressure and flow of fluid changes depend on the load applied and are measured by flow and pressure sensors outside the setup. However, the drawback of this setup is the difficulty in the maintaining constant air flow rate in the sensor, as well as overcoming problem of the occurring slip.

As experience shows, the most successful devices are those developed by employing combined sensing and mechanical principles. For example, in [8] a hybrid sensor developed for catheterization procedures uses both the piezoresistive effect and optical fibre sensing (Fig. 2.10). The sensor is capable of detecting the deformation of an object via the deformation of reflective diaphragm by

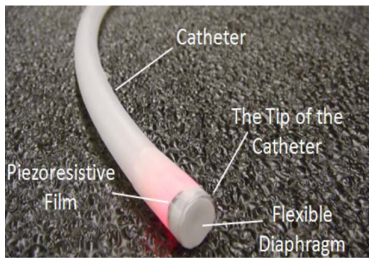

Figure 2.10: Catheter tip which measures relative stiffness of contact tissue [8].

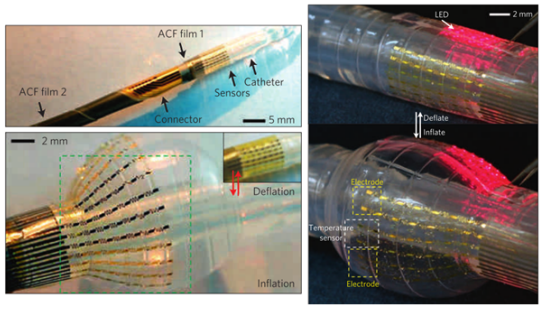

Figure 2.11: Design of multifunctional catheter tip [9].

means of optical force sensing, as well as force feedback using the piezoresistive film. Thus, the relative stiffness of the contact object can be obtained.

In the context of tactile devices developed for catheters it is necessary to mention the work described in [9], where a multifunctional balloon catheter is presented (Fig. 2.11). The original method of fabrication allowed the employment of tactile, temperature and flow sensors. In addition, the device showed good accuracy parameters and was tested in-vivo, which is a necessary step towards the implementation of the device in real surgery.

2.4.4 Layered Structures

This section discusses layered structures, a tactile sensor design, which involves the employment of various materials or transducers placed one upon the other. The method has got various advantages, as several transduction principles as well as different materials can be combined in the same measurement device. Tactile sensors built on the layer principle can be successfully integrated in a surgical instrument, such as graspers, as well as in tactile probes used for soft tissue exploration.

Tactile sensing devices employing various materials in a layered configuration can be compared with the structure of the human finger, which is composed of several different layers, possessing various mechanical properties and acting in a different ways during object exploration [76]. Similarly, tactile sensors with a layered structure can use a layer of silicone or rubber material. However, the viscoelastic properties of measured soft tissue must influence the choice of soft material for the sensor layers during, because the sensitivity of the device will depend on the mechanical interaction between the tool and tissue, such as in [10, 77].

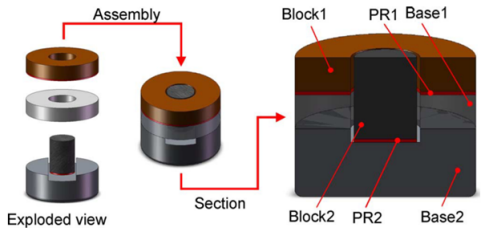

Figure 2.12: Layered structure of soft tissue sensor: Block 1 and Block 2 are composed from rubber with different Young's modulus, PR2 - piezorezistive film, Base1 and Base2 - steel components [10].

The combination of various materials in one device allows measuring both feedback force and the stiffness of the tissue. In [10], two rubber blocks with different values of Young's modulus are placed concentrically upon pressure sensing elements, which allows the determination of the Young's modulus of soft tissue (Fig. 2.12). Another example of a layered structure is the micro electromechanical systems (MEMS) stiffness sensor. It measures soft tissue properties based on a relative displacement of two elements with the help of capacitive sensing membrane [78]. MEMS technologies have a good potential for various sensing applications, however the current fabrication process is relatively difficult due to various challenges in science and engineering [79].

The viscoelastic properties of the outer surface of a tactile sensing device hamper its ability to move fast over the organ due to friction. Thus, such a structure is more suitable for static point measurements of soft tissue and can be successfully integrated in surgical instruments. Surgical grippers equipped with tactile feedback are able to provide the surgeon with information about grasping force as well as to detect the presence of small blood vessels, thus reducing the risk of damaging soft tissue. Such devices with sensing capabilities can estimate tactile information more accurately, as the target area is fixed between the instrument and no significant displacement occurs. As it is seen from relevant examples of grippers [80, 81], the elastic material incorporated in a

layer can enhance stability of a grasp due to its toothed structure. However, vibration or shaking of an instrument can produce data variability in this case.

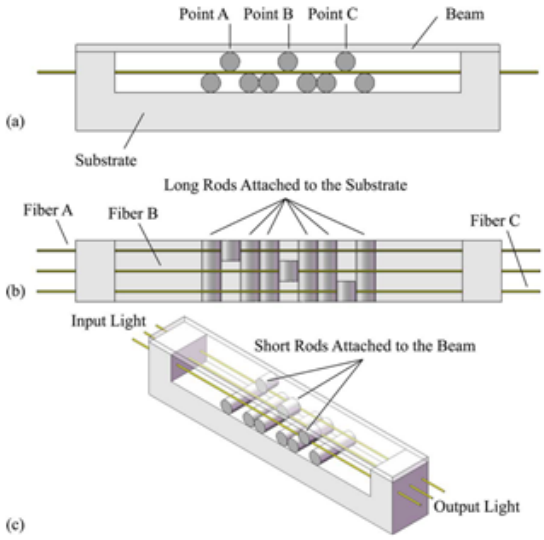

Figure 2.13: Structure of layered sensor working on fibre-optic sensing principle [11].

The typical transducer used in a layered structure sensor should be thin and robust; examples of transducers include piezoresistive films [10, 77, 80], PVDF (polyvinylidene fluoride) films [81,82] capacitive sensing elements [8] or conductive polymer with electrodes [83]. However, all these transducers are not MRI compatible. In [11] the tactile sensor uses the fibre optical sensing principle (Fig. 2.13). This layered sensor is composed of three fibres sandwiched between perpendicular rods of different lengths and several elastic materials. The configuration of rods allows measuring the relative deflection of the sensor structure, therefore detecting the tactile information from the contact surface.

A tactile sensor with a layered structure can be used to measure both force and indentation at the same time, thus providing stiffness information. However, the fabrication process of layers can be relatively complex. In addition, such a sensor can provide more stable results during static measurements, as elastic materials that can be used in the design can lead to the delayed non-linear response. Therefore, one can conclude that a layered tactile device should be integrated in surgical instruments, such as graspers or forceps.

2.4.5 Arrayed Structures

Tactile devices designed as spatially distributed sensing elements in arrays can be very advantageous for RMIS. Arrayed structure sensors are inspired by the design of the human fingertip sensory system with its multiple mechanoreceptors. The structure of a sensor array can be built up from different transducers and their combination. In addition, various tactile sensors can be integrated in one sensing array. One of the advantages of arrayed tactile sensors is that their output can be directly used as the visual information [83] or in the form of a tactile display [84–86].

The sensitivity of the array depends on the number of sensing elements and the accuracy of each of it. However, the more the sensing elements the bigger size and weight of the device, which is undesirable in case of surgical instruments. Therefore, one needs to use small size transducers to increase the sensitivity of the device. For example, in [87] this problem was solved using an array of conductive microchannels embedded in an elastic deformable environment. This technology allows the use of sensors suitable to be used on surgical microgrippers (typical width of an instrument is 1 mm). Another promising technology involves the use of MEMS [88, 89], which has got various advantages such as easy production and miniature size, and can be easily integrated in a surgical instrument. The most suitable transducers for this approach can be PVDF films [88] and capacitors [90] due to their small size. In [89], the measurement sensitivity of a MEMS stiffness sensor has been improved employing an array of force sensing units with two different mechanical stiffness parameters. Thus, a sensing diaphragm was created and can be integrated in a surgical grasper.

The arrayed structure of a tactile sensor can be useful for device flexibility and adaptability to the environment. This approach has been validated in research on robotic

skin in [91–94], where the tactile sensing structure presented is able to cover large curved areas. Looking forward, this approach can be integrated in RMIS instruments, as its flexible structure allows it to cover the entire surface of an organ. However, to achieve miniaturization of this type of sensors further research is required.

2.4.6 Non-contact Devices

As an alternative to contact methods, stiffness can also be measured using non-contact devices. Non-contact stiffness measurement can be used only for devices that are developed for the localization and detection of hard tissue areas, and it is not applicable for integration in surgical instruments. The basic working principle of non-contact devices is based on the detection and measurement of applied deformation and resulting indentation. The advantage of this method is that it allows for the measurement of properties of soft tissue over continuous path in real-time. In addition, the effect of mechanical friction from tool and tissue interaction cannot influence the dynamics of the movement.

The most convenient approach to indent the tissue in a non-contact way is the application of an air jet to the target tissue [95, 96]. This can be easily achieved in the operation theatre, as air supply is broadly available during the surgery. The pressure of an air jet can be regulated, thus it is possible to control the flow applied to the tissue and to reduce the risk of tissue damage during examination. The effect of the resulting indentation can be estimated using a visual feedback system. In [97], similar approach is applied to solve the inverse problem of estimation of the viscoelastic parameters. However, the main limitation of vision based indentation evaluation is the necessity to keep the camera position fixed with respect to organ surface and to avoid shaking and

vibration of the device. This is not possible during surgery due to the natural movement of internal organs. In addition, data processing during this type of measuring is time consuming.

Another way of noncontact measurement of soft tissue parameters was proposed in [12], where a fibre optic displacement sensor is used to estimate the changes in the tissue, which is assumed to be homogeneous. In this work (Fig. 2.14) in order to detect tumour, phase shift difference between air pressure input and displacement sensor output are measured. Therefore, the change in stiffness between two measurements will be detected.

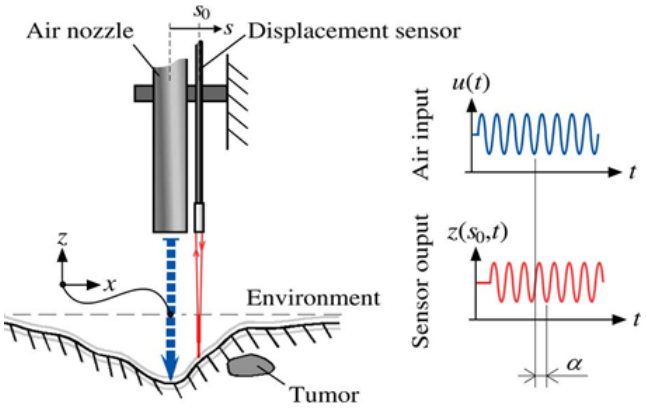

Figure 2.14: Working principle of non-contact stiffness probe [12].

2.5 The Importance of Probing Behaviour

As detailed in the previous sections there is a broad variety of tactile devices that are developed for surgical purposes. The main progress in the development of such devices are made in terms of the mechanical design and measurement principle. It is possible to conclude, that at the moment there exist relatively robust devices, which are capable of providing accurate tactile information during static measurements from

one point. However, as it was already mentioned, to detect the information about an organ's mechanical parameters, it is required to scan soft tissue in a dynamic way.

Therefore, it is possible to conclude that there is a strong need to develop not only tactile devices to measure tissue stiffness, but also algorithms and control methods that can be used to enhance tactile perception. It is beneficial to develop devices and algorithms, which could operate in real-time and provide stable measurements for variable environmental conditions. The concept of autonomous robotic palpation is presented in [98], where hard areas are segmented in a soft environment with the help of elastography and stiffness mapping. The algorithmic approach to localise stiffer areas is used, however, it does not take into account the variability of environment and, therefore, its implementation in real surgical applications might be challenging.

More research is needed to better understand the challenging conditions of the surgical environment, such as in [99], where the interaction dynamics between viscoelastic tissue and the force measuring instrument tip are taken into account. The focus should be on accounting for the force applied, soft tissue restitution dynamics versus time, the shape of an organ and many other factors. These factors can be understood by studying the methods of manual physical examination. Manual palpation techniques are described in detail in Chapter 4.

Currently, only few devices have been approved following clinical in-vivo studies. This is because only robust and safe devices, which fulfil all surgical requirements, can be tested on a live organism. These tests are very important, as the properties of live tissue differ from the properties of ex-vivo tissues. Tests on live tissue represent the final and most significant stage of the development of a tactile device, and it requires preparation and meticulous work.

2.6 Conclusions

The general purpose of a tactile device for stiffness measurement during minimally invasive surgery is to substitute manual palpation and to provide tactile sensations during surgical intervention. The desirable requirements, which should be taken into account in the design of a tactile probe for medical application are summarised below:

- The tactile device should be able to conduct relatively fast measurements over a continuous path on the whole surface of the organ.
- The tactile device should be miniature in size, sterilizable and safe for the patient, that is meet all the necessary requirements for use in RMIS.
- The device should perform equally well in different scenarios under variable dynamic conditions of the measurement process;
- The design of a tactile device should incorporate algorithms and control policies that are used to enhance the obtained perception, to compensate for the effect of the environment on the stability of measurements and to segment stiffer areas in case of artificial tissue palpation.

This thesis focuses on the investigation of palpation strategies and behaviours that can be used to improve tactile perception. More specifically the thesis focuses on how behavioural examination strategies can be used in conjunction with a simplistic indentation tactile probe that measures contact forces from the indentation of the tissue.

Chapter 3

Simulation of Tool Interaction with a Viscoelastic Environment

3.1 Introduction

This chapter discusses one of the obstacles to the practical implementation of artificial surgical palpation, namely variability induced by the dynamical responses of soft tissues. Variability of results from artificial tactile sensing to locate sites of abnormalities, during RMIS depends on non-homogeneity of tissue viscoelasticity distribution and the resulting non-linear temporal dynamics of indentation. The aim of this chapter is to explore the relationship between the probing behaviour and the accuracy of the estimated pre-defined viscoelasticity.

A hardware-based soft tissue simulator (Kelvin-Voigt model) that can provide a repeatable spatial distribution of viscoelastic parameters, was developed to test a repertoire of probing behaviours. Numerical simulations and experimental evidence has shown

that the speed of traversing for a given indentation depth influences the variability of estimating the viscoelastic parameters of the tissue.

As the presented experimental study does not deal directly with soft tissue property measurement, it is worth mentioning various examples describing impedance estimation of soft material by means of an analytical approach [100–102]. For example, [103] considers the nonlinear Hunt-Crossley model, describes the behaviour of soft environment and presents an online property estimation algorithm. Experimental studies and algorithm validation have been implemented for a single point contact and the resulting dynamics. In [104] dynamic finite element estimation was used to define the properties of soft tissues. The results show good accuracy; however, they are highly dependent on boundary conditions, and prior input parameters, and also require high computational power. The above mentioned research works demonstrate that it is important to take into account the dynamics of a target material in order to define an accurate estimate of the viscoelastic environment. Taking that into account, the purpose of this thesis is to study the influence of variable probing dynamics performed over continuous paths of examination.

A hardware simulator able to mimic viscoelastic properties of soft tissues is used for the experimental studies. In this case, the advantage of a physical simulator over an analytical one is that the first is able to test various tactile probes and hardware configurations. The use of a physical simulator eliminates the need to mathematically model the interaction of the tool and material and provides more realistic results. Previous works have used physical setups to represent the properties of viscoelastic materials. For example, in [105] an experimental setup for impedance estimation was created to represent a one-dimensional Kelvin Voigt (spring - damper) physical model with fixed properties of viscosity and elasticity. While in the case described in this chapter,

the viscoelastic parameters can be variable in order to represent the complex structure of soft tissue. Thus, the aim is to quantify the impact of different dynamical modes applied to the material and to correlate them with pre-defined viscoelastic parameters.

Here, the following hypothesis is studied: during dynamical mechanical measurements of soft tissue viscoelastic parameters, the measurement dynamics should be considered in the planning of probing behaviour. Further on, the experimental setup and the way soft tissue modelled for the simulator is described in the methodology section. Then, the results and analysis are presented and are followed by the conclusions.

3.2 Methodology

3.2.1 Hardware Simulator of Viscoleastic Response

A hardware setup was designed to simulate the viscoelastic responses of soft tissue. Fig. 3.1 displays a side view of the experimental system - a one-degree of freedom platform, placed perpendicularly to the force-measuring probe, and controlled by a motor. In addition, the mechanical principle of the proposed hardware simulator is displayed on Fig. 3.2. A weight compensating mechanism is used to minimize the effect of the platform mass. A brushless DC motor (MAXON EC-max 40, 120 Watt) is connected to a position controller (EPOS 2), which is setup to hold the supporting lever attached to the shaft of the rotor in the pre-set position with the variable output torque. The 140 mm long lever transforms rotation and torque of the motor into a vertical translation movement and resistive force of the platform respectively. The PD type controller is used to keep the angle of the lever constant at 30°. Each time the load was applied to the platform, it tended to return to the nominal position with

defined viscoealsticity.

Changing the parameters of proportional and derivative gains (k_p and k_d) allows for the simulation of the responses of the material with desired viscoelastic parameters and exhibits time-dependent strain and stress relation. Furthermore, a known distribution of the parameters enables the possibility to evaluate their influence on the behaviour of measurements of force feedback. In these experimental studies several distributions of the viscoelasticity were used to test the proposed hypothesis. To execute the required distribution, the control of the motor was implemented by reading proportional and derivative gains from the look-up table.

Force feedback is measured with a force and torque sensor (ATI technologies F/T Sensor Nano 17), which has got resolution of up to 0.0013 N for force measurements. The spherical indentation tip, which is 6 mm in diameter, is attached to the sensor. The driving speed and the path of the probe are kept constant during each experiment, and the movement has been implemented with a pre-programmed Fanuc M-6iB robot. The movement of the robot was implemented in the tool space using position control. To reduce the effect of contact friction, which can influence the correct readings of force and torque sensor and introduce undesired noise, a thick lubricant film is applied to the surface of the platform. The advantage of the chosen measurement procedure is that it allows fast and efficient acquisition of results for the same conditions.

To summarize the above-mentioned description, Fig. 3.3 provides the schematic arrangement of the working principle and measurement arrangement of the hardware setup. The input of the simulator is the displacement of the probe and pre-programmed distributions of k_p and k_d. The force and torque sensor is used to measure the responses of the simulator. A mathematical simulation is performed to calculate the theoretic re-

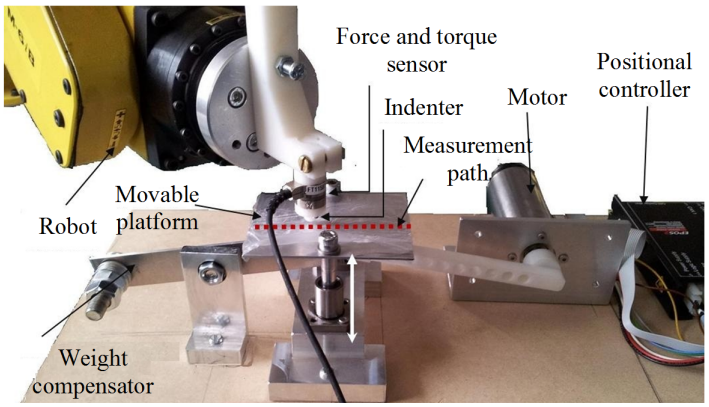

Figure 3.1: Experimental setup used to simulate and measure responses of soft tissue.

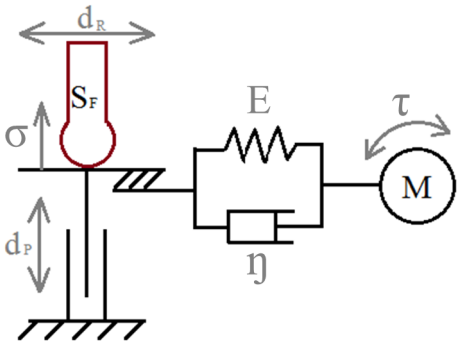

Figure 3.2: Schematic diagram of experimental setup used to simulate and measure responses of soft tissue: motor M produces torque τ with controlled viscoelastic parameters - E (elasticity) and η (viscousity); d_p is the displacement of the movable platform; σ is the stress response produced by the motor; sensor S_F measures the force produced by the platform via a spherical indenter; d_R is the displacement of the sensing probe produced by the robot arm.

sponse of the probe. Next, the comparison of the calculated response and measured forces is performed.

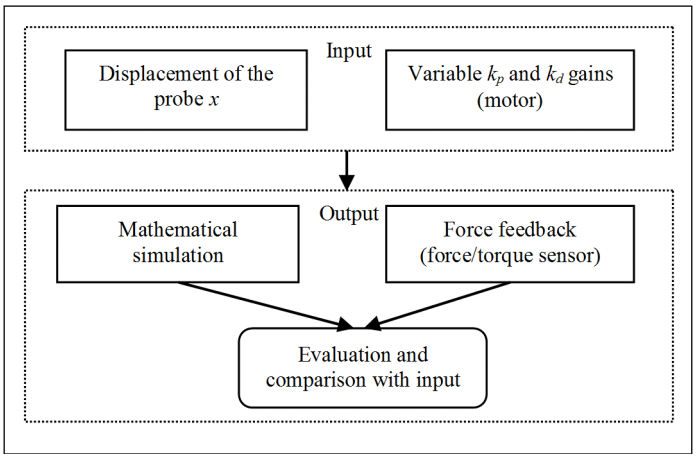

Figure 3.3: Block diagram of the experimental setup.

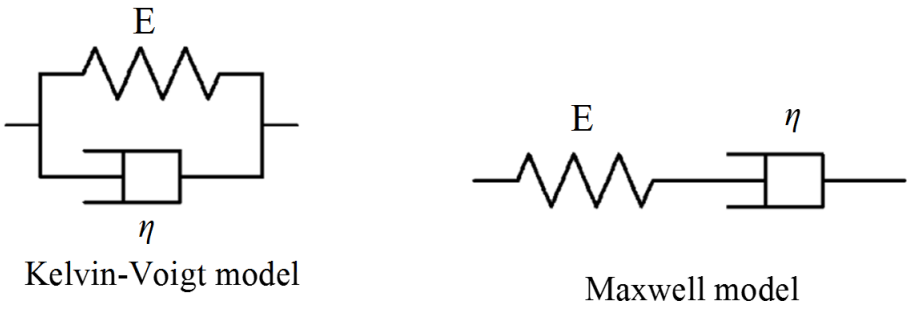

Figure 3.4: Soft tissue viscoelastic structure: Kelvin-Voigt and Maxwell models.

Soft Tissue Modelling

One needs to understand the behaviour of viscoelastic materials in order to model their responses. Viscoelastic material exhibits time-dependent stress in relation to strain. Biological soft tissues exhibit viscoelastic behaviour [106] and therefore that the constitutive linear models for the simulation can be used. There are several types of viscoelastic models in which elastic and viscous parameters are linearly combined and arranged differently, such as Maxwell, Kelvin-Bolzman, Kelvin-Voigt or Zener mod-

els. Various studies show the advantages and shortcomings of these models [107–109] in relation to such phenomena as creep, relaxation and hysteresis. Stress exhibited by an elastic component σ_E can be expressed as a product of elasticity or elastic modulus E and strain ε:

$$\sigma_E = E \cdot \varepsilon \tag{3.1}$$

Stress created by viscous element σ_η depends on the derivative of strain and viscosity η:

$$\sigma_\eta = \eta \cdot \frac{d\varepsilon}{dt} \tag{3.2}$$

Due to the simulator hardware properties, only a model with two parameters can be considered (Fig. 3.4). The Kelvin-Voigt model is composed of an idealized spring (elasticity - E) and a damper (viscosity - η) in parallel and represents a material which is subject to viscoelastic reversible strain. The benefit of this representation is that it produces realistic results for constant stress (creep). The constitutive equation is represented as:

$$\sigma(t) = E\varepsilon(t) + \eta\frac{d\varepsilon(t)}{dt} \tag{3.3}$$

, where t is time. The Maxwell model is represented by a spring and a dashpot placed in series. The model can be represented as:

$$\frac{d\varepsilon_{Tot}}{dt} = \frac{\sigma}{\eta} + \frac{d\sigma}{E \cdot dt} \tag{3.4}$$

, where the ε_{Tot} is the total strain. The limitation of Maxwell model is that when there is a constant load it produces an unrealistic creep prediction. Therefore, when constant load is applied to the simulator, the Kelvin-Voigt model is suitable to represent the viscoelastic response of the simulator.

Input to the Simulator

During medical examination elevated tissue viscoelasticity is treated as a hard formation or a tumour. The main objective of probing during RMIS is to localize hard and abnormal regions of the model. In this experimental study elastic response was implemented by a variation of a proportional gain k_p while viscosity was realized by a derivative gain k_d. Variable elasticity and viscosity was pre-programmed as an input to the simulator (Fig. 3.5). In order to match the desired viscoelastic distribution it was required to calibrate the proportional and derivative gains of the motor accordingly. The calibration of these two parameter was achieved using manual tuning of the controller. At the same time, during tuning it was required to preserve the stability of the system and to avoid vibrations of the motor. In this studies two combinations of viscosity and elasticity responses are tested - the elasticity distribution is combined with one of the two distributions of viscosity. The distribution of the viscoelastic parameters in the simulated tissue was implemented using time-dependent lever impedance, as shown in Fig. 3.1.

To avoid the hardware vibrations, the elasticity E was set to the range of 6 to $11{\cdot}10^{-3}$

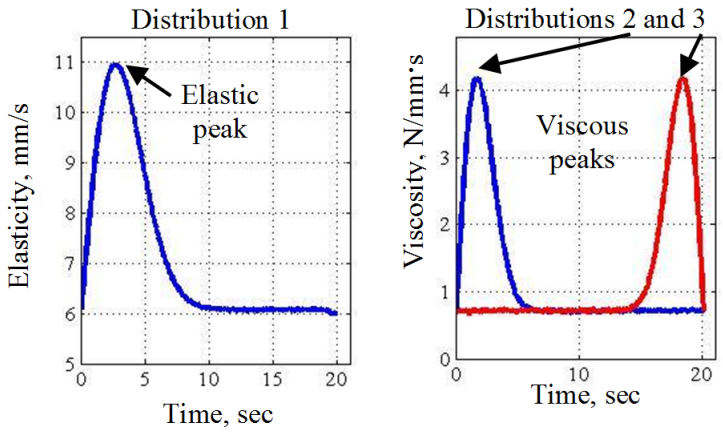

Figure 3.5: The input simulated profiles of viscoelastic response for hardware-based simulation.

(N/m) and damping η was set to the range of 0.7 to 4.2·10^{-3} (N/m·sec). The lever of 0.14 m translated the rotational movement of the motor (gear ratio 1:1) to the linear displacement of the simulated viscoelastic tissue (moving platform). Therefore, the ranges of k_p and k_d variation were: k_p - from 840 to 1535 N·rad^{-}1, and the range of k_d from 95 to 585 N·sec·rad^{-1}.

As shown in Fig. 3.5, in the first model (distribution 1), elasticity distribution had a peak of 11·10^{-3} N/m, that is around 200% above the base level (6 ·10^{-3} N/m) at the beginning, when simulating a hard lump, and then dropped by $\pm$ 5 % around the base level. Viscosity for the first case was kept at the same level with $\pm$ 2.5 % variance around the base level (0.7·10^{-3} N/m·sec) while the peak (4.2·10^{-3} N/m·sec) was simulated at the same region of the elasticity peak (distribution 2). In the second case (distribution 3), viscosity formed a peak of 600% (4.2·10^{-3} N/m·sec) above the base level, which was located at the end of the distribution. For all other parts, viscosity variance was set to $\pm$ 5 % of the base level. The input to the simulator was created using a combination of distribution 1 with distributions 2 and 3.

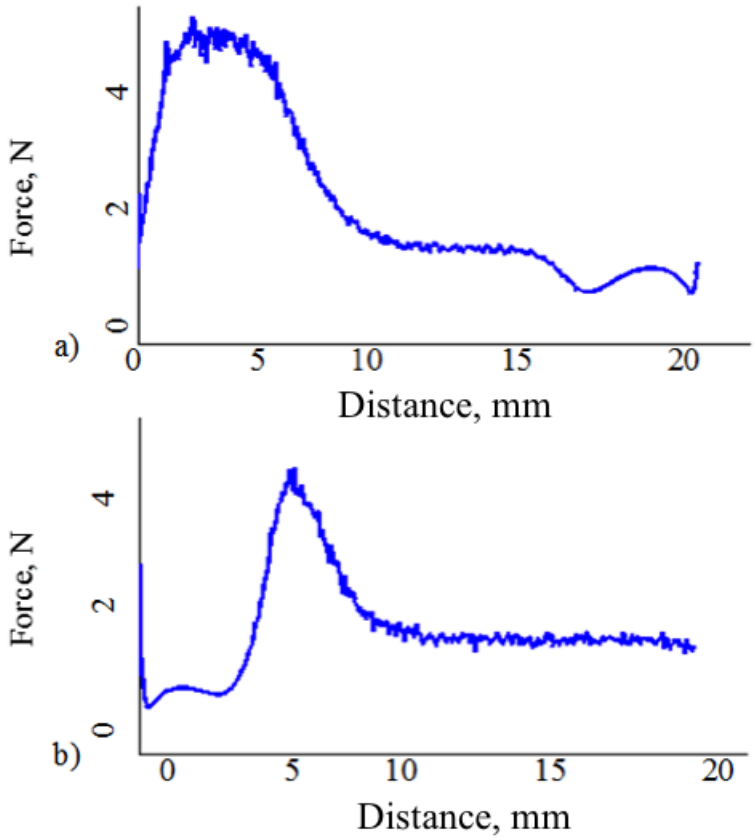

Figure 3.6: The profiles of elastic and viscous gains obtained from simulation.

Experimental Condition and Analysis

Experimental studies comprised two sets of tests employing three different traversing speeds for combinations of input 1 and input 2, and input 1 and input 3 - six tests in total. Two models of viscoelastic soft tissue were simulated in order to evaluate the performance of force measurements in different conditions (Fig. 3.6). Different speeds of probing were tested to estimate a known distribution of the viscoelastic impedance in order to establish a relationship between the accuracy of the impedance parameter estimation and the probing behaviour. To reduce the effect of creep and relaxation during force measurements, the platform was preloaded for a short period of time

before the tests. The load applied to the platform, was not varied during the tests. The normal force from the probe, indentation depth of the platform, and its velocity were recorded at 100 Hz for each type of experiment across 20 trials.

Data analysis was performed to evaluate the accuracy of estimation of impedance parameter for combinations of the pre-programmed distributions. In particular, the regions of variability of parameters, such as the locations of elastic and viscous peaks, were analysed. The displacement of the probe in the vertical direction was kept constant, thus this value did not influence the measurements of the probe. Experimental data was normalized and compared with the theoretical estimation of the parameters. The analysis was carried out across models for the same probing speed and among the measurements for the same model with different speeds. Force feedback data was filtered with a second order Chebyshev low-pass filter in order to minimize the noise naturally occurring during measurements. Normalized stopband edge frequency was empirically selected to be at 0.005 and the stopband ripple at - 45 dB.

3.3 Analysis and Results

3.3.1 Evaluation of Experimental Results

The measurements of impedance data, or stiffness, obtained during probing of soft tissue are commonly used for the representation of tumours during haptic or visual feedback in virtual reality systems [110, 111]. Therefore, it is important to evaluate the experimental results not only from the statistical point of view, but also from a dynamic point of view. Fig. 3.7 and Fig. 3.8 display the mean results of the measurements for different speeds, as well as for the simulated response, as shown in Fig. 3.6.

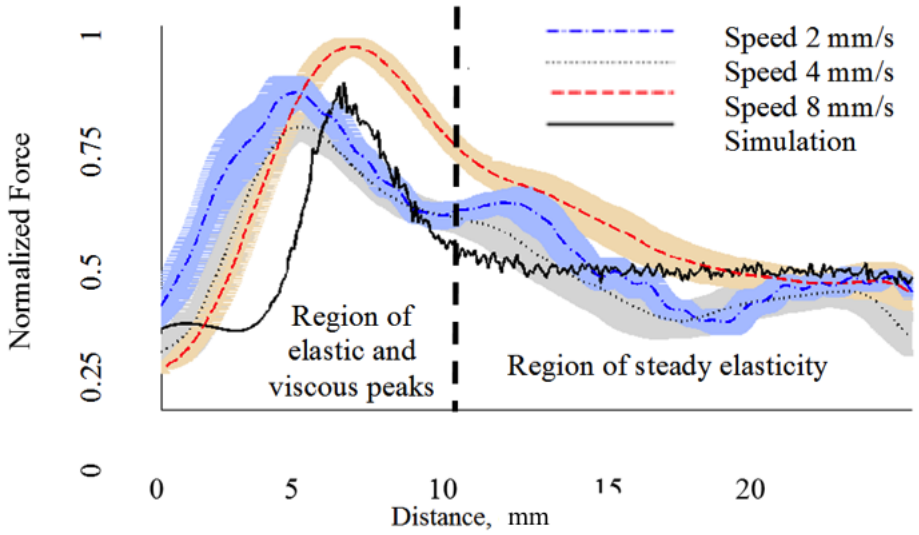

Figure 3.7: Mean values of force readings for the same model (viscous peak inside the elastic peak) for data obtained with different speeds.

The velocity of the simulation was not adjusted, as it was required to observe the theoretical response only. One can observe that the detection of the stiffer area depends on the probing speed. In addition, the locations of the stiff peak in the results of the mathematical simulation do not correspond to the measurements. The effect of hysteresis which appears on the decay of the elastic peak is observable in all graphs. This is typical for viscoelastic material and is explained by the effect of relaxation in soft tissue [106]. Moreover, such response might be explained by the mechanical behaviour of the simulator.

To understand the impact of viscoelastic parameters on probing at different speeds, two regions of the measurements of force were focused on during data analysis: the area with elastic peak, simulating hard formation in soft tissue and the region with steady elasticity. At the first part of the graphs (Fig. 3.7, 3.8) it is seen, that for the same input parameters the location of the simulated hard formation (elastic peak) is detected

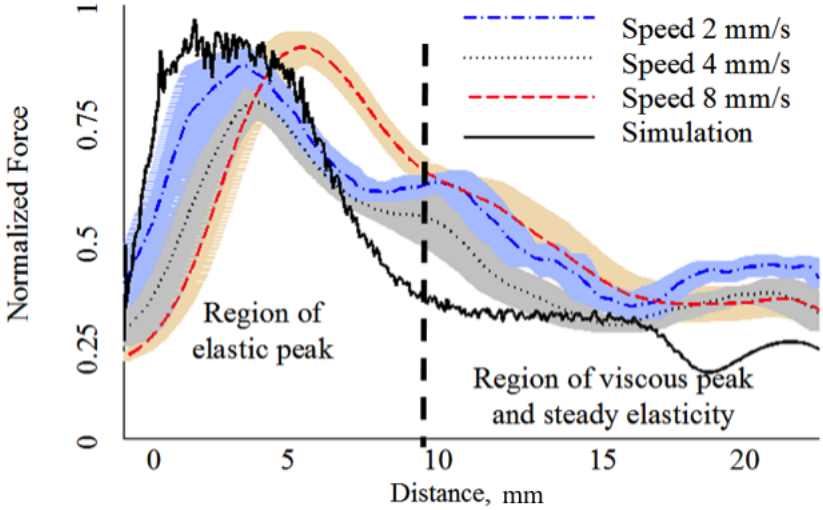

Figure 3.8: Mean values of force readings for one model (viscous peak outside the elastic peak) for data obtained with different speeds.

differently, and that gives the possibility to continue the analysis.

Table 3.1 shows how separate elastic and viscous parameters influence the detection of the peak value in comparison to the mathematical simulation (the input). Interestingly, the higher the probing speed, the longer it takes for the he stiff area to be detected (the peak is detected for lower values of the pre-programmed peak of elasticity). This trend is observed in all three models and shows how the effect of the static-dependent parameter decreases as the dynamical component - speed increases. In a surgical examination, this would lead to the variable localization of the tumour, and thus to an to ambiguous clinical diagnosis. The lowest detection of force magnitude was observed at the average driving speed of 2 mm/s.

Table 3.1: Viscosity, elasticity and force for different velocities and theoretical simulation

Velocity	***Viscous peak inside elastic peak***	***Viscosity, N/mm***	***Elasticity, N/mm·sec***	***Force, kN***
2 mm/s	Yes	1.20	9.4	0.36
	No	0.73	9.3	0.37
4 mm/s	Yes	9.10	9.5	0.41
	No	0.72	9.8	0.43
8 mm/s	Yes	7.60	7.7	0.44
	No	0.72	7.7	0.47
Mathematical Simulation	Yes	4.20	8.5	0.42
	No	0.70	10.5	0.45

3.3.2 Statistical Evaluation

The time constraints of surgery mean that it is not possible to perform several probing trails to determine the most precise tissue stiffness parameters and the location of a tumour. The premise of this thesis is that the optimal probing behaviour can enhance the result of the procedure. Therefore, the analysis was carried out in such a way that the determining factors for the probing behaviour could be outlined.

To study the effect of viscoelastic parameters in the model and the impact of traversing speed, force profiles were cross-compared. The relationship between two variables - force profiles and different speeds across the same input - was established with regression analysis, with the regression step of one second. The results of regression coefficients are displayed in Fig. 3.9. When comparing minimal with maximum speed (2 mm/s versus 8 mm/s) and average with maximum (4 mm/s versus 8 mm/s) for both models, high variation of parameter is seen for the region with an elastic peak (seconds 6 to 8). This highlights the importance of choosing an optimal probing behaviour and variability of results for different dynamical conditions. Another conclusion, which

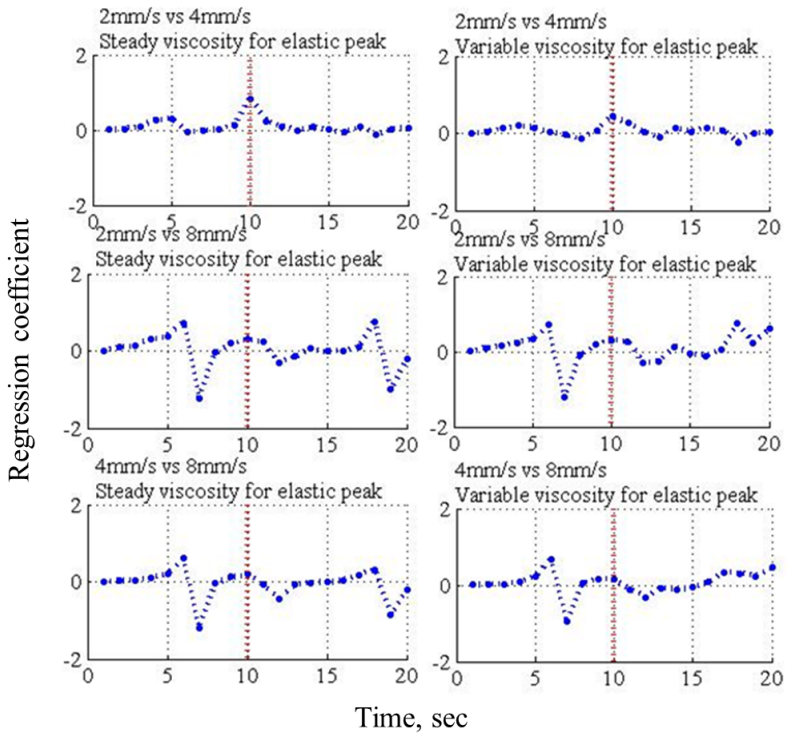

Figure 3.9: Regression analysis of the models with viscous peak outside and inside the elastic peak, comparison of different speed modes; first part of each graph shows the region of elastic peak and second part the steady region of elasticity.

can be drawn from the regression analysis, is that the viscosity for steady elastic distribution (seconds 17 to 20) causes increased variability of data. The model with viscous peak inside the elastic peak does not show such variability for the corresponding speed comparison. Moreover, some increased variation in regression coefficients can be observed in the transient region - on the decay of the peak of elasticity (second 10).

Furthermore, in order to see the impact of the change in viscosity during measurements with different speeds, the standard deviation of error σ for two conditions of elasticity (peak and steady period) was analysed. Table 3.2 reflects the deviation of error for the region of elastic peak while Table 3.3 shows the standard deviation for the steady

Table 3.2: Parameters of variability for the region with elastic peak

Velocity	***Viscous peak inside elastic peak***	**Parameters of Variability**	
		Deviation of error (Σ)	***Mean of standard deviation(μ_σ)***
2 mm/s	Yes	0.0060	0.00198
	No	0.0055	0.0190
4 mm/s	Yes	0.0052	0.0174
	No	0.0083	0.00176
8 mm/s	Yes	0.0043	0.0150
	No	0.0097	0.0267

Table 3.3: Parameters of variability for the region with steady elasticity

Velocity	***Viscous peak for steady elastic part***	**Parameters of Variability**	
		Deviation of error (Σ)	***Mean of standard deviation(μ_σ)***
2 mm/s	Yes	0.0030	0.00147
	No	0.0041	0.0149
4 mm/s	Yes	0.0046	0.0162
	No	0.0036	0.0245
8 mm/s	Yes	0.0016	0.0241
	No	0.0035	0.0209

elastic part. The mean of the standard deviation μ_σ and the standard deviation of σ, designated as Σ, were calculated to achieve a fully fledged analysis. The deviation of error for slow probing speed (2 mm/s) for the region with elastic peak remains at the same level of distribution ($\mu_\sigma \sim 0.02$). The same pattern is observed for the steady elastic region, where the mean of the error is equal to $\mu_\sigma \sim 0.0148$. This happens, as the influence of viscosity minimizes in slow speed, and the elastic parameter prevails. In high speed (8 mm/s) over the region with the viscosity peak, the range of variability of error is decreased compared to the other values in the same region. In the part with both elastic and viscous peaks Σ is equal to 0.0043, while in the last region of the model with viscosity peak only, the value of Σ is equal to 0.0016. Therefore, it can be

concluded, that variability of error decreases in the regions with viscosity dominance for high probing speeds. These results provide initial evidence about the impact of dynamical parameters, such as velocity, on the detection of non-homogenous areas.

3.4 Conclusions

During RMIS, only a limited number of scans can be performed while due to the complex viscoelastic structure of data, it is difficult to locate accurately a tissue abnormality. A hardware-based soft tissue simulator has been shown in this chapter. The simulating setup has the ability to program any given spatial distribution of impedance to test different probing behaviours and transducers. In general, the created approach for the simulation of soft tissue response parameters can be used for the evaluation and testing of soft tissue measuring probes and other surgical instruments, for the definition of optimal measurement dynamics during the measurement of viscoelastic parameters. In this chapter, the accuracy and variability of reconstructing a known bimodal impedance distribution (elastic and viscous parameters) using three probing behaviours within the mechanical limitations of the hardware was presented.

The results can be summarised as follows:

1. This experimental study showed that not only the tactile probe plays an important role for accurate soft tissue examination but also the probing behaviour applied during examination matters.

2. It is shown that increased speed of measurements results in less variability of error at the expense of accuracy to detect the harder area. By means of experimental evidence, it was proved that the probing dynamics for a given viscoelastic

structure can influence an accurate estimation of soft tissue mechanical parameters. Therefore, there might exits an optimal probing behaviour, which will reduce measurement error and variability for a given viscoelastic parameters of soft tissue.

In the next three chapters the studies of a set of probing behaviours based on the examination of manual palpations using soft tissue samples with hard formations will be described. Thus, it will be possible to outline the specific behaviours used in soft tissue examination.

Chapter 4

Modulation of Applied Force

4.1 Introduction

This chapter presents experimental evidence for the existence of a set of unique force modulation strategies employed during soft tissue palpation to locate non-homogeneous hard formations, such as tumours. The active probing strategies to define local areas are explored and the role of force control is outlined. In addition, it is investigated whether the applied force depends on the degree of non-homogeneity of soft tissue.

To achieve artificial palpation for surgical applications, the detection of hard abnormalities and measurements obtained by tactile sensing devices should be reliable and repetitive. However, it is difficult to fulfil this requirement due to the variability of conditions introduced by the surgical environment. Variability is caused by the viscoelastic nature of soft tissue as well as by external factors, such as movement of internal organs and flows of bodily fluids.

There are several examples where the properties of a soft medium are measured using active modulations of applied force, such as vibrations. One of the possible technologies that can be used to measure soft tissue stiffness during RMIS is resonance-frequency based method. For instance, technologies described in [5, 67] are based on the combination of linear variable differential transducers (LVDT) with a mass-spring mechanism. The system measures a shift of accruing resonance frequency during the indentation of the probe inside a soft tissue. Thus, it is possible to measure viscous and elastic properties of soft tissue.

Soft tissue manual palpation strategies used by expert surgeons should also be taken into account in the development of a medical tactile device for palpation. These strategies can provide guidelines not only for the design of the sensor but also for the development of an optimal examination process, which can lead to a higher tumour detection rate and better efficiency [112]. Soft tissue palpation is a mechanically complex process whose performance requires expertise and continuous training. It is broadly applied for initial breast and prostate examinations to detect the presence, location, shape, mechanical properties, and texture of abnormalities.

There are several palpation techniques in use, depending on the organ examined and the shape and depth of the abnormality [113, 114]. Palpation methods can be subdivided into three main techniques, namely global movement (discussed in Chapter 6), local movement (Chapter 5) and palpation pressure. These techniques are often combined in order to achieve the best possible result [115].

At the start of the process to detect areas of possible abnormalities, a global finger movement (GFM) is applied, as a general scanning technique. For further examination it is necessary to explore those areas more thoroughly. Therefore, the local finger

movement (LFM) technique is applied and performed only within a selected section. This type of palpation helps physicians to understand the shape and depth of an abnormality. Due to the different shape and location of organs, the approaches of LFM though similar are specific to the target organ. In particular, three methods of LFM can be outlined for palpation examinations performed with one finger on the prostate [115]. The first technique is tapping - a fast striking discontinuous touching of the tissue. The second technique is vibration, where the finger is kept at constant contact with the tissue and the force direction of the finger is varied during examination. Finally, there is the sliding pattern - a smooth movement over a defined area at a relatively constant pressure. In the scope of this work the particular focus is on one-finger palpation, as it can emulate probing of the tissue with a tactile examination probe.

The third palpation technique, is finger movement pressure (FMP), which corresponds to the average intentional finger pressure applied during the palpation procedure, such as light and deep palpation [116]. Light pressure is mainly used with GFM to access the general mechanical properties and temperature of the organs. Indentation of this type of palpation does not exceed 2 cm and pressure is as light as possible. Deep palpation is performed with heavier pressure, mainly used for LFM, with an indentation of about 4 cm, and is used to evaluate the stiffness, size, contours and shape of the formation or of the organ. The focus of this Chapter is on local FMP.

Based on the relevant literature, it is possible to formulate the following questions that are discussed in this chapter:

1. Is there a generic template or pattern of applied force that is used to probe a localized area of viscoelastic non-homogeneous environment?

2. Is there a mathematical model that can represent the pattern of force modulation?

3. Can a robotic probe of embodiment different from a human finger achieve a substantial level of palpation effectiveness only by following the pattern found from human demonstrations.

4.2 Methodology

4.2.1 Subjects and Experimental Protocol

This chapter explores the general force control principles for tactile exploration of soft environments, such as artificial palpation during RMIS. More specifically, the way humans are performing manual palpation is investigated. The research carried out for these studies was approved by the King's College London Biomedical Sciences, Dentistry, Medicine and Natural & Mathematical Sciences Research Ethics Subcommittee. A total of ten subjects participated in the experimental studies that are described in this chapter. These subjects did not have any surgical experience, as here it was important to understand low level primitive strategies that are used to explore unknown environments. Surgeons and other physicians who practise manual palpation can be biased by their training and experience, whereas subjects that do not have such experience apply their natural behaviours. In this study naive subjects without any previous palpation experience were used to test whether there is a common behavioural structure for manual palpation so that the abstractions can be generally applied across a wide range of palpation applications. The difference in performance between experts and novices is discussed in the next chapter.

4.2.2 Design of Artificial Silicone Phantoms

Design of Experiments - Types of Abnormalities

To fabricate realistic phantoms of soft tissue with a lump inside it is necessary to understand the biological background and properties of the lumps. Lumps can be benign and malignant (cancerous) and are formed due to abnormal cell growth. In this work it is important to replicate the properties of malignant formations. From a biological point of view all malignant lumps are classified depending on the type of cells they are formed from. For instance, the majority of breast and prostate cancers are called carcinomas and are formed from the epithelial cells. Therefore, it is desirable that the fabricated formation in the phantom tissue is similar to this type of abnormality.

According to TNM (tumour, nodules, metastasis) classification malignant tumours are divided into four classes. First parameter T (tumour) characterizes the level of propagation of the abnormality. As reported by [117], the first stage can be defined depending on the size or on the growth level of the formation. The first level of cancer is easier to treat but more difficult to diagnose. For instance, prostate cancer of this stage is difficult to palpate or it is not visible. Therefore, in this research the focus is on small tumours of the first stage.

Malignant tumours can have even and irregular shapes. In addition, tumours can have non-homogeneous stiffness distribution, such as soft edges. However, homogeneous nodular tumours are frequently present in prostate, lung, breast and other carcinomas [118, 119]. For simplicity, the shape of malignant formations in this research is approximated to solid spherical formations.

Fabrication of Silicone Phantoms with Artificial Hard Formations

Artificial silicone phantom organs were used as an exploration medium to study the behavioural patterns of manual palpation. The analysis of healthy and cancerous prostate tissues shows that the stiffness of malignant tissues is significantly higher than that of healthy tissue or benign formations [120]. To comply with the common natural stiffness ratio in healthy and cancerous tissue, artificial soft phantom with hard nodules was fabricated with the hardness ratio 1 : 4. According to [121] silicone gel RTV6166 (Techsil Limited, UK) with mixture ratio 4:6 and 900 mPa·s viscosity was used to create soft artificial tissue of homogeneous stiffness. Hard transparent nodules or artificial tumours were embedded in the soft phantom tissue. To fabricate the spherical nodules, hard silicone rubber compound RTV615 (Techsil Limited, UK), ratio 10:1 and 4000 mPa·s viscosity, was used. The stiffness of the hard nodules was not varied across experiments. The depths of the hard inclusions were varied across experiments. Each silicone phantom was exposed to multiple examination rounds. Therefore, it was necessary to ensure that the nodules are not displaced inside the phantom, as it might affect the results of the analysis. In case it was noted, that the nodule was moved in depth, new silicone phantom was used.

The participants were asked to explore the appointed areas of an artificial soft tissue phantom. Six out of seven phantoms contained an embedded nodule. Hard nodules of different diameters - 3, 6, 9, 12, 15 and 18 mm - were fabricated to simulate tumours, all embedded at a depth of 5 mm from the surface. These sizes correspond to cancer stage T1, according to TNM classification [122]. Each participant performed five probing trials for every nodule location. To prevent the effect of learning, subjects were asked to explore embedded nodules in a pseudo-random order. In addition, sub-

jects were given time to get familiar with the task, performing three palpation trials on a different phantom tissue. The task stated during the experiment was formulated in such a way as to stimulate the most effective exploration pattern using one-finger palpation. Subjects were asked to estimate the depth and the diameter of the embedded nodules. Most of the time, the estimated dimensions did not correspond to the real values as the depth and the diameter of the nodule are related: a deeper nodule with a large diameter can be perceived as a smaller nodule closer to the surface. These results were considered as subjective, and are used to stimulate the exploration. The answers of all subjects are shown in Appendix A. Subjects were instructed to avoid any movement of the finger in the lateral direction. It was observed that all subjects intuitively have used their index finger for palpation. For the investigation of manual palpation described in this chapter, four silicone phantoms were created to study the forces applied during exploration movements, including the phantom that was used in the preliminary studies.

4.2.3 Data Measurement

The experimental setup (Fig. 4.1) was designed to measure the applied force during palpation of an artificial soft tissue. Three-dimensional force readings were recorded using 6 degrees-of-freedom force and torque sensor (Mini 40, ATI industrial automation). The resolution of normal force is 0.01 N and the sensing range in that direction is $\pm$ 30 N. The range of lateral forces is $\pm$ 10 N with a resolution of 0.05 N. The sensor was mounted under a support base plate that held the phantom tissue. The sample of artificial tissue was placed in such way that the area of examination was located just on the top of the sensor. To avoid the unnecessary effects of friction, the surface of the silicone was lubricated with silicone gel. During palpation, the silicone block was stably

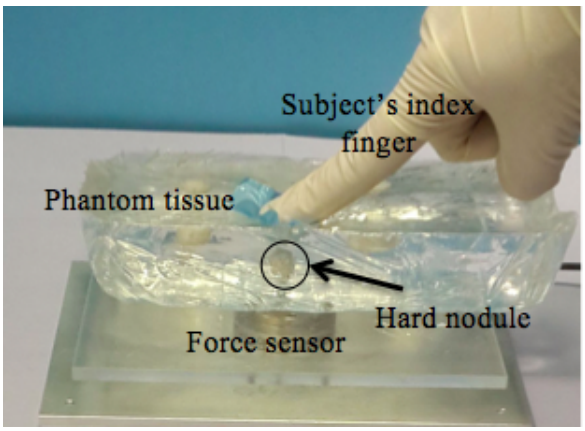

Figure 4.1: Experimental setting used for studies of local palpation behaviour

attached to the base under its own weight, and any sliding or bending was avoided.

4.2.4 Data Analysis

To analyse the recorded palpation behaviour, and to evaluate palpation factors, such as force modulation, data analysis was carried out. The approach described below and the methodology of data processing were both applied for the analysis of all experiments on manual palpation that are described in the two following chapters. Statistical analysis and data processing were conducted using R statistics i386 2.15.2 and MATLAB 7.12.0 software packages. To smooth out noisy peaks from the force measurements, a second-order Chebyshev low-pass filter was used with a cut-off frequency of 0.2 Hz and stop-band attenuation of 60 Hz. These parameters were chosen based on the empirical evaluation. The measurements of the trials with negative detection results were excluded from the analysis for the locations that contained the nodules. A Kolmogorov-Smirnov test was used to check whether the data was distributed normally. To analyse the significance of possible factors and conditions of probing strategy, analysis of variance (ANOVA) and two-way t-tests were used. The impact of a factor was considered

significant if the null hypothesis was rejected with a 95% confidence level (p <0.05).

4.3 Analysis and Probing Results

This chapter focuses on the investigation of a possible pattern of force modulation that can be applied in the exploration of a given point. The aim is to determine whether there exists a specific force control strategy that is used to detect non-homogeneous areas in a soft environment. To achieve a better understanding of the ways humans detect hard nodules in viscoelastic environments, modulations of applied normal (F_z) and lateral forces (F_x and F_y) are evaluated separately.

4.3.1 Variability of Force Magnitude

It is interesting to observe how the range of the magnitude of applied forces changes across different nodules and subjects. Fig. 4.2 displays the distribution of the mean range for three different forces - magnitude of lateral forces, normal force and overall force magnitude. Magnitude of lateral forces equals $\sqrt{F_x^2 + F_y^2}$. Similarly, the overall force magnitude was calculated using all three measurements. The observation of the dynamics of the data indicates that there might be no strong dependence between the range of force magnitude and the diameter of the nodule.

Furthermore, to observe the variability of the normalized force measurements for three force components across subjects and all trials, standard deviations of these values were analysed. Fig. 4.3 reflects the histograms showing the variability of standard deviation values for three force components for all trials. The magnitude of lateral forces is kept relatively at the same level with the average standard deviation σ =

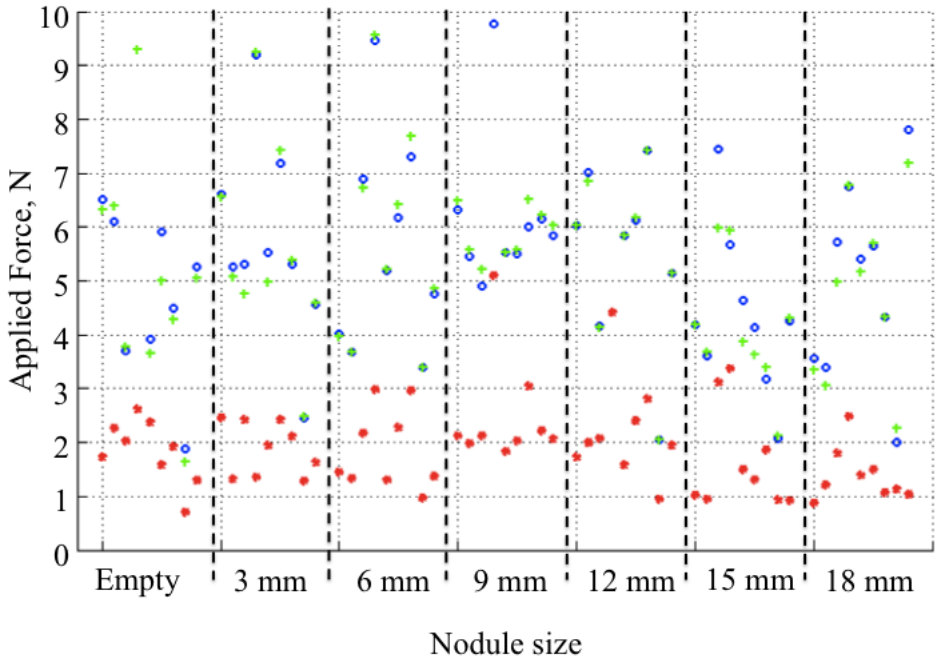

Figure 4.2: Distribution of the mean range for the magnitude of lateral forces (red dots), normal force (blue dots), and overall force magnitude (green dots). Values are plotted for different nodule sizes from empty location to 18 mm (X axis), and across different subjects (for each size, subjects are not numbered, number of subjects is equal to ten).

0.04 (for normalized force values). However, the magnitude of normal force is varied more: the mean standard deviation for normalized force is equal to $\sigma = 0.16$. The diameter of the nodule was not significantly influencing the value of standard deviation for lateral forces ($p = 0.73$ for F_x, and $p = 0.57$ for F_y). Conversely, standard deviation of normalised normal force significantly depends on the diameter of the nodule (p <0.005). In addition, this value also varies significantly across subjects (p <0.0001). The average magnitude of the normal force is 3.2 N across all subjects. Therefore, this might suggest that rather than using lateral forces subjects predominantly use normal force as a control variable to explore hard nodules in soft tissue.

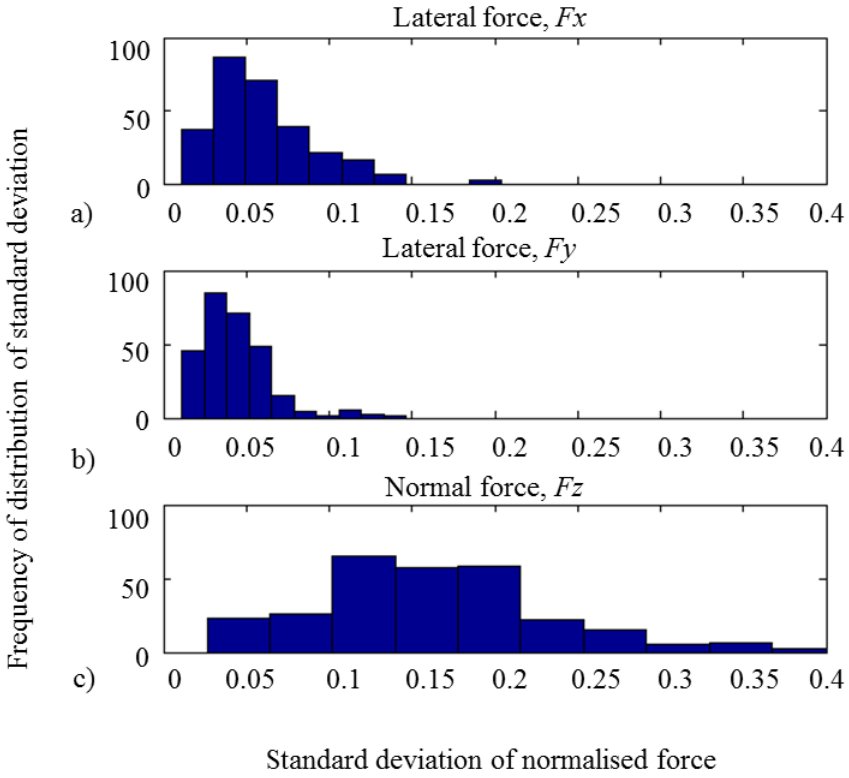

Figure 4.3: Histogram of standard deviations across all trials for normalized measurements: a) lateral force F_x, b) lateral force F_y, and c) normal force F_z

4.3.2 Modulation of Lateral Forces

To understand the possible patterns and the role of modulation of lateral forces, F_x and F_y measurements were analysed. These two forces are mechanically related as the force modulation is performed on the same plane. The correlation analysis was carried to support this interpretation. According to this analysis 94% or 328 trials had significant correlation with mainly negative trends, as shown on Fig. 4.4 ($p < 0.05$). This confirms the fact that the two forces are inversely related. A sinusoidal pattern of the magnitude has been found to be the main feature of such forces. The mean range of magnitude of lateral forces across all trials is 1 N.

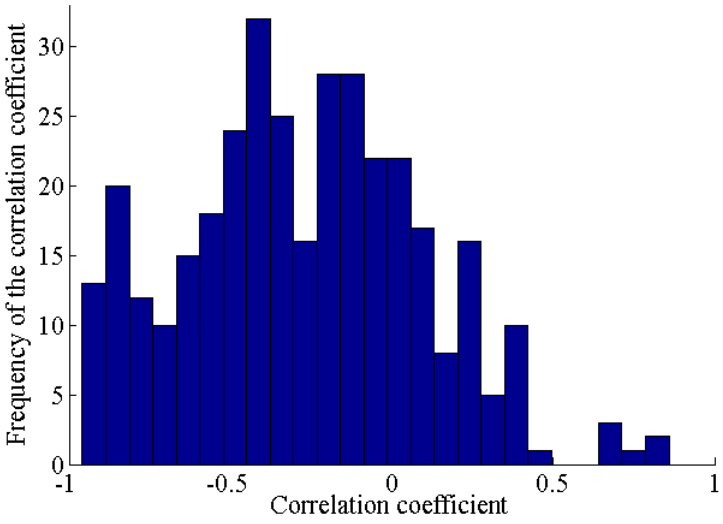

Figure 4.4: Histogram of correlation coefficients for measurements of two connected lateral forces F_x and F_y.

Fig. 4.5 displays the distribution of magnitude of lateral forces for one selected subject and one trial. It is possible to observe that the magnitude of applied force might vary depending on the size of the nodule. A curve linear regression analysis was used to check if it is possible to model the relationship between the nodule diameter and the magnitude of the lateral force, characterized by the area of an ellipse. According to the evaluation of the coefficient of determination for polynomials of different orders, the mean order of best fit is as high as 3.7 ± 1. A statistical evaluation was carried out in order to explore whether there exists a connection between the applied force modulation and the diameter of the embedded nodule. To characterize the magnitude of lateral forces in one variable the area of a fitted ellipse (Fig. 4.5) was used. However, the results of statistical analysis show that the magnitude of lateral forces is independent with respect of the probing location and the preferences of the subject (p >0.05).

Another variable that characterizes the behaviour of lateral forces is the frequency

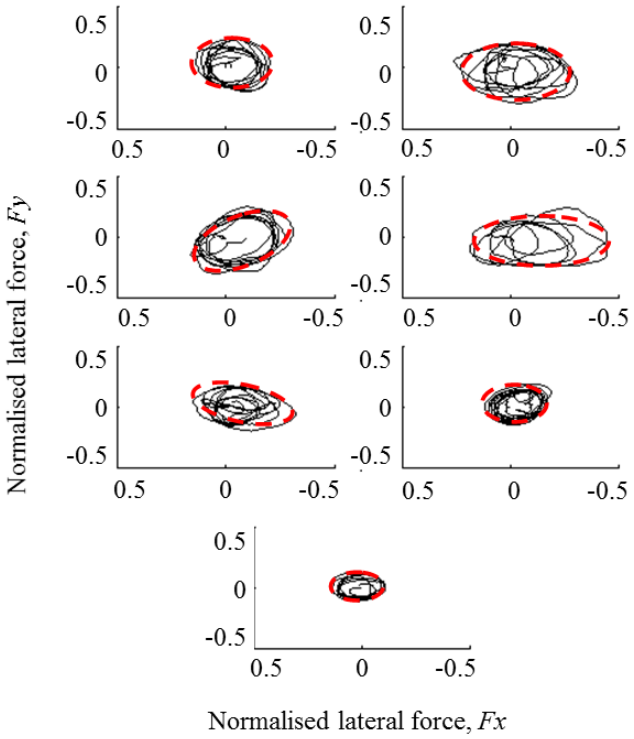

Figure 4.5: Distribution of lateral force with fitted ellipse (red dashed line) for one selected subject, one trial, and for different nodules a) to g): Empty, 3, 6, 9, 12, 15 and 18 mm, respectively, normalized force values.

of the applied sinusoidal pattern. Fig. 4.6 displays the distributions of the applied frequencies for all subjects. Frequency is calculated as a mean value for each trial. According to statistical analysis there is no significant relation between the modulation of the applied frequency of the lateral forces and the diameter of the nodule ($p = 0.66$). In addition, the frequency value does not depend on the subject ($p = 0.38$). Thus, it is possible to conclude that there exists a specific bandwidth of frequencies for lateral forces that is used during exploration of soft non-homogeneous environments. The mean value of such frequency is 1.8 ± 0.66 Hz. Therefore, there is clear evidence that vibrations of lateral forces are used to enhance the tactile perception in a viscoelastic non-homogeneous environment. It is possible to conclude that there is a stereotypical

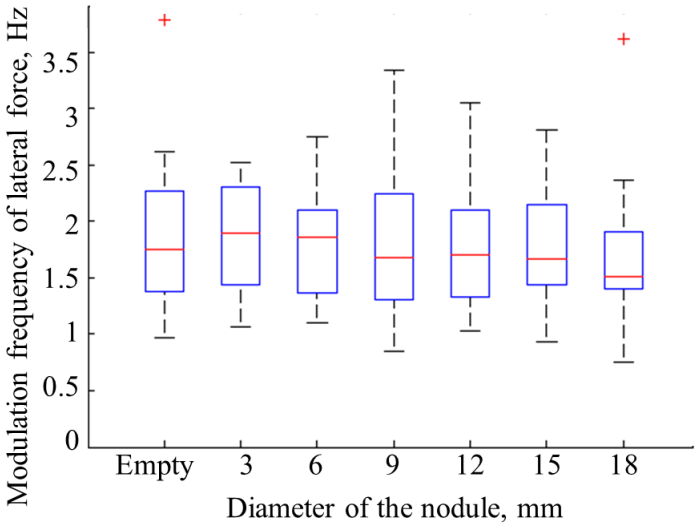

Figure 4.6: Distribution of frequency for the modulation of lateral forces for different probing locations for all subjects.

force modulation frequency used by all subjects. The developed frequency of force modulation might occur due to the natural constraints of the human hand ligaments in combination with the given viscloelastic environment [123].

4.3.3 Modulations of Normal Force

The obtained results lead to the question as to whether the normal force follows any specific pattern during exploration, or whether its variations are random. First, the relationship of normal force in respect to the lateral force is studied. For this purpose correlation analysis is performed. Fig. 4.7 shows that there is a significant negative correlation between the magnitude of lateral forces and the normal force ($p < 0.05$ for 93 % of all trials). The mean value of correlation coefficients for all trials is equal to -0.45. This indicates that the probing strategy should include modulation of both lateral and normal forces in an autonomous robotic palpation.

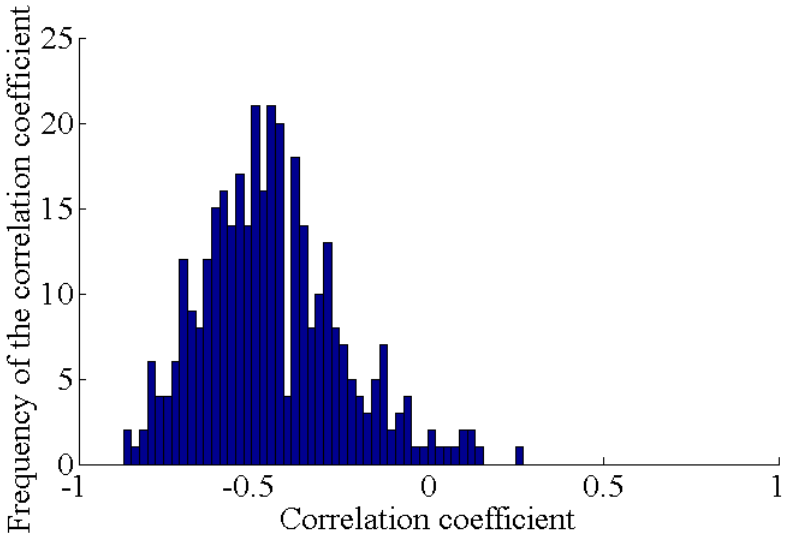

Figure 4.7: Histogram of correlation coefficients for measurements of the magnitude of lateral and normal force F_z.

As was observed in sections 4.3.1 and 4.3.2 there is no significant variation of lateral forces among all subjects and across all trials. In other words, the strategy of lateral forces is similar in all trials. Therefore, it can be concluded that the normal force can be modelled separately.

Normal force can be the main force vector that is used to produce stiffness from the exploration area to detect a hard formation. In this subsection the mathematical representation that can be used to model the normal force is presented. The results lead to the question as to whether the normal force follows any specific pattern during the exploration, or if it is just a random variation.

Modelling of Normal Force Using Linear Model

A linear regression model was evaluated in order to determine to what extent a simple mathematical model can be used to explain temporal normal force patterns for probing.

The minimal order fitting polynomial was used to find the model of lowest order that produces the best fit. Coefficient of determination R^2 was used as fitness measure for defining the best model order. This value represents the fraction of the variability of the dependent variable explained by the variance of the independent variable.

In order to define an indicative pattern of evolution and a model order, linear models of increasing order were interpolated for each individual trial assuming $R^2 > 0.7$ as a good fit. It was observed that 41% of the data followed a 4th order linear model pattern and the rest of the data followed a sinusoidal pattern. The sample profiles of normal forces for two types of profiles are shown on Fig. 4.8 - sinusoidal is shown in red dotted lines and step-like is shown in black solid lines.

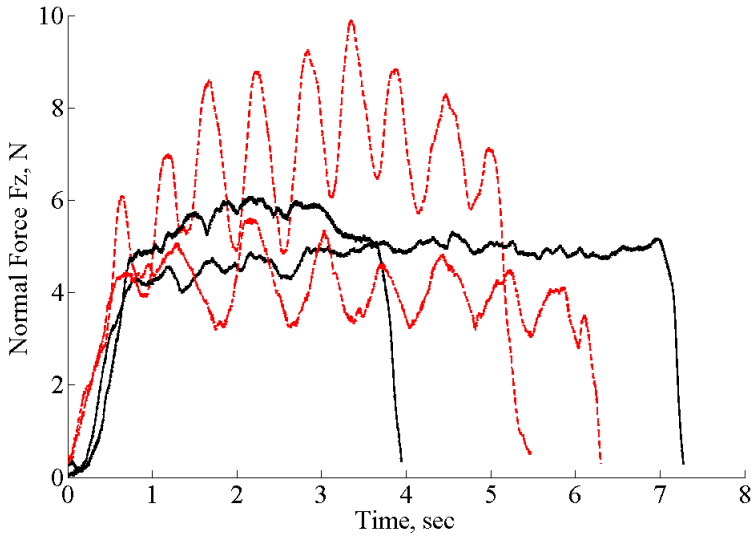

Figure 4.8: Sample profiles of normal forces for sinusoidal (red dotted lines) and step - like response (black solid lines)

Next, it needs to be determined whether a 4th order model can be assumed as general behaviour or more complex dynamics have to be taken into account. To describe the nature of the polynomial, the process was modelled as stochastic equation with variable

polynomial coefficients. The structure of the model is:

$$F_z = a + bx + cx^2 + dx^3 + ex^4 \tag{4.1}$$

where F_z is the normal force, x is trial time in milliseconds and a = - 0.59 $\pm$ 0.40, b = 0.12 $\pm$ 0.56, c = 0.18 $\pm$ 1.21, d = - 0.13 $\pm$ 1.33, e = 5.24 $\pm$ 2.31 are the coefficients. 80% of the data was used to learn the coefficients while 20% was used for cross-validation. It was found that a 4th order polynomial did not optimally fit the data in the general sense, as the average R^2 value was around 50%.

The responses that did not fit with the linear model were analysed separately. It was found that all of them followed the sinusoidal pattern. According to statistical evaluation some subjects preferred one pattern of normal force over the other (p <0.01). In addition, the interaction effect of two influencing factors, namely the subject and the probing location, is highly significant as concerns the choice of probing pattern (p <0.001).

Fig. 4.9 shows the distribution of frequency modulation for normal force across different probing locations. There were no significant differences among frequency values across trials and subjects (p >0.05) for the sinusoidal pattern. Therefore, the distribution of frequency can be considered to be common in all trials. The mean frequency value of normal forces for the sinusoidal pattern is 1.9 +/- 0.7 Hz.

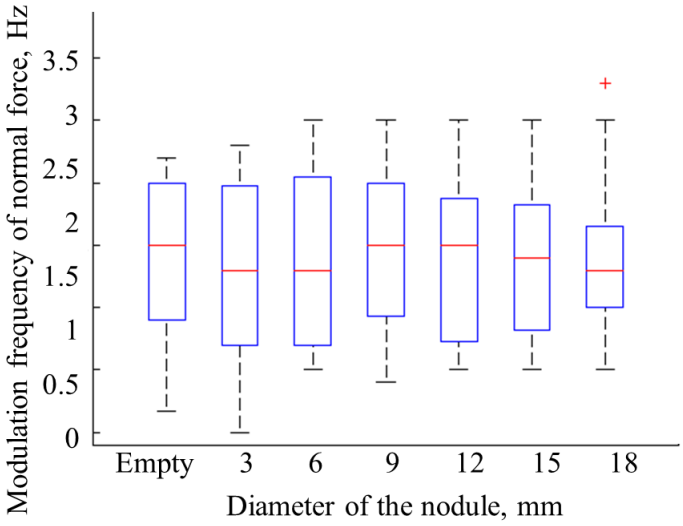

Figure 4.9: Distribution of frequency for the modulation of normal forces for different probing locations for all subjects.

Prediction Using Autoregressive Model

The autoregressive model is used to model the modulation of applied normal force as a second approach. In this section both reactive and predictive models are tested. In the first instance it is assumed that subjects are planning the applied stress using previously perceived information about stress values, while in the second model the estimated or predicted stress is used. The autoregressive model can be defined with the following equation:

$$X_t = c + \sum_{i=1}^{n} a_i X_{t\pm n} + \varepsilon_t \tag{4.2}$$

where a_i are the autoregression coefficients, ε_t is white noise, c is constant, X_t is the stress output, t is the sampling step, and n is the model order. In our case the constant

c is equal to zero. In case of $(t + n)$ the model is predictive; in the case of $(t - n)$ it is reactive. To understand the order of the autoregressive model for both cases the Akaike Information Criterion (AIC) was used. To statistically validate and choose the model order, the non-parametric Wilcoxon rank sum test was implemented across AIC values for different orders. This test is equivalent to the Mann-Whitney U-test and is used to determine whether the rank of related samples is different. Table 4.1 below reflects p-values for reactive and predictive models.

Based on these results, it can be concluded that the subjects use either the reactive model of second order (p <0.001), or the third order predictive model (p <0.05). Further on, the coefficients of the autoregressive model were obtained. Stochastically distributed coefficients obtained from the individual fitting are the obtained from the learning phase. There can be various methods of estimating the value of the coefficients. In our case it was found that the centroid values of the distribution of coefficients produce the model with the best fit. The coefficients of the second order reactive model were estimated as: a_0 = 1, a_1 = -1.706, a_2 = 0.721. The predictive model of the third order can be characterized by the following coefficients: a_0 = 1, a_1 = -1.980, a_2 = 0.819 and a_3 = -0.164. It is worth noting that the autoregressive model is applied to

Table 4.1: Selection of Order Number for Autoregressive Model

Order Number	*Reactive model, p-value*	*Predictive model, p-value*
One vs. Two	$p < 0.0001$	$p < 0.0001$
Two vs. Three	$p = 0.38$	$p < 0.05$
Three vs. Four	$p = 0.76$	$p = 0.34$
Four vs. Five	$p = 0.84$	$p = 0.63$
Five vs. Six	$p = 0.98$	$p = 0.74$

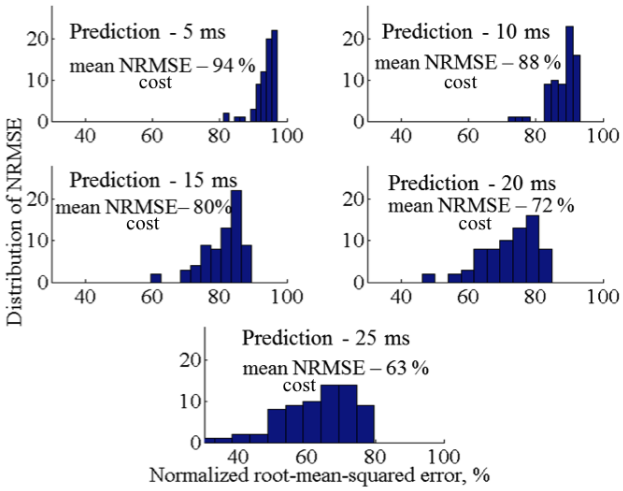

Figure 4.10: Histograms of prediction horizon and NRMSE costs for second order reactive model; where 100% assumes perfect fit.

both sinusoidal and step-like patterns,as mentioned in the previous section.

The two obtained models were tested on the validation data using normalized root-mean-squared error (NRMSE) costs as a measure of the goodness of fit. This parameter is a non-dimensional version of root-mean-squared error (RMSE) that allows the comparison of data of different dimensions for the range of the observed data. If the NRMSE cost of the training data set exceeds 70% it is assumed that the model produces good results, considering 100% a perfect fit. It was found that the reactive model produces a good fit for up to 20 ms prediction horizon. Fig. 4.10 shows the corresponding average NRMSE cost value for the reactive autoregressive model for prediction horizon 5 to 25 ms. On the other hand, the predictive model is not able to produce good fitness results. The average NRMSE cost value for prediction horizon 5 ms is 95%. However, the higher prediction horizon results in bad fitting. Therefore, it can be concluded that the data of normal force can be best explained with the second order reactive model.

Prediction Using Markov Chains

An alternative approach that can be used to model the transient behaviour is a Markov decision process with the steady state treated as an absorbing state. This process describes the dependence between the adjacent elements of the chain. In this case the chain represents a set of force readings of different magnitude. The first stage of the process is the creation of a stochastic matrix that describes the probability of transitions. Each entry of the matrix corresponds to a probability of transition from one state to another. The states of the matrix correspond to physical values of applied force. The chosen resolution of the physical force for each step influences the accuracy of prediction. High number of elements in the chain leads to small transition probability values between dependences. Therefore, a very large stochastic matrix will have equal probability values for each transition. In contrast, low number of elements would lead to coarse prediction of the applied force. In this case it was chosen to use 0.4 N resolution steps. The range of force applied by humans varies from 0 to 10 N. Based on that, the size of the matrix is 24 by 24. The created matrix is smoothed using box blur linear filter where the element is assigned an average value of eight neighbourhood values. Then, the matrix is normalised to obtain the total probability value for the chain which equals one. The resultant stochastic matrix and the distribution of eigenvalues are shown in Fig. 4.11. In addition, the figure shows the distribution of eigenvalues for the matrix, which is useful in the understanding the transition properties of the described process [124]. A steady-state vector s of a transition matrix P satisfies the equation $s \times P = q$. This corresponds to the first largest eigenvector of matrix P to be equal $\lambda = 1$. The second largest eigenvalue is equal to 0.7, and affects the convergence to the steady state. In other words, this value is useful to understand the earliest failure of he system. Time to converge to an absorbing state is equal to

$$t = 1/(1 - \lambda_2) \tag{4.3}$$

where, λ_2 is the second eigenvalue. Once the dynamic system reaches an absorbing state, it cannot be avoided. The convergence time is defined by the value of the second largest eigenvector. The settling time to an absorbing state in this case is just 3.3 seconds, which is too short to be modelled as a stochastic decision process. In this case, the autoregressive model converges to steady state very fast and is more influenced by state and environment driven.

In addition, to test the proposed approach using Markov chains, each experimental trial was used to evaluate the prediction. However, the results did not show the good prediction with R^2 value equal to 25%.

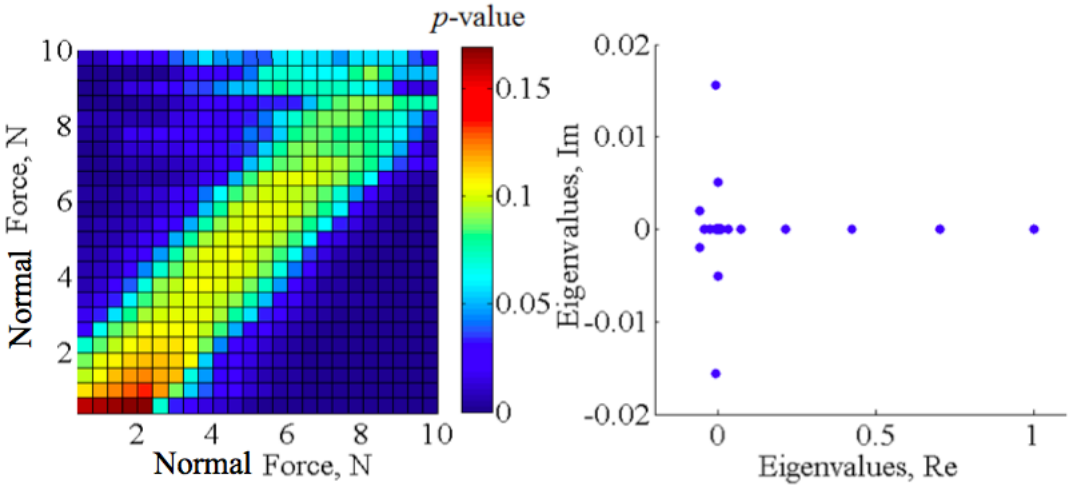

Figure 4.11: Transition probability matrix for applied normal force from human experiments, and eigenvalues for the same matrix.

4.4 Robotic Implementation of the Algorithm for Local Palpation

To validate whether the obtained reactive model of force modulations can be used during artificial palpation, experiments were performed using a robotic setup. The goal is to verify whether human-like palpation can be replicated during robotic palpation, and whether this type of artificial palpation can enhance the perception of embedded nodules. In particular, it is important to test the effectiveness of this approach for exploration of the nodules that are difficult to perceive, such as very small or deep nodules. For the prediction of the behaviour of the normal force, a second order predictive autoregressive model was used according to the findings of the human experiments.

4.4.1 Design of the System

Experimental Setup

To perform autonomous robotic palpation, a tactile probe was attached robotic arm Fanuc M-6iB with R-J3iB controller. The robot arm has 6 DoF and $\pm$ 0.08 mm repeatability of the motion. The control of the robot arm was implemented in the tool space using position control. The tactile probe has a spherical indenter 8 mm in diameter. The position of the probe is measured from the position of the end effector of the robot. A commercially available force and torque sensor NANO17 (ATI industrial automation, force resolution 1/320 N) was used to measure applied forces during probing. The probe is positioned on the surface of the silicone in the desired location before the palpation. The maximum possible indentation depth of the probe is 6 mm. The palpation algorithm autonomously controls the modulation of the applied normal force, but not the indentation depth. Therefore, this safety threshold is needed to avoid breakage

of the tissue or of the probe. Fig. 4.12 displays the arrangements of the experiments.

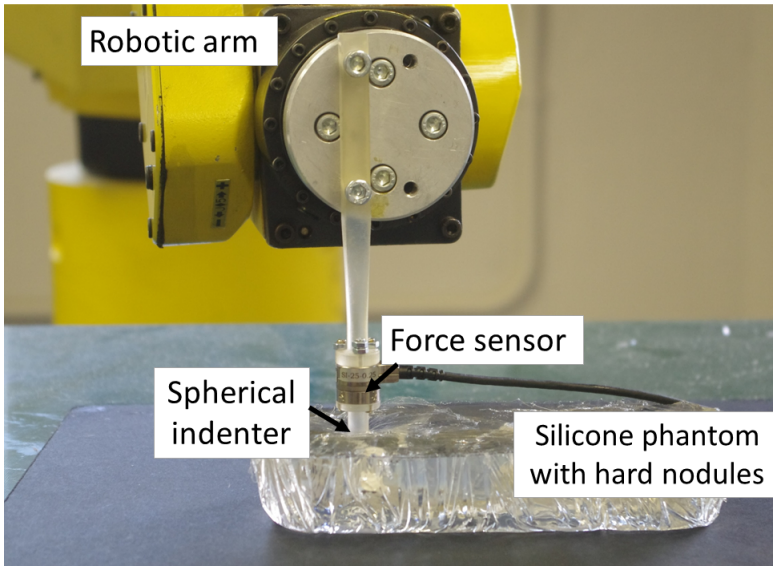

Figure 4.12: Experimental setup to validate autonomous palpation based on force modulation strategy

Design of Validation Experiments

The target of the validation experiments is to determine whether the outlined mathematical model of human behaviour can be implemented in robotic applications. It is required to compare the performance of the proposed force-based modulation strategy with simple indentation-based or passive palpation, such as in [55], when the stiffness is measured after the indentation of the probe on soft tissue.

The Young's or Elastic modulus is used to evaluate the perceived stiffness values during the autonomous palpation. It is reported [125] that for a spherical indentation tip and a small indentation depth, the Young's modulus of soft tissue can be calculated as follows:

$$E = \frac{3f(1+v)}{8d_{in}\sqrt{rd_{in}}} \tag{4.4}$$

where, E is the Young's modulus, v is the Poisson's ratio, f is the normal interaction force, r is the radius of the indenter, and d_{in} is the indentation depth. Poisson's ratio for the assumed incompressible soft tissue is 0.5.

For this experiment silicone phantoms with hard nodules of different diameters are used. Similarly to studies with human subjects the diameters were chosen to be 3, 6, 9, 12 and 15 mm, all embedded at a depth of 5 mm. Therefore, the robotic identification is performed both for nodules that can be difficult for humans to sense and for those that are easier to perceive. In addition, to evaluate perception between harder areas and soft uniform environment, the stiffness of the location with no nodule is evaluated as well.

First, it is required to obtain the stiffness of each test location during static probing. The probe is indented 5 mm down into the chosen location on the silicone phantom. The force is measured at this point and the corresponding stiffness is calculated. This measurement can be called indentation-based stiffness. These stiffness values are used to validate the performance of the proposed autonomous palpation.

In the second stage of the experimental studies, autonomous palpation is performed on the same areas, that is, on five nodules and on empty locations. Five trials were performed for each separate location. This type of behaviour is based on human tactile demonstrations and is formulated with the help of an AR model.

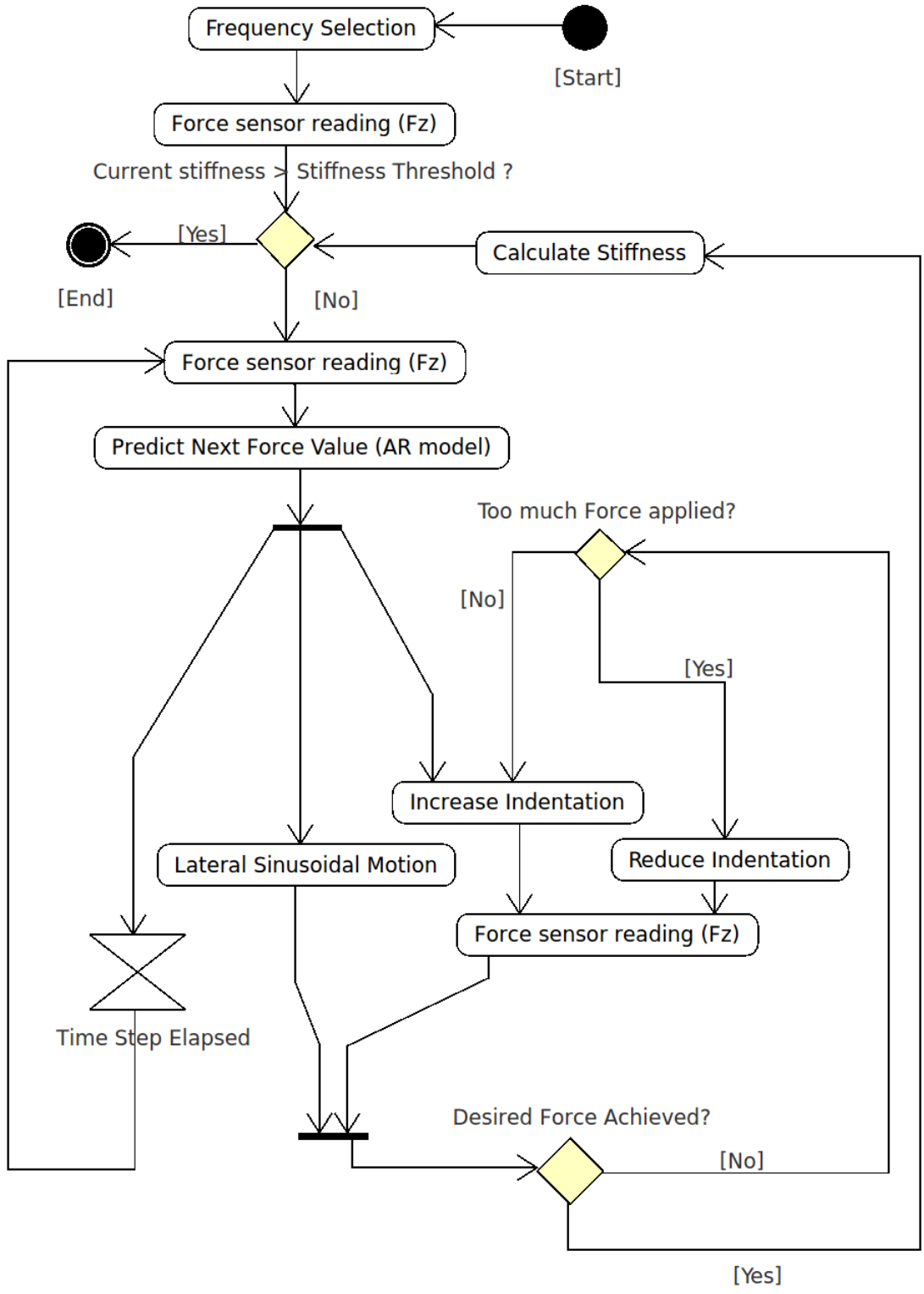

Figure 4.13: Algorithm of validation studies for robotic palpation.

Control Algorithm

The design of the control algorithm for autonomous palpation was based on the proposed experimental design. The flowchart of the autonomous palpation algorithm is displayed in Fig. 4.13. The initialisation of the system is implemented at the first steps of the algorithm. Initially, the frequency of the whole system is selected based on the empirical evaluation and set to 120 ms. This is the time allowed to achieve the required force given by the autoregressive predictor. Another constituent parameter of the system is the selection of stiffness threshold. This is the value obtained during indentation-based stiffness measurement and is used as a termination and assessment criteria for the system.

The first force readings are used to initialize the second order AR model. They are recorded for two indentation steps, each 0.25 mm deep. The initialization stage is crucial for correct execution of the palpation as the AR model requires two input parameters. Subsequently, the system enters the palpation loop. Two types of motions are performed iteratively: lateral sinusoidal motion and normal motion. Lateral movement creates the sinusoidal modulation of lateral force according to human studies, with the frequency 1.8 Hz. The range of the motion is 2 mm in order to correspond to the desired frequency. Normal motion is generated according to the desired force that is defined by the AR model.

In each iteration, the system reads force measurements according to the current position of the probe; predicts a desired force, using the AR model; and translates the force into position. This translation is performed via incremental or decremental indentations of 0.25 mm in order to match the perceived force with the desired force within a tolerance of 0.01 N. If the desired force is not achieved within the given time limit

(120 ms), current force value is fed into AR model for the next prediction. At the end of each iteration the stiffness is evaluated according to Eq. 4.4. As soon as the value (threshold set by indentation-based palpation) is achieved, the autonomous palpation continues for 30 seconds to observe the variation of the stiffness dynamics.

4.4.2 Analysis of Stiffness Measurement for Autonomous Robotic Palpation

The results of stiffness measurement for autonomous robotic palpation for different sizes of nodules and for the location without a nodule are displayed on Fig. 4.14. These results demonstrate the modulation of stiffness caused by the variable dynamics of the probe during autonomous palpation (blue solid line). The obtained stiffness modulations are compared with the indentation based stiffness (red dashed line). It can be observed that the recorded stiffness oscillates around the value of indentation based stiffness. Thus, the motion of the probe generates dynamic gain of stiffness that can be used to enhance the perception. To understand the nature of such response and to validate whether the proposed model can enhance the stiffness perception, variance and magnitude of the signal should be considered.

Mean variance of measured stiffness during autonomous palpation is displayed on Fig. 4.15a). According to Wilcox rank test, there is a significant difference between silicone with no nodules and nodules of 12 and 15 mm ($p < 0.05$). Thus, temporal differentiation of the signal caused by the palpation behaviour can enhance the perception of hard nodules in case of high variability. In addition to variance of the stiffness measurement, it is important to see the difference between real stiffness magnitude (indentation based measurement) and enhanced magnitude from autonomous palpation (mean value). The values are represented on Fig. 4.15b). It can be observed that the difference is negative

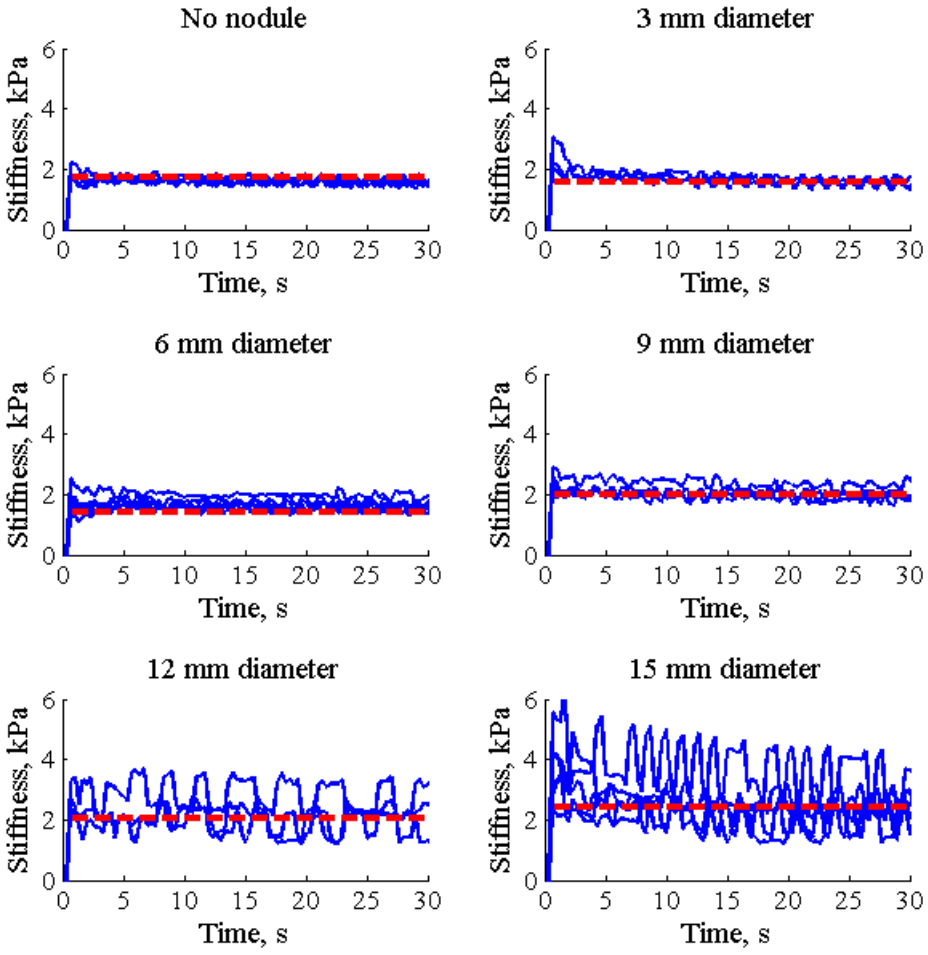

Figure 4.14: Stiffness measurements for indentation-based measurements (red dotted line) and autonomous palpation based on AR model (blue solid line) for silicone with no nodule, nodules of 3, 6, 9, 12 and 15 mm.

only in the case of soft silicone palpation with no nodule inside. Therefore, the stiffness calculated during autonomous exploration exceeds the stiffness threshold that was measured during the simple force indentation test. In other words, the static value of stiffness is enhanced with some dynamic gain that helps to perceive the environment.

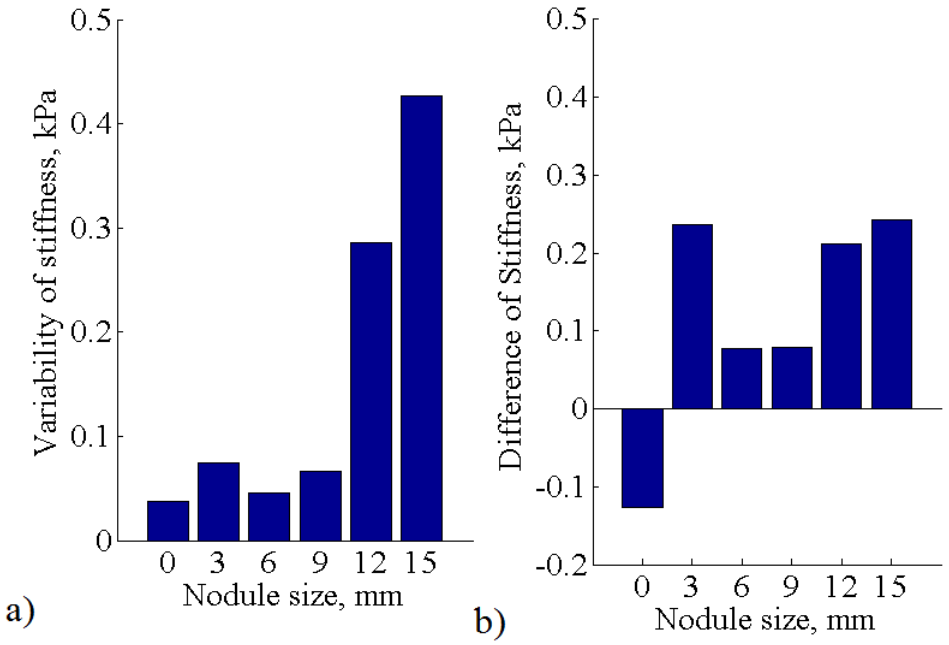

Figure 4.15: a) Variability of stiffness measurements for autonomous palpation; b) Difference of stiffness for autonomous palpation and indentation based measurement, for silicone with no nodule, nodules of 3, 6, 9, 12 and 15 mm.

Validation of the Components for Autonomous Palpation

A final step in the analysis of stiffness for autonomous palpation is the validation of two components of the system - sinusoidal modulation of lateral force and autoregressive modulation of normal force. Here it is interesting to establish whether whether it is really required to apply both sinusoidal variation of the lateral force and the change of normal force according to AR model during one single palpation. The analysis of human experiments described in Section 4.3.3 shows that there is a significant negative

correlation between the magnitude of lateral forces and the normal force. This means that there is a significant statistical relation between normal and lateral forces.

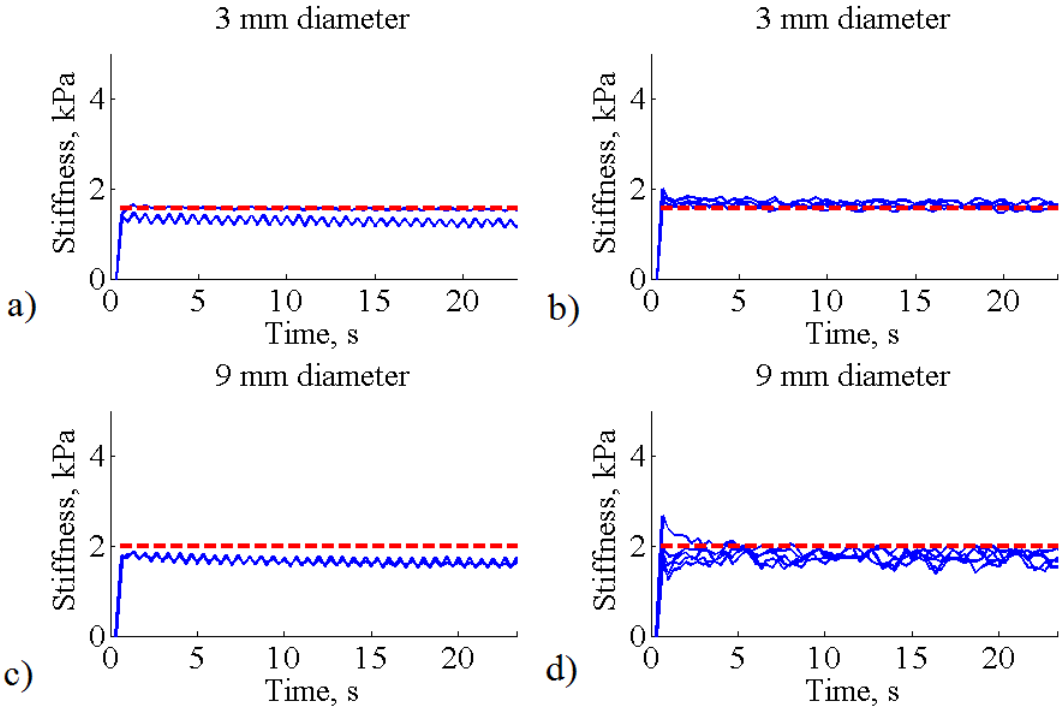

Figure 4.16: Stiffness for nodules with 3 mm (a) and (b); 9 mm diameter (c) and (d); stiffness for lateral force modulation only (a) and (c) and for AR based palpation with no lateral movement (b) and (d). Red dotted line shows stiffness measurements for indentation-based palpation

To validate this assumption, two behaviours are tested separately on two small nodules, 3 mm and 9 mm respectively, which might be difficult to detect. Lateral force modulation was performed with 5 mm indentation that corresponds to the depth of the embedded nodules.

Fig. 4.16 reflects the stiffness measurements of two separate behaviours of each nodule. It can be observed that modulation of lateral force only does not produce sufficient magnitude and has low variability (Fig. 4.17).

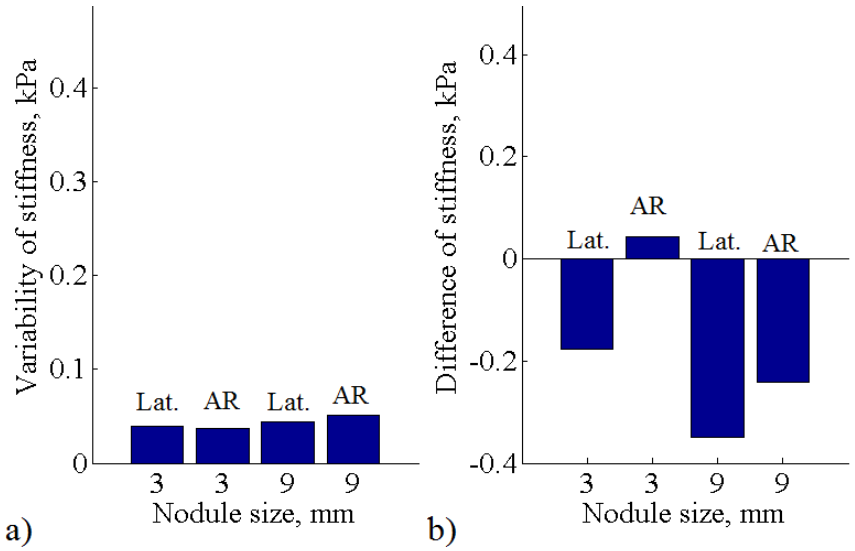

Figure 4.17: Diagram (a) shows the variability of stiffness measurements and diagram (b) shows the difference of stiffness for autonomous palpation and indentation based measurement for silicone with nodules of a diameter of 3 mm and 9 mm. Results from validation studies for lateral force modulation (Lat.) only and for AR based palpation with no lateral movement.

Fig. 4.18 displays the variability and difference of stiffness during autonomous palpation in respect to the indentation-based palpation for all robotic experiments. This figure is used to understand better the results obtained by the autonomous palpation, and to evaluate the separate components (lateral and normal modulations of forces), as well as to evaluate the performance of robotic palpation based on the distance to the zero point. Zero denotes the stiffness that was measured during indentation based palpation. The closer the point is from zero, the less difference is between autonomous palpation and indentation based stiffness. When the measurement is below the zero line threshold, then the performance is considered less efficient. The combination of high variability (from the mean stiffness) and high positive difference of stiffness (from the indentation-based palpation) demonstrates the effectiveness of autonomous robotic palpation.

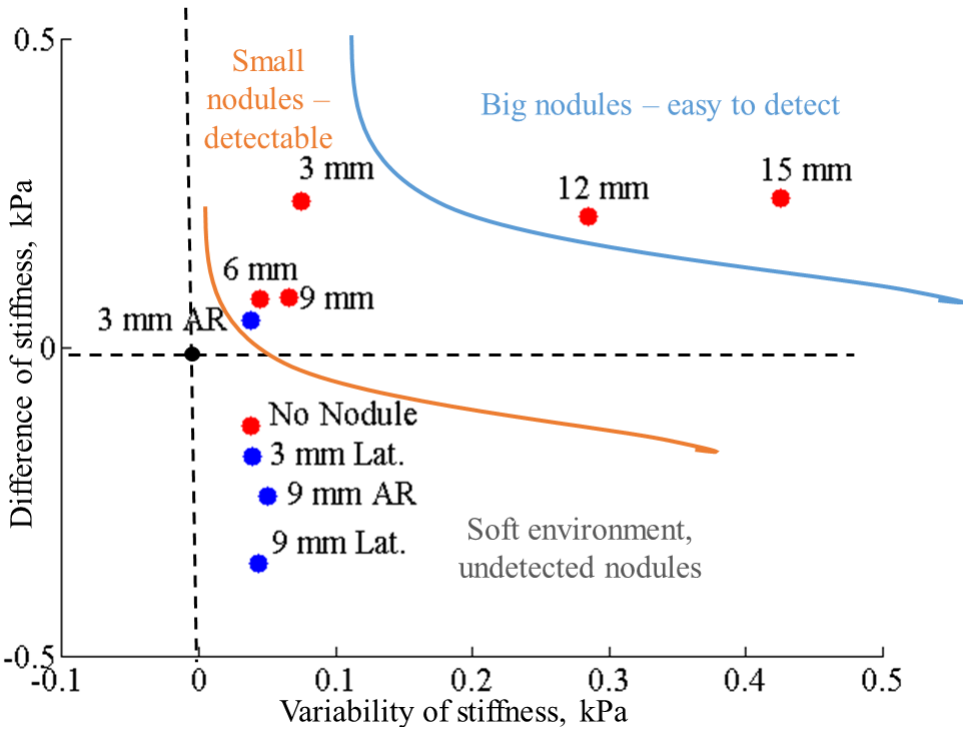

Figure 4.18: Variability and difference of stiffness of hard nodules and soft environment for robotic palpation. Red points show the results of autonomous palpation, blue points correspond to validation of lateral and normal motion respectively.

It can be seen that autonomous palpation with both lateral and normal (AR model) motion enhances the stiffness of all nodules tested during first experiments (red points). Therefore, the dynamical interaction with the tissue containing non-homogeneous areas increases the stiffness perception. Whereas, palpation of soft silicone without a nodule (red point "No nodule") does not lead to stiffness enhancement. The silicone at the point of palpation is homogeneous, and the indentation-based stiffness already produces correct estimation of the measurement.

The results obtained during the separate tests of normal AR and lateral sinusoidal motion (blue dots) support the effectiveness of the simultaneous use of both lateral and normal AR motion. Negative difference between indentation-based palpation and low

variability of stiffness does not indicate the presence of the nodules and can lead to misinterpretation by the user. The stiffness coefficients for small 3 mm nodule, palpated using normal AR motion only, are located above the zero point. This might suggest that in some cases lateral motion can be omitted. However, the palpation of the same nodule using both motion components produces better results with higher variability.

4.5 Conclusions

In this chapter modulation of applied force during palpation is studied. First, palpation behaviour as demonstrated by humans is explored and formulated. Then, to validate the concept, autonomous robotic palpation is performed. Robotic behaviour is created using recorded human demonstrations of tactile exploration. The advantage of force control strategy for robotic application is that it can be used with simple probing devices that are based on the indentation and force measurement principles. Therefore, there is no need to use mechanically complex frequency and vibration based tactile devices. The main conclusions for this chapter are listed below:

1. The analysis of human behaviour during palpation of hard nodules shows that the applied normal force can be modelled using second order AR model. In addition to this, humans perform sinusoidal modulation of lateral forces to enhance the perceived tactile information.

2. Autonomous palpation learned from human tactile demonstrations showed its effectiveness during exploration of hard nodules. The results have demonstrated that the applied behaviour enhances the perceived stiffness of hard nodules with the help of an increased magnitude as well as variance of the perceived signal.

Chapter 5

Localized Palpation Pattern

5.1 Introduction

Simulations on soft tissue palpation show that particular stress-velocity patterns during tissue probing lead to constructive dynamic interactions between the probe and the tissue, enhancing the detection and localization of hard nodules. In this chapter, the hypothesis that specific human palpation behaviours for localized palpation pattern (defined by the fingers' velocity, trajectory and exerted force) directly influence the result of manual palpation and diagnosis of soft tissue organs, is evaluated. Here, simulation studies involving human participants are used to establish open hypotheses on the interaction and influence of relevant behavioural palpation variables, such as finger trajectory, its velocity, and force exerted by fingers on the accuracy of detecting embedded nodules. This hypothesis is validated through the investigation of palpation strategies used by humans during straight unidirectional examination to detect hard nodules inside silicone phantoms and ex-vivo porcine organs. In addition, experiments

on remote palpation with the help of tele-manipulation setup are carried out.

The objective of this chapter is to test several probing behavioural hypotheses to identify the most effective manual palpation strategies for the localization of tumours in soft tissue during straight unidirectional movements. Based on the relevant literature, and the results obtained in Chapter 3 two open hypotheses about the characteristics of manual palpation are tested to understand applied strategies to detect and localize hard formations, such as nodules in soft tissue: 1 the palpation speed influences the correct localization of an embedded hard nodule; 2) the localization and detection rate of nodules can vary depending on the palpation force and velocity.

This chapter is organised as follows: first, the methodology is presented; then, the ways of investigating localized manual palpation techniques is presented using: 1) unrestricted manual palpation to extract the behaviours that are used for examination of smaller areas, and 2) finite element analysis to outline the above mentioned hypothesis. Thus, assessment of localized unidirectional palpation techniques is carried out, analysing the impact of force and velocity. Finally, the validation studies are performed with the help of FE simulations and remote tele-manipulated palpation.

5.2 Methodology

5.2.1 Manual Palpation Studies

The experimental arrangement (Fig. 5.1) was designed to detect the finger pressure, trajectory and velocity, thus allowing the main characteristics of the finger movement to be recorded. The force values of the applied pressure were measured with a 6

degrees-of-freedom sensor force-torque sensor (Mini 40, ATI industrial automation), with a force sensing range of ± 10 N in X and Y direction, ± 30 N in Z direction and ± 0.5 Nm for torque readings; normal force resolution is 0.01 N. The sensor was mounted under a base plate, supporting the examined target material (i.e. the silicone phantom or the animal organ). To reduce the effect of friction the surface of the sample tissue was lubricated (*Pharmaceuticals Intrasound Gel*).

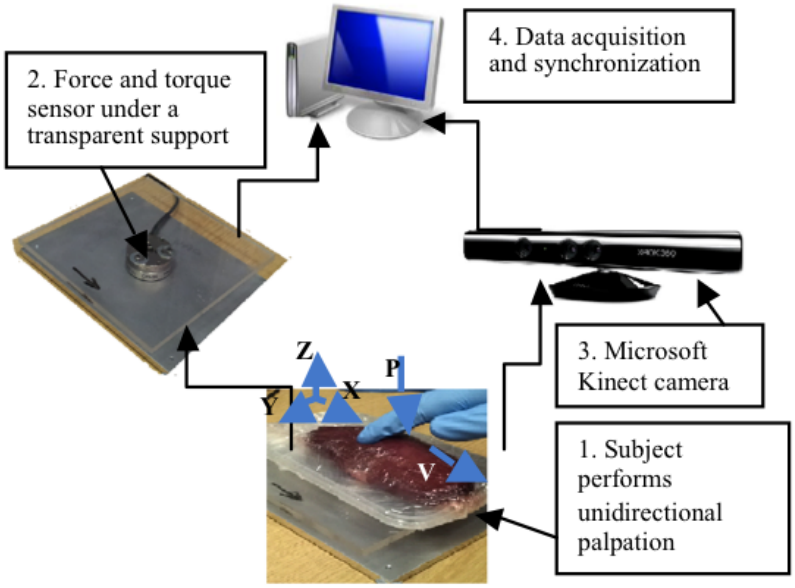

Figure 5.1: Experimental setup to measure position and applied force during manual palpation.

A three-dimensional vision system (Microsoft Kinect camera system) was used to record the trajectories of the finger during the palpation tests. The Kinect system was equipped with a depth sensor and a video camera (640×480 pixel resolution, image acquisition 30 fps). The OpenCV package for Microsoft Visual C was used to track the three-dimensional movements of a subject's hand while performing palpation. Spatial position readings were recorded and used to obtain the magnitude of the finger's tangential velocity. Evaluation tests were carried out to check the measurement accuracy

of the camera. The value of position accuracy depends on the velocity of the moving object, in this case, the finger. Therefore, to test the accuracy of the Kinect system, the mean velocity of palpation was applied. First, the hand position was recorded with the Kinect-based system, using a hand-tracking algorithm. Concurrently, the trajectory of the hand was recorded using stereovision (two separate cameras), and the position was obtained from a coloured marker on the finger using the MATLAB Computer Vision Toolbox. The two-dimensional position values of the marker on the moving finger were analysed from each camera separately; then the three-dimensional position of the marker in space was reconstructed. Comparing the obtained three-dimensional values from the Kinect sensor and the stereovision system, the position accuracy for the Kinect camera was found to be 1-2 mm. This value satisfies the goal of the experiment which is to understand the trends of the dynamics of the motion.

5.2.2 Finite Element (FE) Simulations

FE analysis is the first step in the study of the patterns of localized manual palpation. Simulations can promote the understanding of the stress responses experienced by the soft tissue during tactile examination [126]. The detection rate of hard nodules, an important feature of manual palpation is directly related to the magnitude of stress applied to the contact area with a finger. The higher the force per unit area is applied, the more stress is induced on that area. The analysis presented in this section will be used to explain the behavioural patterns of manual palpation. The process of unidirectional one-finger manual palpation over a silicone phantom was simulated in an FE modelling environment. Validation experiments on manual palpation were used to obtain the input parameters, such as the velocity and force exerted by the finger. To understand the impact of palpation behaviour, these parameters were varied during our

simulation study.

FE simulations were conducted in ABAQUS 6.10. The silicone phantom was modelled based on the studies described in [121] - a non-linear, isotropic, incompressible, and hyperelastic Arruda-Boyce model was used. The silicone phantom was modelled as a rectangular cuboid with dimensions $50 \times 50 \times 30$ mm ^{3}. The element size of the mesh of the FE model was 1 mm, using elements of quadrilateral type. The diameter of the embedded spherical nodule was set to 10 mm and its depth at 2 mm, as shown in the experimental studies presented in Section 5.4. The fingertip contact was modelled as a discretely rigid (undeformable) sphere with 20 mm diameter. Based on validation simulations, it was found that the rigid sphere can be modelled with 20 mm diameter. The contact between the soft tissue and the indenting body was modelled as friction-less, assuming a perfectly lubricated surface. At the start of all simulations, the soft tissue was indented by 3 mm, based on the initial indentation used by subjects during palpation experiments.

For demonstration purposes, Fig. 5.2 shows the FE simulations with the deformation at the contact point above the nodule; in the shown example, the tangential velocity decreases while the normal force decreases.

5.2.3 Tele-manipulation Setup for Validation Studies

The tele-manipulation setup was developed in collaboration with Dr. Min Li and Dr. Vahid Aminazdeh in King's College London. The setup was used to validate the results of force-velocity modulation strategies, as well as during experimental studies in Chapter 6.

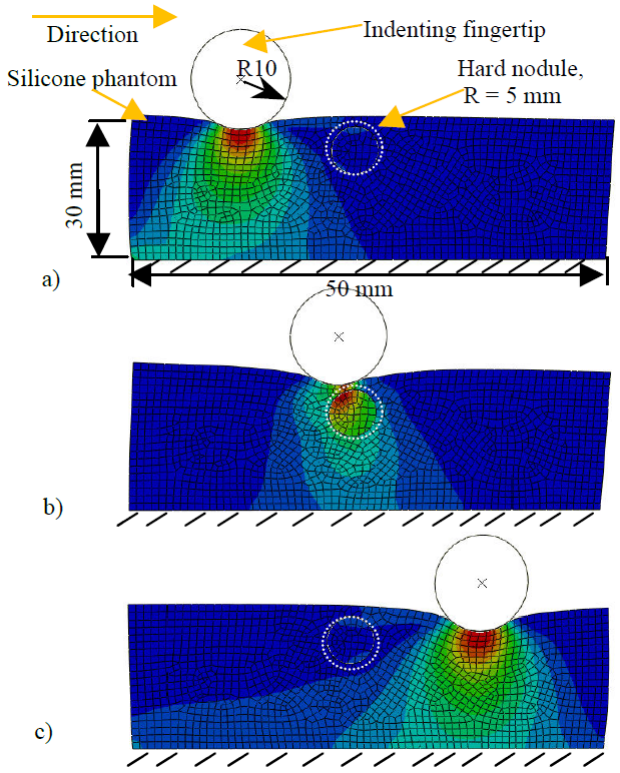

Figure 5.2: FE simulation of stress in the silicone phantom indented with a fingertip (diameter 20 mm) above the nodule location (diameter 10 mm) for the location above the nodule. Here, the tangential velocity and the normal force are decreasing during the palpation movement.

Main Components

Fig. 5.3 shows the arrangement of the setup. A user implements the position control of the robot arm (Fanuc M-6iB) with the help of a haptic device (PHANTOM Omni, Sensable). A sliding tactile probe with a spherical indenter (6 mm diameter), attached to the end effector of the robot, was used to measure force feedback from the phantom tissue. The stylus of the haptic device is moved by a user to control the desired position of the robotic probe. The displacement of tip of the stylus corresponds to the displacement of the spherical indenter of the robotic probe. The scaling factor of four was applied for the displacement of the haptic device the convenience of a user. The

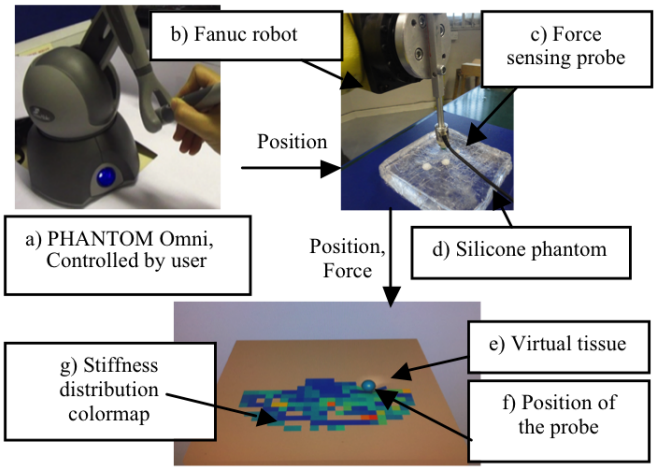

Figure 5.3: Tele-manipulator setup: a) Haptic device PHANTOM Omni (master) is used to control the position; b) Fanuc robot (slave) is following the trajectory; c) Force sensing probe is scanning the silicone phantom (d); e) Virtual tissue is displayed on the computer monitor; f) Position of the probe is displayed in real time; g) Stiffness distribution colour map is generated using force and indentation depth data.

robot arm acted as a slave and repeated the movements of the haptic device. The control of the robot was implemented in the tool coordinate system using position control. Then the position of the probe was displayed on the monitor in the virtual environment in real-time using the position displacement of the robot. The pointer on the virtual model of as silicone phantom moved following the trajectory of the robot and showed the position of the probe in real-time. Depending on the depth of the indentation, the deformation of the silicone phantom was displayed in the model. A force / torque 6 DOF sensor Nano17 was employed as a sensing element integrated at the tip of the robotic probe to measure normal and tangential forces from the silicone phantom. In order to reduce the effect of friction the surface of the phantom was lubricated. The obtained forces were used to calculate the measured stiffness, as well as for the display of the visual stiffness information for the user, as it is described below.

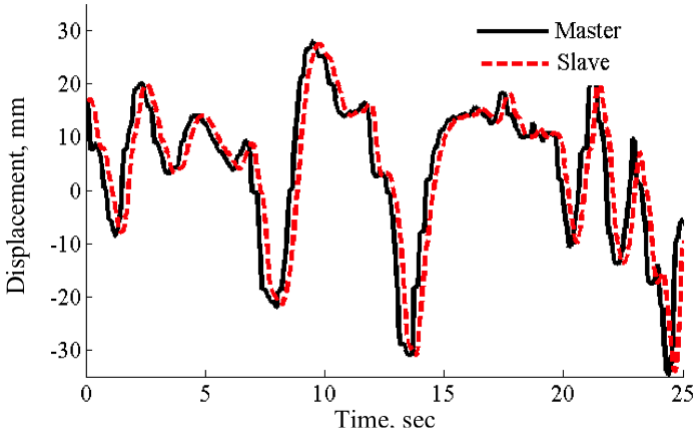

Figure 5.4: Trajectory in tangential direction for tele-manipulation setup: solid line shows the movements of the master device, and the dashed line displays the trajectory of the slave.

The accuracy of the position tracking for master-slave communication is 0.2 mm. Fig. 5.4 shows the trajectories of the haptic device and the end effecter of the robot arm. The mean delay of the slave trajectory for the changed direction of movement is 0.5 sec with standard deviation of 0.04 sec. The frequency of communication between master and slave devices is 21 Hz.

Stiffness Feedback for Tele-manipulation Setup

The obtained force information from the silicone phantom is combined with the normal displacement data in order to calculate the stiffness in real time, which is defined as the Elastic or Young's modulus in (4.4).

The operator receives both visual and haptic feedback in real-time to enhance the perception of stiffness. Haptic feedback (force) is exerted via a haptic device in three dimensions during palpation of a target object. Three-dimensional force feedback al-

lows the display of not only normal force but also tangential dragging forces.

Visual coloured stiffness information of the Young's modulus is represented on a virtual model of an object, which is generated before the palpation task. The colour which changes from dark blue to red represents the magnitude of stiffness; displayed stiffness values which are relative to the previous measurements. The colour map is being constantly updated as the range of stiffness changes.

5.3 Manual Palpation Strategies

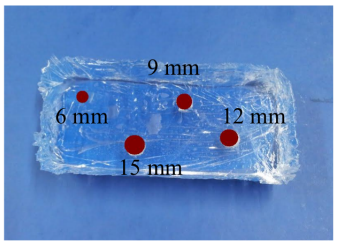

Figure 5.5: Silicone phantom tissue with the locations of embedded hard nodules used for evaluation palpation tests.

Previous clinical studies on manual soft-tissue examination behaviours for different organs [127, 128] suggest that patterns of finger movements influence the effectiveness of detecting hard nodules in soft tissue. However, there is no fundamental evidence supporting the argument that temporal modulation patterns of movement variables play a role during palpation. First, validation palpation tests were carried out to understand the possible influence of variable palpation behaviour on the process of the localization of hard nodules. This test is designed to analyse the strategies and evaluate the velocities, trajectories, and palpation forces that humans apply to detect hard inclusions. The subjects were first asked to apply "unrestricted" palpation, i.e. to palpate a phantom tissue with one finger in an unprescribed and unconstrained way with the aim of detecting embedded nodules. One-finger palpation is used to create a meaningful comparison with

artificial palpation approaches involving a single probe during RMIS.

A total of twenty subjects participated in these experimental studies. In the study group, ten of the participants were certified experts in palpation techniques with at least five years of surgical experience, more specifically, they were were gynaecologists accredited by the Royal College of Obstetricians and Gynaecologists (London). The remaining subjects were considered novices with regards to soft-tissue palpation.

The first silicone phantom used for evaluation studies ($130 \times 85 \times 30$ mm^3), Fig. 5.5, contained four nodules of different diameters - 15, 12, 9 and 6 mm - and were all embedded 9 mm from the surface. This particular depth was chosen to raise the level of difficulty in detecting the nodules.

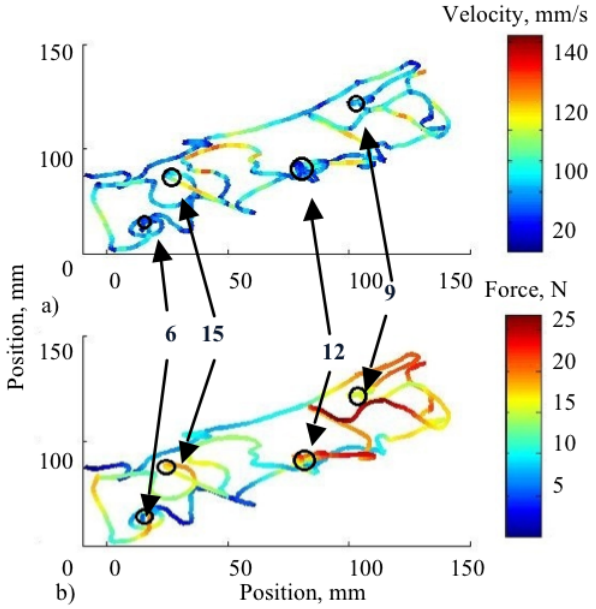

Figure 5.6: Representative example of palpation path over a phantom tissue with four embedded nodules (diameters in mm marked with arrows): a) modulation of velocity magnitude, b) modulation of applied finger pressure.

5.3.1 Results of Validation Studies

As part of the analysis, it is interesting to establish whether there is a correlation between the palpation variables (force and velocity) during hard nodule localization, based on results from validation palpation studies. To understand the mechanisms and behaviours used by subjects to obtain explicit information about the properties of the embedded nodule, the experiments on "unrestricted" one-finger palpation were examined. Fig. 5.6 demonstrates the distribution of palpation velocity and applied finger pressure over the phantom organ. Naturally, palpation parameters are variable and are based on the judgement of the subject. However, one can notice dependencies between applied force and velocity as well as a certain type of behaviour applied to the tissue at locations above the nodules. However, it is not possible to draw any conclusions about the impact of palpation force and velocity, based solely on the representation of the parameters' magnitudes.

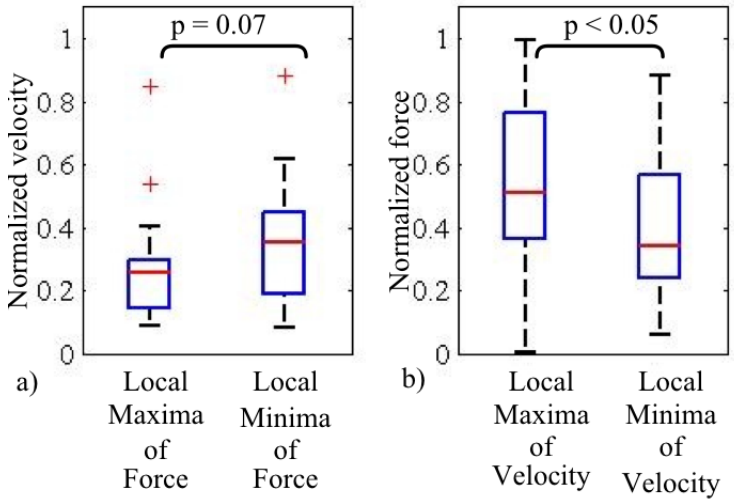

Figure 5.7: Distributions of a) normalised force magnitude and b) normalised velocity magnitude; the y-axis shows the local minima (1) and local maxima (2) peaks of force and velocity measurements, respectively.

To observe the cross-modulations of applied pressure and velocity, the local extrema of each measurement (force and velocity) and the associated concurrent values of the other measurement (velocity and force) were investigated. Local extrema in this case are considered the local maxima and local minima of force or velocity magnitude, and are found using a second derivative test. Fig. 5.7 shows the distribution of force and velocity for the local maxima and minima of the other measurement. The presented data are separately normalized with regards to the maximum value of each variable. The general trend is for velocities to increase in response to the application of higher forces. The velocity magnitude Fig. 5.7a does not vary significantly for maximum and minimum force. In addition, according to the two-way t-test there is no significant difference between the velocity at local minima and that at local maxima of force pressure ($p > 0.07$). However, the force values which correspond to the extrema values of velocity (Fig. 5.7b) belong to two different distributions ($p < 0.05$). The force magnitude tends to decrease for higher velocities, but shows a large deviation. These observations demonstrate that to explore a soft environment and to locate some hard inclusions in an efficient way one applies variable examination behaviours. However, to understand the characteristics of manual palpation one needs to examine the modulations of force and velocity in the vicinity of a buried nodule. For this purpose, FE simulations were carried out using force and velocity parameters, obtained during evaluation palpation studies, followed by additional palpation experiments that are focused on unidirectional manual palpation.

5.3.2 Finite Element Simulations

To understand the possible combination of force-velocity modulations during palpation, four types of palpation behaviours in the vicinity of a hard nodule were simulated:

a) decreasing tangential velocity (from 100 mm/s to 50 mm/s) whilst decreasing normal force (from 15 N to 8 N); b) increasing tangential velocity (from 50 mm/s to 100 mm/s) whilst decreasing normal force (from 15 N to 8 N); c) constant tangential velocity (75 mm/s) and decreasing normal force (from 15 N to 8 N); and d) no modulation in force (12 N) and velocity (75 mm/s), that is both variables remain constant whilst moving across the nodule. FE simulations were designed according to the methodology that is described in Section 5.2.2.

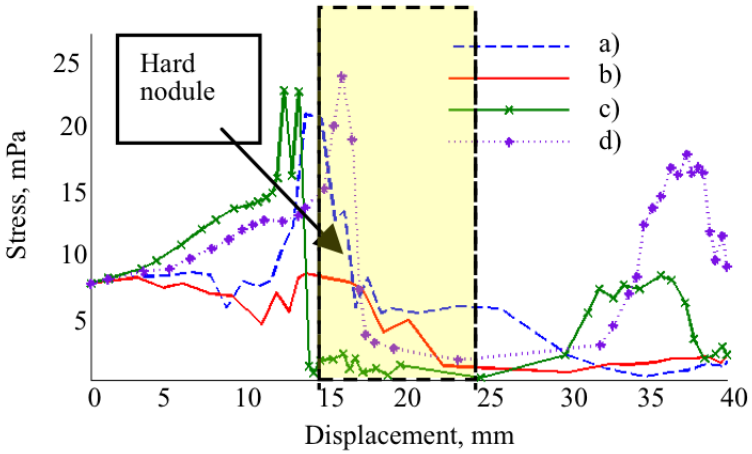

Figure 5.8: FE simulation of stress for different palpation strategies: a) increased velocity and decreased force; b) decreased velocity and decreased force; c) constant velocity and decreased force; d) constant velocity and force.

The results of the simulations with hard nodule buried 2 mm from the surface are shown in Fig 5.8. One can observe that applied force-velocity modulations cause different stress responses in the area around the hard nodule. The decrease of the stress magnitude can be observed after the nodule location has been reached. The responses from the simulations c) and d) show some peaks in the area of the nodule even after it has been detected. However, these peaks are not observed for the strategies shown un-

der a) and b). For the decreased velocity strategy (b) the stress distribution is relatively uniform and less intense. The result of simulation with increasing-velocity strategy (a) shows one high peak before the nodule, only.

Different palpation behaviour strategies, described by finger velocity and applied force, result in different stress responses, and can potentially lead to enhanced human tactile experiences. Therefore, taking into account the simulation results, it is required to test further the validity of the proposed hypotheses with the help of palpation studies.

5.4 Assessment of Localized Palpation Techniques and Data Analysis

Two sets of palpation tests involving human participants and a test rig with silicone phantoms were carried out to determine the features of manual palpation in the context of hard nodule localization during unidirectional movement. In the first test, manual palpation strategies to detect hard embodiments within the silicone phantoms were studied. The impact of the velocity of the subject's finger traversing over the tissue surface was recorded and examined during the second test.

5.4.1 Strategies to Detect Hard Embodiments

Experimental Protocol

In order to further understand what kind of behaviour is used particularly for nodule localization, the recordings of movements of the finger when positioned in the vicinity of the buried nodules are investigated. During this test, subjects were asked to palpate

a silicone phantom block (100 $\times$ 100 $\times$ 30 mm^3) in a linear unidirectional way in order to sense three hard inclusions, 9.4 $\pm$ 0.8 mm in diameter, along a pre-defined path (Fig. 5.9). According to Classification of Malignant Tumours (TNM), the T1 stage tumours vary from 0.5 mm to 20 mm in size. The range of tumour sizes for TNM classification was modelled as a normal distribution (9.75 $\pm$ 1 mm) and then compared to the fabricated distribution. The distribution of the size of fabricated hard nodules was 9.4 $\pm$ 0.8 mm, which was not significantly different from that of the corresponding tumour nodules ($p > 0.7$ according to one way t-test). Each subject performed five trials. Hard nodules were embedded 30 mm apart at depths of 2 mm, 6 mm and 11 mm from the surface. The selected depths presented the subjects with easy, average and difficult localization tasks.

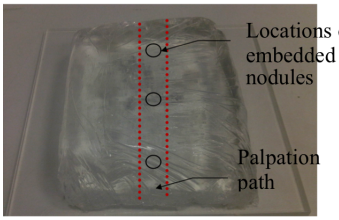

Figure 5.9: Silicone phantom sample used for unidirectional palpation with marked palpation path.

During evaluation palpation tests, subjects were encouraged and allowed to apply any desired palpation trajectories and use various patterns, such as those learnt and developed during their professional practice. To measure the variability of applied force and velocity when the finger is in the vicinity of a hard nodule, subjects were asked to palpate the tissue in a unidirectional fashion. This type of palpation is one of the possible patterns for soft tissue examination. For instance, the work in [129] validates the autonomous exploration of the soft tissue with a snake robot employing a circular pattern. However, this work focuses on a straight unidirectional palpation, as this pattern is the easiest for artificial palpation and enables fast and efficient coverage of the target area [55].

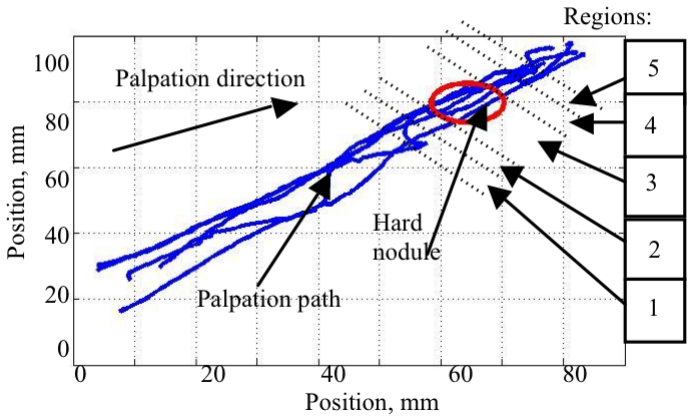

Figure 5.10: The trajectory of palpation path - several trials of one selected subject; area of interest around the third nodule (2 mm deep) is shown with five interval regions (1-5).

Results

Three nodules were placed along the palpation path for this test. Only the third nodule (buried at a depth of 2 mm deep from the surface) was sensed by all subjects. As the aim is to study the force and velocity modulations in the area of a detected hard nodule, the measurements from the region of the third nodule were analysed separately. To observe the modulations of palpation behaviour, the area around the nodule was separated into five interval regions. Fig. 5.10 demonstrates the location of the regions in respect to the location of the third nodule and displays the trajectory of the palpation path for one selected subject.

Each region represents a facet of the palpation movement in the vicinity of the nodule, (Fig. 5.10). The area around the nodule is divided up into regions as follows: the region closest to the nodule (Region 3) has a width of 10 mm, while the regions further

away from the nodule (1, 2, 4, and 5) have a width of 5 mm. An experimental evaluation of the variables, force and velocity, for each region shows that the variance of each variable does not exceed 5%. The chosen unidirectional palpation path allows arranging the regions sequentially, forcing the subjects to conduct the experiment along a straight line. However, the experimental study does not explore circular pattern based palpation, which would be more appropriate if the trajectory was following a curve or any other non-straight trajectory around a nodule, as it is often the case in the medical environment.

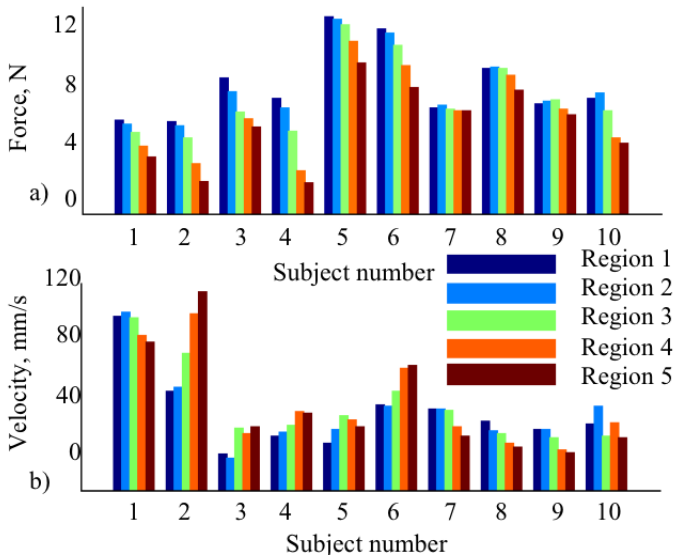

Figure 5.11: Force (a) and velocity (b) distribution trends across ten selected subjects: subjects 1 to 5 are experts, and subjects 6 to 10 are novices.

Fig. 5.11 shows the mean force and velocity for each region applied by ten selected subjects - five experts and five novices. To identify possible trends in force and velocity modulation, the effects of force and velocity magnitude on the particular location (region) in the area around the nodule and the influence of each individual subject were tested with the help of three-way ANOVA tests. The velocity computed based on the smoothed position profile was compared with the optimal estimate of the velocity us-

ing a Kalman filter to obtain the average velocity error in each region. The average velocity error was found to be 0.11 $\pm$ 0.79 mm/s. The result showed that the pressure applied by the finger (F(3.94) = 7.92, p $<$ 0.00001) depends on the distance between the finger tip and the location of the hard inclusion. The effect of velocity and the impact from each individual was not significant (F(3.94) = 0.37, p = 0.55 for force measurements and F(3.94) = 0.02, p = 0.9 for the influence of each subject). These results show that the modulation of finger pressure is consistent for all trials, when the finger is in the vicinity of a detected nodule. However, the insignificance of the velocity magnitude in this context may suggest that the modulation of velocity varies among individuals due to some difference in their palpation behaviour. Alternatively, the modulation of velocity may not be a significant factor to the detection of a nodule.

To check the presence of different behaviours of palpation force and velocity, a first-degree polynomial was fitted to the normalized mean values of force and velocity for each region (1 - 5). Fig. 5.12 confirms the statistical significance of force across all subjects and demonstrates the consistent decay of this variable. The velocity trends can only be observed when the fitted line is displayed on two separate plots, as shown in Fig. 5.13. One can observe that there are two behaviours of velocity strategy that either decreases or increases.

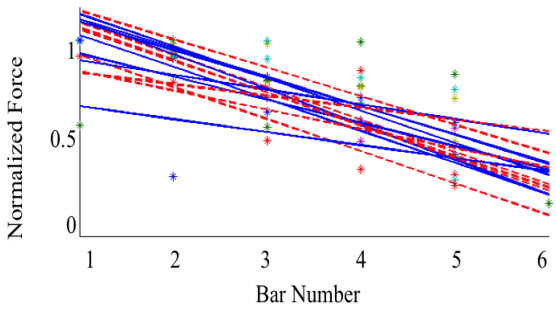

Figure 5.12: Distribution of force for each subject shown with data points for each bar; fitted lines show inclination of force (dotted red line - experts, solid blue line - novices).

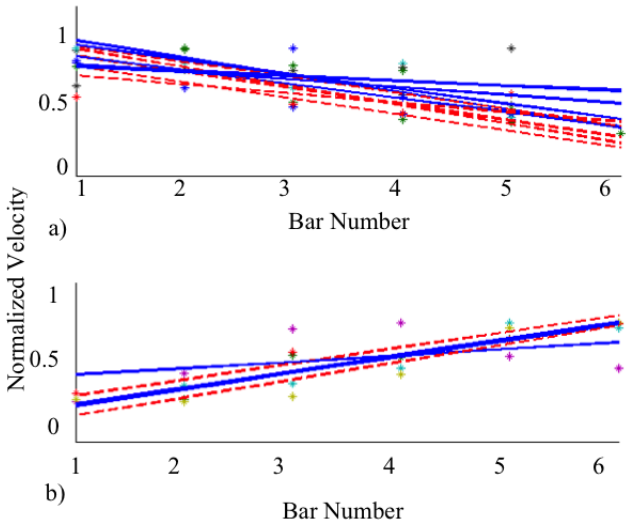

Figure 5.13: Distribution of force for each subject shown with data points for each bar, fitted lines show inclination of force (dotted red line - experts, solid blue line - novices).

In order to confirm the presence of two strategies in palpation over a hard nodule, the slope (gradient) of the polynomial fit of the force was plotted versus the slope of the corresponding velocity polynomial (Fig. 5.14). Two distinctive strategies were observed. It appears that 50 % of subjects have decreased both finger pressure and velocity while conducting an examination in the vicinity of the nodule. 30% of subjects have increased the velocity magnitude while at the same time decreasing the applied force. 20% of the subjects did not vary velocity and force significantly. The group of experts who participated in the studies performed at the same level as other subjects, i.e. showing similar behaviours like all other subjects.

To validate the statistical significance for separate behaviours with different variation of velocity, a three-way ANOVA test was conducted for two separate strategies, i.e. increasing velocity with decreasing force and decreasing velocity with decreasing force. The impact of both finger velocity ($F(4.00) = 9.16$, $p < 0.0001$) and finger force (F(4.0)

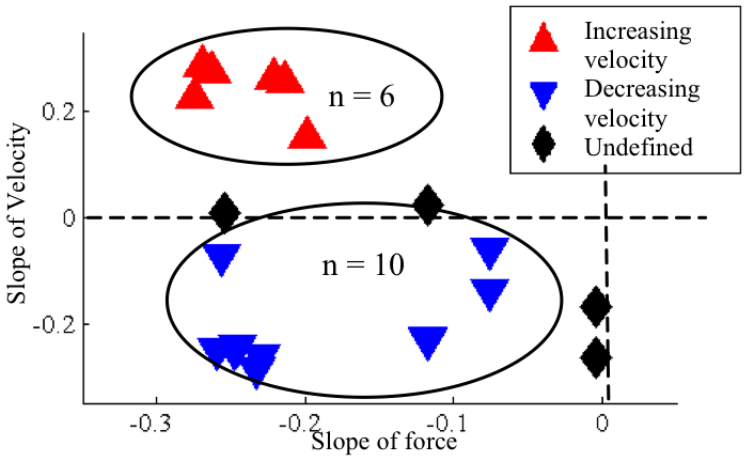

Figure 5.14: Slope of force versus slope of velocity for subjects: two distinctive strategies can be identified - increasing and decreasing velocity. Outlier results are classified as "undefined strategy".

= 4.83, p <0.01) in the vicinity of a nodule were significant for the strategy with decreasing velocity. Similar observations can be made for the strategy where the velocity increases: the impact of both velocity and force are significant for locations near the nodule (F(4.17) = 4.59, p <0.01) and (F(4.17) = 4.36, p <0.01). Thus, one can see that during a soft tissue examination and hard nodule probing, the finger palpation properties can be varied in two different ways. In particular, the subject either increases or decreases the finger velocity while, at the same time, reducing the applied pressure. In addition, the small group of subjects (20 %) does not apply any force-velocity modulation.

5.4.2 Impact of Traversing Velocity

Experimental Protocol

The second set of experimental studies for examination of localized palpation patterns was designed to evaluate the impact of the velocity of the subject's finger during palpation on the detection rate of hard nodules. To perform manual palpation of an organ sample in a way as close as possible to real organ palpation, subjects were asked first to localize embedded nodules during three sets of experiments, applying unidirectional palpation across the surface of a semi-spherical silicone phantom that was fabricated to match to the size of an average human kidney (length 120 mm, width 65 mm, depth 30 mm).

This was followed by three sets of experiments where unidirectional palpation was applied to an ex-vivo porcine kidney of average length 125 mm, width 80 mm and depth 30 mm. Hard nodules of 9.4 ± 0.8 mm in diameter were embedded at depths of 1 mm, 3 mm and 5 mm from the surface - (Fig. 5.15), in a such way that an average subject would be able to detect their presence. The nodules in the tissue sample were inserted through skew cut from the posterior part, and the depth was assessed using a needle test rod. Each experimental set had different applied palpation velocities, namely slow, natural and fast. "Natural" palpation velocity is defined as the speed of palpation that feels most comfortable to the subject. Consequently, slow

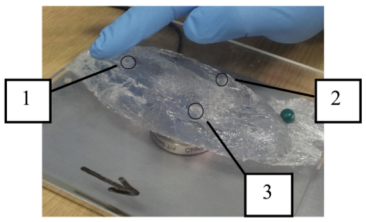

Figure 5.15: Silicone phantom sample for Test 2; embedded nodules are marked (1, 2, 3).

and fast traversing velocities were defined as velocities that are lower and higher than the natural velocity. The range of the velocity magnitude is different for each subject, and is discerned during an analysis. One of the aims of this study was to evaluate how the velocity range varies across trials and across subjects.

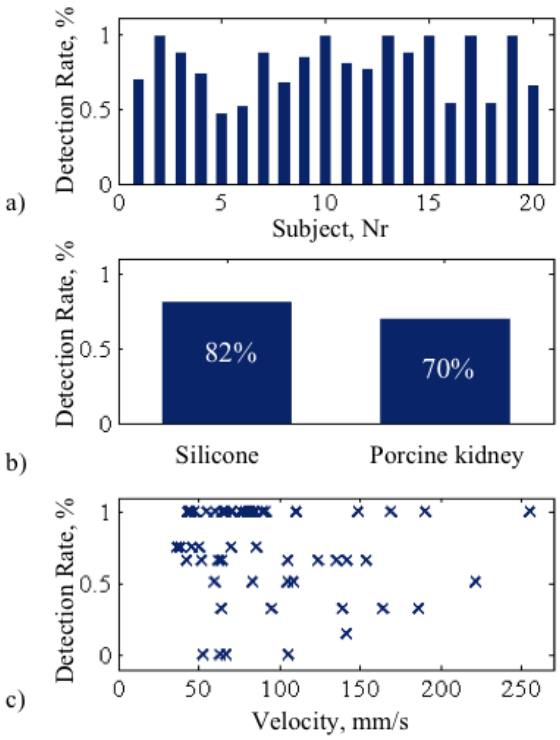

Figure 5.16: Summary of hard nodule detection rate for a) different subjects (novices: 1-10, and experts: 10-20), b) silicone and porcine kidney, c) velocity.

Results

In order to acquire a better understanding of the impact of the finger velocity on the detection of hard nodules, additional studies were carried out. Fig. 5.16 shows the summarized data for Test 2 which presents the influence of separate factors such as subject, palpation medium, and traversing velocity, with regards to the detection rate

of hard nodules. A three-way ANOVA test was carried out, to evaluate the importance of each separate palpation behavioural element and its influence on the detection rate. To compensate for the individual bias, a weight was applied on the detection rate of hard nodules in all sets of experiments for all subjects. The weight was calculated from the best performance of each subject with no false positives. We found that the type of palpation medium had a significant effect on the results ($F(3.99) = 6.23$, $p < 0.0001$) while on the other hand, the subject ($F(3.99) = 2.27$, $p = 0.14$) and the palpation velocity ($F(3.99) = 0.61$, $p = 0.44$) did not influence the detection rate of hard nodules. Therefore, it is important to emphasize the significance of choosing correctly a palpation technique for a given environment and of analysing the process of soft tissue examination taking into consideration the features of the target material.

To evaluate the impact of the traversing velocity for the silicone phantom a three-way ANOVA test was performed on the set of palpation cases. The group of subjects with a low level of palpation experience was studied first. Three factors influencing the detection rate were considered, namely subject sequence number, applied pressure and the magnitude of palpation velocity. The velocity had a significant effect on the detection rate ($F(4.17) = 3.14$, $p < 0.001$) while both force and subject sequence numbers - ($F(4.17) = 0.61$, $p > 0.3$) and ($F(4.17) = 1.01$, $p > 0.4$), respectively - had virtually no effect. Secondly, the same analysis was carried out for the group of experts. There, the impact of velocity was also found to be significant ($F(4.24) = 8.97$, $p < 0.00001$). In addition, experts have used variable finger pressure to detect hard nodules ($F(4.24) = 16.67$, $p < 0.00001$). This result confirms the importance of correctly choosing the traversing velocity and applied force. As the results have shown, the experts achieved a higher detection rate.

To understand how the magnitude of velocity influences the detection rate of hard nod-

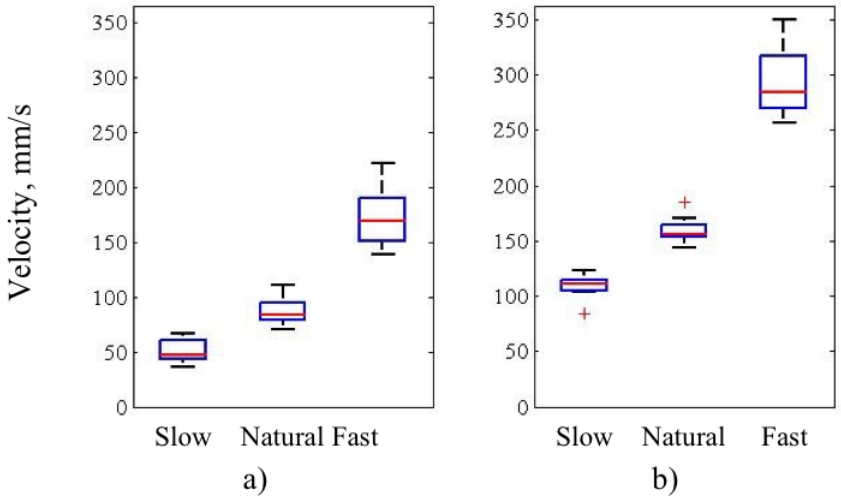

Figure 5.17: Clusters of velocity distribution for a) novices and b) experts.

ules, an analysis of different velocity magnitudes is carried out. In Test 2 three trials were performed using fast, natural and slow palpation velocities. The magnitudes of velocity were defined by the participants, based on their personal preference. Therefore, the values of the chosen palpation velocities for different subjects for the same trial (for instance, for natural velocity) are not the same. Thus, velocity data, which was defined experimentally, was divided into three groups based on magnitude. For this purpose, k-means clustering was used. The data for experts and novices was processed separately. The results of the velocity distribution of both participant groups for three clusters are presented in Fig. 5.17. Compared with the experimentally defined velocities, there was 100%, 50%, and 61% correlation for the group of novices and 75%, 38%, and 55% correlation for the group of experts with sets of fast, natural and slow magnitudes of velocities respectively.

To evaluate the impact of the velocity magnitude, the detection rate for each cluster for each group was calculated as shown in Table 5.1. It can be observed that the

velocity magnitude applied by the group of experts is higher. However, the results for the detection rate for each set of velocity are similar. These results demonstrate the importance of the correctly chosen velocity magnitude. According to the data, the highest detection rate of nodules for the silicone phantom is observed for slow palpation velocity.

Table 5.1: The Impact of Palpation Velocity for Experts and Novices

Cluster	*Experience*	*Detection Rate, %*	*Velocity magnitude, mm/s*
Slow	Novice	87	36 - 67
Natural	Novice	83	70 - 110
Fast	Novice	69	139 - 222
Slow	Expert	96	85 - 123
Natural	Expert	82	144 - 220
Fast	Expert	53	256 - 350

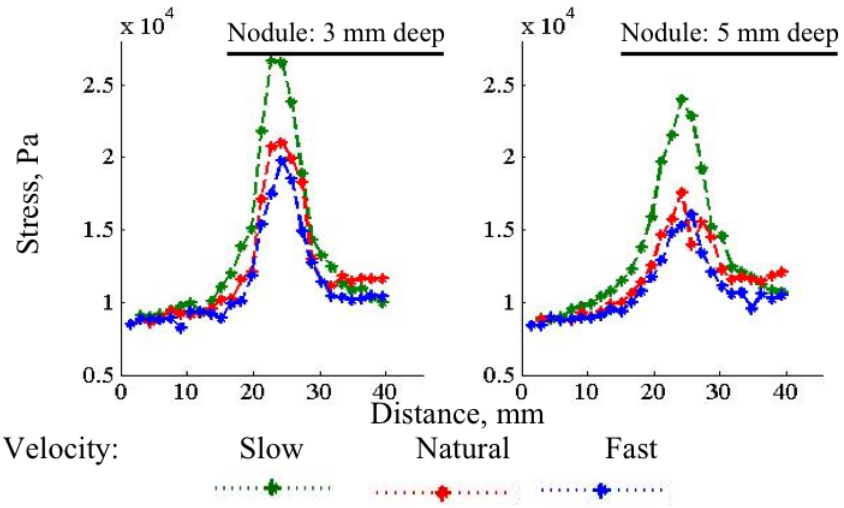

Figure 5.18: Stress distribution for different depths of nodules - 3 and 5 mm, (green - slow velocity, red - natural; blue - fast).

5.5 Validation of Results for Robotic Applications

5.5.1 Impact of Velocity

The experimental measurements of velocity magnitude are used in the FE simulations. The detection rate of a hard nodule depends on the stress magnitude in the target tissue. A subject senses the higher force in the unit area when the stress on the material is higher. Fig. 5.18 displays the stress magnitude for the indentation contact point for two different depths of the location of a hard nodule. As expected, a slower speed of palpation induces a higher magnitude of stress. A larger depth of the nodule leads to a smaller stress response from the area above it, especially for fast and natural velocity.

5.5.2 Impact of Force and Velocity Modulation for Tele-manipulated Examination

In order to understand the feedback forces from the soft tissue phantom perceived with the finger during manual examination or with a probe during artificial palpation from the silicone phantom subjects were asked to perform experiments with tele-manipulated palpation setup. For the experiment described in this section, subjects were given the following instructions. It was required to detect a hard nodule on the predefined palpation path, similarly to the experimental studies with subjects. The task was considered complete as soon as the nodule was detected. It is necessary to note that such instructions lead to the reduction of force after the nodule is detected, as is shown later. The results of forces recorded during tele-manipulation (path over the nodule, ten trials) are shown in Fig. 5.19 and Fig. 5.20. As expected, the feedback force profiles are different for each probing strategy and can provide information about the

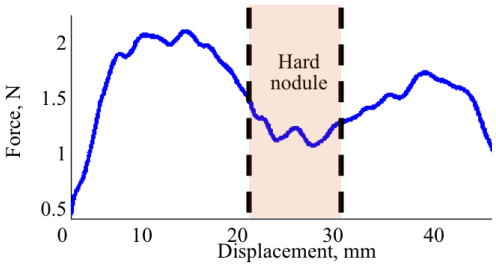

Figure 5.19: Force feedback sensed with probe based on decreasing velocity strategy.

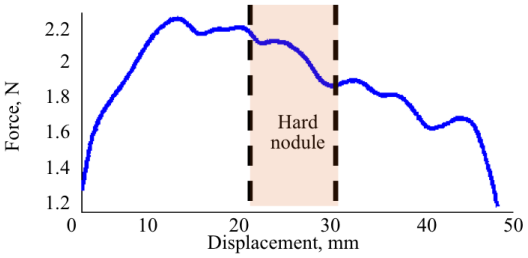

Figure 5.20: Force feedback sensed with probe based on increasing velocity strategy.

palpation behaviour, applied during each strategy. If the indentation depth of the probe is constant during examination, the areas of high stiffness (hard nodule) are denoted with increased force feedback. However, the indentation depth is not controlled for this experiment. Thus, force feedback for decreasing velocity (Fig. 5.19) has two peaks and a steep trough around the location of the nodule. This means the indentation depth above the nodule has reached a minimum. In other words, the probe has followed the shape of the nodule, while subjects were relying on kinaesthetic sensing, that is, on the location of the finger in space during palpation. This observation corresponds to the simulation shown in Fig. 5.8 b), as stress magnitude did not vary significantly around the location of the nodule. Assuming constant contact area, a subject receives higher feedback force as the stress of that area is higher: this allows for the comparison between force feedback detected by the tactile probe and stress magnitude from FE simulations.

The force profile, measured by the probe, for the increasing velocity strategy (Fig. 5.20) gradually decreases within the marked area. First, the peak is reached just before

the location of the nodule. The force drops along with the decrease of the velocity, i.e. when an inclusion is sensed. As discussed, the force feedback can be the determining factor for hard area localization if indentation is kept constant. Thus, as opposed to the first strategy, it is most likely that in this case the received force feedback is the determining factor for the localization of the hard nodule. The drop of the force can be explained by the fact that the location of the nodule is already detected. The simulation in Fig. 5.8 a) supports the results obtained during tele-manipulation, namely the stress magnitude has reached its peak before the nodule.

5.6 Summary and Conclusions

In this chapter two hypotheses are tested to understand the characteristics of manual palpation to localize hard nodules in soft tissues: 1) the speed of palpation influences the detection rate of hard nodules; and 2) force - velocity modulations during manual palpation influence the localization and detection rate of hard nodules.

The main conclusions of this chapter are presented below:

1. During random exploration of soft tissue humans use various modulations of force and velocity. Therefore, there are different ways that can be employed to augment and enhance the feedback from hard nodules.

2. Subjects that are unfamiliar with the techniques of manual palpation mostly use the modulation of velocity only to detect hard formations, as shown in Fig. 5.16; statistical evaluation has shown that the impact of exerted force is insignificant on the detection rate.

3. The expert subjects take advantage of both force and velocity. The analysis clearly shows two distinct strategies (Table 5.2) that are applied during finger-based palpation of soft materials that contain embedded hard inclusions.

4. For each strategy, FE simulations and validation experiments were carried on the tele-manipulation setup to support the experimental results. The state variables of the palpation strategies are summarized in Table 5.2.

Table 5.2: Possible determining factors that are used to detect the location of hard nodules

Strategy	**State variables with respect to the nodule location**		
	Velocity	*Pressure Applied*	*Most likely determining factor*
1	Decreasing	Decreasing	Kinesthetic feedback/Displacement
2	Increasing	Decreasing	Force Feedback

Chapter 6

Global Palpation Pattern

6.1 Introduction

During clinical organ examination, global movements are used to scan the whole surface of an organ, and then local movements are applied on locations of abnormal formations. This chapter discusses the application of global palpation pattern during remote examination of soft tissue. It studies the hypothesis that a manual palpation trajectory pattern can be used in the framework of a tele-manipulation setting and can provide efficient results to promote the detection of simulated abnormalities in the silicone phantom. The detection rate and the time consumed during remote palpation with manual palpation pattern is tested and compared with a user-defined pattern.

The global finger movement (GFM) manual palpation technique - is used with the aim of increasing palpation efficiency and accuracy by covering the whole surface of the organ. GFM reduces the risk of missing a suspicious formation and can provide general information about the state of the organ. In prostate examinations, GFM is performed

following four main different movements: U, L, V - shape, as well as straight line movement [115]. Clinical breast examinations (CBE) are usually performed with the following three patterns: concentric circles, radial spokes, and vertical stripes [130]. The pattern choice mainly depends on the preference and training of the practitioner. In general, a successful palpation should be performed in such a way that the chosen pattern completely covers the selected area in the shortest time possible.

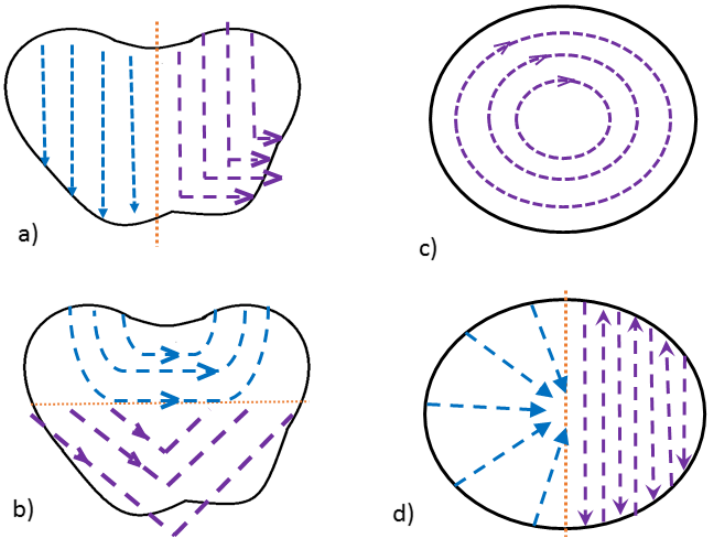

Figure 6.1: Global palpation patterns: a) Line pattern and L-shape pattern for prostate examination, b) U-shape and V-shape patterns for prostate examination; c) Concentric circles for breast examination; d) Radial spokes and vertical stripes for breast examination.

The above described shapes of patterns can be divided into two primitive movements - lines and curves. These primitives will be used as a base for the pattern during tele-manipulated palpation.

6.2 Methodology and Experimental Design

The experimental protocol is developed to study the hypothesis that application of palpation patterns during tele-manipulated examination of soft tissue can improve the efficiency of examination. The design of the tele-manipulation setup was described in Chapter 5.

To represent soft tissue with hard formations inside, the silicone phantom tissue ($120 \times 120 \times 30$ mm^3) with hard nodules was fabricated according to the standard approach used in this research, (Fig 6.2). Three nodules were embedded at a 5 mm depth from the surface and had diameters of 6, 8 and 10 mm respectively. Ten subjects participated

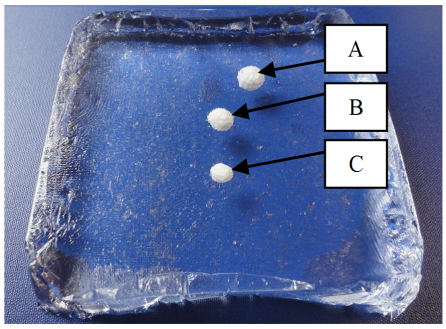

Figure 6.2: Silicone phantom sample ($120\times120\times30$ mm^3) with three embedded hard nodules: a) 10 mm in diameter, b) 8 mm and c) 6 mm.

in experimental studies and performed two tests on remote tele-manipulated palpation. Subjects, previously inexperienced in tele-manipulated palpation, were given time to familiarize themselves with the device, haptic and visual stiffness feedback. In addition, three practice runs on a silicone phantom with different locations of hard nodules were conducted. The number of embedded nodules was unknown to the subjects. There were no time restrictions imposed during the tests; subjects were only asked to report the time that the task was completed.

Test 1: This test was developed to evaluate the general performance of detecting nodules during tele-manipulated palpation. Subjects were asked to perform any type of pattern to scan the silicone phantom described above. The trajectories of the probe and measured forces were recorded on a log file.

Test 2: The second test was developed to establish whether the manual palpation trajectory pattern can be successfully applied during remote palpation. Generally, manual palpation is not standardized [131] and there are various techniques specific to a certain body part. Taking into account the relatively large surface area of the used silicone phantom sample, a clinical breast examination pattern is applied [132] that comprises two primitive movements - lines and curves (as described in Section 6.1). Participants were familiarised with the principles of manual palpation and asked to perform consequent scanning of the silicone combined with circular movements over suspicious areas, where a hard nodule might be located (Fig. 6.3). The orientation of the silicone phantom was changed for the second experiment. The palpation trajectory, detected force and a number of detected nodules were recorded. At the end of two trials, each subject was asked about their assessment of the remote palpation experience and of the efficiency of nodule detections in each trial.

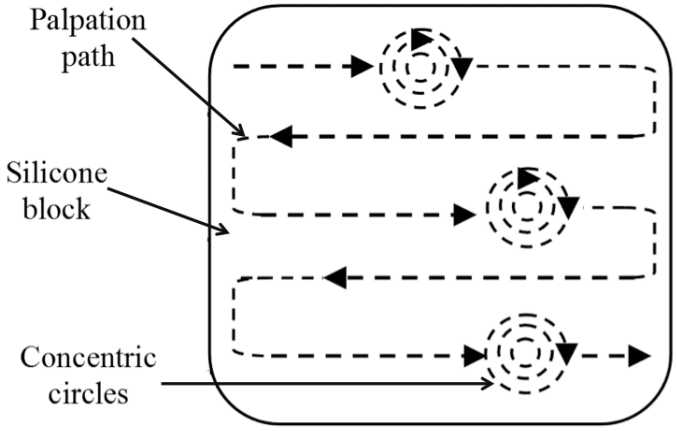

Figure 6.3: Schematic palpation trajectory pattern used in Test 2 to scan the whole surface of the target area with concentric circles applied in the areas of possible inclusions.

6.3 Results

6.3.1 Evaluation of Palpation Patterns

In order to determine whether the applied trajectory pattern for the second test corresponds to the desired pattern an analysis of applied movement was carried out. The trajectory of the probe in a lateral plane over a silicone phantom as performed by each subject in the second test was evaluated. It was observed that all ten subjects applied the circular patterns in the areas of possible nodules and followed the direction of the movement as prescribed.

Fig. 6.4 displays the sample trajectory of one selected subject for both tests. One can observe the unstructured movement used in the first test, followed by the applied pattern, which corresponds to the desired trajectory, during the second test. This participant spent 150 seconds to detect two nodules during the first test and 80 seconds to detect all the nodules during the second test. However, the circular motion applied in the second trial can be clearly observed only in two locations of hard nodules (nodules A and B) and is less obvious in the third nodule (nodule C). Not every participant has applied such random palpation trajectory for the first test. It was observed that two of the participants applied some circular motions in the palpation trajectory. This demonstrates the intuitiveness of the trajectory pattern that was used for the second test.

To demonstrate the visual feedback observed by the same participant, during the second test, Fig. 6.5 displays the stiffness distribution colour map, captured during the experiment. The biggest nodule A is marked with red, nodule B is orange, and the smallest nodule is reflected with yellow.

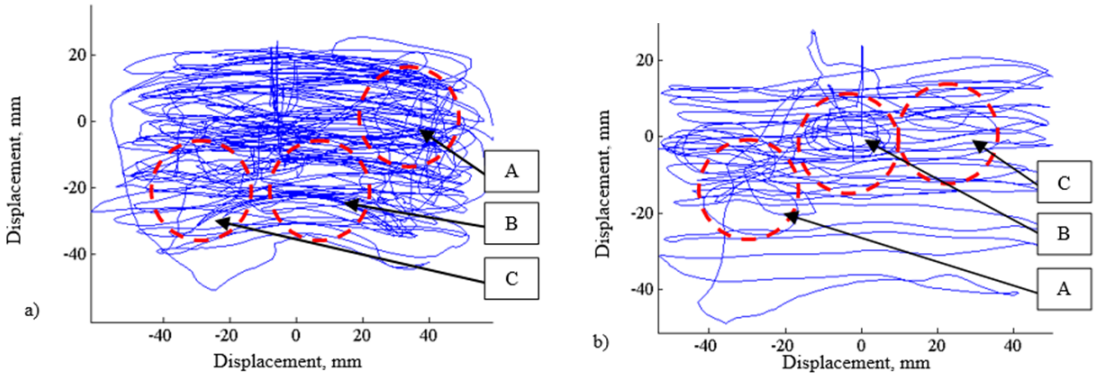

Figure 6.4: Trajectory of remote palpation for: a) unrestricted and unstructured user-defined movements - Test 1, and b) pre-defined pattern - Test 2; the orientation of the silicone phantoms is different in each of the two tests; the locations of hard nodules are marked A, B, C.

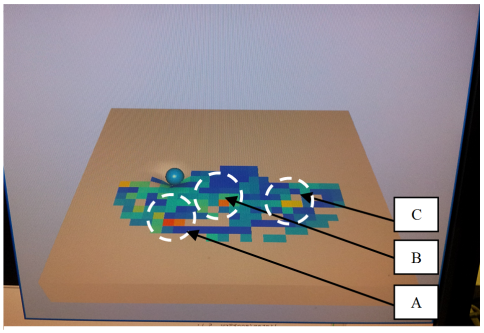

Figure 6.5: Stiffness distribution map captured during the second test: nodules A, B and C are detected with high saturation colour code (from red to yellow).

6.3.2 Evaluation of Effectiveness

To understand the effect of manual palpation trajectory pattern (Test 2) on the nodule detection rate, in comparison to the unconstrained remote palpation (Test 1), the evaluation of each test is carried out. The detection rate of hard nodules is used to assess the effectiveness of remote palpation in two different tests. Table 6.1 summarizes the results of two tests, excluding false positives. The overall detection rate across all subjects is higher in the tests with application of manual palpation pattern. In particular,

the detection rate for the largest and smallest nodule had increased in the second test.

Table 6.1: Detection of embedded nodules

Nodule, diameter	**Detection of hard nodules for all tests, %**	
	Undefined pattern (Test 1)	***Defined pattern (Test 2)***
A, 10 mm	80 %	100 %
B, 8 mm	90 %	90 %
C, 6 mm	50 %	80 %
All together	73 %	90 %

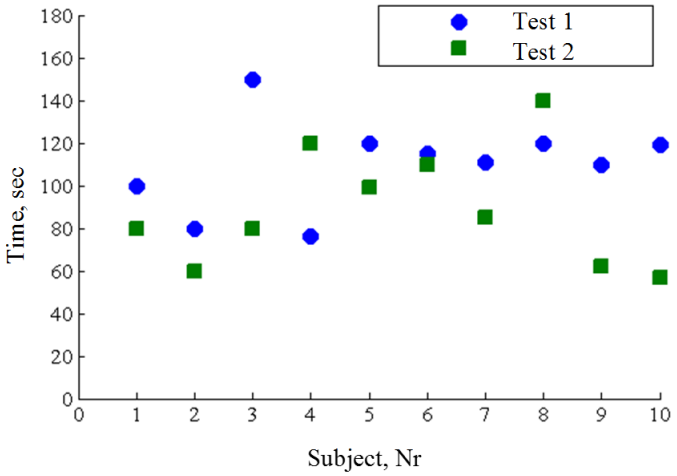

Figure 6.6: Time spent by each subject for Test 1 (random palpation) and Test 2 (pattern is applied).

In order to check the influence of the palpation pattern on the detection rate of hard nodules, a statistical evaluation was carried out. With $F(4.38) = 3.56$ and $p < 0.01$ the trajectory pattern was influencing the detection rate. There was no impact on the detection rate of hard nodules by each subject.

It is important to evaluate the time required by each subject to perform remote palpation tasks. Fig. 6.6 displays time spent by each subject to complete Test 1 (unconstrained trajectory of palpation) and Test 2 (defined trajectory pattern of palpation).

The time spent to detect nodules during Test 1 exceeds that of Test 2. In total, the time spent by all subjects for remote palpation with random pattern is 1101 sec while for specified pattern is 893 sec.

The two-way ANOVA was carried out to test the influence of palpation type implemented during each test, and the possible impact from the performance of each subject had on the completion time. The result shows the significance of the palpation type (Test 1 or Test 2) and its impact on time needed to perform the detection of hard nodules ($F(4.38) = 3.26$, $p < 0.01$).

Lastly, all subjects were asked about their experience during tele-manipulated palpation at both trials. All participants indicated that they were comfortable to use the developed setup during remote palpation. Moreover, none of them indicated any difficulties in the detection of embedded hard nodules. Nine out of ten participants agreed on the efficiency of the second trial with the defined palpation pattern. Therefore, the above results demonstrate that remote palpation implemented with a specified examination pattern can be successfully applied during tele-manipulation.

6.4 Conclusions

The results presented in this chapter aim to demonstrate the effectiveness of applying manual palpation trajectory pattern to remote palpation. Various surgical procedures are implemented using robotic tele-manipulators. Consequently, tactile representation of stiffness data can improve the clinical outcomes of surgical procedures. In this chapter the application of remote tactile examination on the tele-manipulation setup was tested to determine the impact of the palpation pattern. It was found that the applica-

tion of a specific manual palpation trajectory pattern during remote tactile examination can enhance the efficiency of the detection of hard nodules in soft phantom tissue. The evaluation of the time consumed for palpation and the detection rate of hard inclusions in the silicone phantom for two different tests was carried out. The unrestricted, user-defined palpation test was compared with remote palpation performed using predefined pattern.

1. It was found, that the second test performed better in terms of detection rate and time needed to perform the task.

2. The results demonstrate that it is feasible to apply patterns of manual palpation during remote soft tissue examination. Thus, skilled surgeons, with good experience in manual palpation, can use the tele-manipulated palpation with higher confidence and better outcomes.

Therefore, there is an indication for the possibility to change the current practice of MIS by enhancing this procedure with the use of tactile devices. However, the experimental studies performed in this chapter can be considered as preliminary evaluation of the application of global palpation. For further understanding and testing of this method it is required to take into account various conditions that are common for real surgery. The influence of the motion of organs during surgery should be studied. In addition, it is required to perform studies using real tissue organs, and, in future, in-vivo experimental trials.

Chapter 7

Discussion and Conclusions

7.1 Summary of Results

Exploring and offering solutions in the area of tactile sensing for soft tissue tactile examination, this thesis contributed to the ongoing research that attempts to resolve the unreliability of artificial tactile perception in complex surgical environments. Manual palpation of soft tissue was studied to investigate the possible ways that can enhance tactile perception during robotic probing. The performed work opens up various directions of research in the areas of robotics, human perception and behaviour.

A number of miniature tactile devices have been developed to enable tele-manipulated palpation of organs during surgical procedures. The most recent developments in the field of tactile sensing for surgical robotics are discussed in **Chapter 2**. Nevertheless, surgical tactile devices are not broadly used in RMIS yet. This is the case mainly because the devices developed for surgical applications need to be accurate and well tested so that they can perform efficient and reliable tactile examinations. Surgical

environments are complex and uncertain due to the non-linear mechanical properties of soft tissue and additional factors, such as the mobility of internal organs and the flow of body fluids. Thus, the results of tactile examination can be subject to high variability of perceived tactile data. Currently, there is a lack of literature on behavioural based approaches of artificial palpation. This thesis maintains that the result of tactile examination depends not only on a device's technical parameters, but also on environmental conditions. As in the case in manual palpation, specific patterns can be used in artificial tactile exploration taking into account the above-mentioned factors and to improve the accuracy of the tactile examination.

Different probing dynamics lead to variable perception of stiffness. This problem is discussed in **Chapter 3**, where a simple hardware-based simulator was used to emulate viscoelastic responses of soft tissue. The chapter establishes the discussion on the importance of probing behaviour for tactile exploration of soft environment. The stiffness recorded during the interaction between the probe and the simulator was compared with the mathematical input to the hardware. It was observed that the recorded responses varied from the input variables depending on probing dynamics. Although the simulation hardware was of a basic mechanical structure which might have led to measurement inaccuracies, it was able to provide robust and repeatable results that proved that the probing dynamics for a given viscoelastic distribution influence the accurate estimation of soft tissue's mechanical parameters. An alternative approach could be the use of mathematical modelling or finite element (FE) simulations. FE studies are extensively used for simulations and in-depth understanding of the probing behaviour in the next chapters.

In **Chapter 4** local palpation and finger movement pressure (FMP) for soft tissue tactile examination were studied in depth. Based on the way humans modulate the applied

force during tactile examination, a mathematical model of finger movement pressure for local palpation was outlined. Participants were asked to detect the size and depth of the nodules so that natural exploration behaviour could be captured and recorded. The obtained mathematical model corresponded to the second order reactive model. This means that every next movement was planned according to the previously perceived information. To validate the obtained result, robotic implementation of the model which was based on the results of human palpation trials was performed. The robotic probe was used to autonomously palpate a soft tissue silicon phantom. Thus, it was proved that the obtained model of modulation of the applied force enhances the perception of a non-homogeneous environment and can be successfully used during robotic-based palpation. Also, it was demonstrated that it is necessary to use a combination of lateral and normal motion to achieve a more efficient exploration of the environment. The advantage of the applied force control strategies is that they can be used with simple probing devices which are based on the indentation and force feedback measurement principles. Therefore, there might be no need to use mechanically complex frequency and vibration based tactile devices.

Chapter 5 focuses on the studies of localised palpation that is used to explore a small area of the tissue. In this case a single palpation path is considered as an exploration area. Two hypotheses are tested to understand the characteristics of manual palpation that can be used to localize hard nodules in soft tissues: 1) the speed of palpation influences the detection rate of hard nodules; and 2) the applied force and velocity modulations during manual palpation influences the localization and detection rate of hard nodules. Thus, manual palpation has been studied with the aim to get a better understanding of how the process of tactile probing during robotic surgery should be implemented. It was shown that the application of the appropriate palpation veloc-

ity improve the performance of the detection of non-homogeneous areas. The results show that experts use both applied force and velocity to locate hard nodules, while in the case of novices just the variability of velocity influences significantly the detection rate. However, the detection rate for novices and experts does not differ significantly. The experts use a complex modulation strategy of both force and velocity; the novices take a simpler approach that involves just velocity modulations while the impact of exerted force is insignificant on the detection rate according to the statistical evaluation. Therefore, the first hypothesis holds more validity for the subjects with no palpation experience. By conducting tests on manual palpation, together with FE simulations and tele-manipulated palpation, the strategies used to detect hard nodules during unidirectional palpation are examined. Based on the experimental evidence, certain manual palpation strategies are applied to detect hard formations in soft tissue. Consequently, force - velocity modulations are applied differently for the detected palpation strategies. The correct combination of these palpation variables for a given examination environment may lead to a higher detection rate of nodules. This supports the second hypothesis that was outlined in Chapter 5. Ten out of twenty participants had at least five years of experience in manual palpation. Therefore their palpation trajectory was expected to follow distinct patterns different from those of non-experts. For instance, during the evaluation test, the majority of subjects have indicated that in order to locate a hard nodule and understand its shape, they have applied circular movements around a suspicious area. Such types of palpation are easier to implement and thus appropriate to be performed during manual soft tissue examination. However, the objective of this study was to provide a basis for the design of optimal robotic behaviours during soft tissue examination to localize hard nodules. To sum up, the detection and localization of stiff abnormalities, such as nodules, in soft tissues is influenced not only by the pa-

rameters of the probe, but also by the employed palpation strategy, that is by the choice of force and velocity components for the given environment. The interaction dynamics of the finger or a probe during palpation is the result of the applied force-velocity modulations on the given properties of soft tissue.

Finally, in **Chapter 6** global examination of soft tissue is discussed as it is an integral part of the assessment of organ stiffness during palpation. For the purpose to study global examination strategies, tele-manipulation setup was used. Apart from the optimal behavioural pattern for global examination, it is important to explore the feasibility of tele-manipulation palpation for surgical applications. All the invited participants were not familiar with tele-manipulation setup or manual palpation before the experiments. Interestingly, some of the participants were naturally applying the suggested palpation pattern before being instructed to do so (user-defined palpation). At the second stage subjects were instructed to execute a specific pattern that is typically used by medical specialists. Therefore, it is possible to conclude that such behaviour is natural and can be easily integrated for practical applications.

The methodological approach presented in this thesis uses the model of certain range and distribution of hard nodules (tumours). As it was described in Section 4.2.2 small spherical type tumours of stage T1 are used to obtain and to validate the findings related to probing behaviour. Such choice is based on the difficulties and significant importance for medical outcomes to detect small nodules. In clinical conditions, there might be different placement of tumours inside an organ or various shapes and structure of tumours. Several nodules can be located next to each other, causing difficulties to separate each one of them. The application of the proposed probing behaviours might be useful to detect the area with abnormalities, but there might be difficulties to separate individual nodule. Taking into consideration such cases it is important to

select tactile sensors with an appropriate range of sensitivity at the tip of the device.

Probing behaviour strategies for artificial palpation were outlined based on the experiments carried out on silicone phantoms and ex-vivo porcine kidneys that contained hard spherical homogenous nodules. However, the presented strategies can be applied for the detect of the harder inclusion of any shape, such as ellipsoids and or tumours of irregular shapes. The presented approach does not intend to measure the exact stiffness of the tissue, but it aims to distinguish areas with relatively harder areas. Therefore, in case a tumour has non-homogeneous structure, technical parameters of the sensing device would influence the result of stiffness measurement.

The experimental protocol of these studies considers the tactile examination of ex-vivo organs and silicone phantoms that a fixed position during palpation. However, in real conditions tissue is not stationary, as it is discussed in Chapter 2. During surgical procedure and in-vivo tactile examination organs are subject to natural reflexes and motion caused by breathing. Therefore, in-vivo conditions can cause significant sensor noise during artificial palpation. The proposed palpation strategies aim to reduce the effect of such disturbances by using dynamic behaviour. However, in future studies, it is required to perform more extensive evaluation of the strategies emulating in-vivo conditions.

Probing behaviour during soft tissue examination is intended to be used during artificial palpation of soft tissue examination during RMIS or MIS. The stiffness information obtained during palpation should be used by a surgeon to make fast on-line decisions regarding to the scenario of a surgery. However, it is necessary to take into account that pre-operative imaging techniques are very useful to define the area of abnormality. Therefore, the process of artificial palpation can be significantly accelerated, especially

for the cases where global examination techniques are applied to detect the area of abnormality.

7.2 Future Work

The work presented in this thesis builds a base for the understanding palpation behavioural strategies that can be used to improve the perception of non-homogeneous distribution in soft tissue. There might be various directions of future research studies, and this section is briefly describing the ones that are considered as the most important. This thesis discusses tactile examination that is relevant not only to the palpation during minimally invasive surgery only, but also can be applied for any other palpation procedure. For instance, in the occasion of a severe epidemic disease where the access to the patients is restricted, it might be very helpful to grant a remote access for the doctors to perform simple abdominal palpation.

The studies can also be applied to the examination of viscoelastic environments for various other applications, such as the examination of the whole range of rubbers and silicones for industrial applications where a robot needs to perform sorting and manipulation of such materials.

One of the prospective future directions can be learning of human tactile examination based on demonstration of the applied behaviour. In particular, it is interesting to study the driving factors for tactile exploration of the particular objects, such as force, velocity and movement trajectory. In such a way it would be possible to demonstrate to the robot various complicated procedures where precise tactile feedback and control is required. For instance, such procedures as painting with a brush, manipulating various

fragile uncertain objects require the understanding of the environmental stiffness.

In this thesis the focus was on the understanding of palpation variables, which are assumed to be velocity, applied pressure and movement pattern. During experimental studies it was observed that apart from variation of these physical parameters, humans are actively using the morphological properties of the finger such as compliance. For instance, finger motion and stiffness can vary depending on the control of the tendons or the flexibility of muscles. Therefore, in future, it will be interesting to perform a study that explores the effect of physiological and morphological features of the human hand on tactile examination.

Studies of manual tactile examination for this thesis were performed based on the data obtained from two groups, namely, experts and novices in manual palpation. However, mostly the conclusions were drawn from the recordings of people that were not familiar with manual palpation techniques, as it was important to observe the natural pattern of exploration. In future, it is required to study in depth the main differences between these two groups, as experts can use additional behaviours to improve the efficiency of examination. In particular, it will be required to observe the performance of surgeons during in-vivo examination of soft tissues or palpation on a medical simulator.

Bibliography

[1] M. L. Cain, H. Damman, R. A. Lue, and C. K. Yoon, *Discover Biology*. W. W. Norton & Company, 2000.

[2] Z. Cui, Z. Han, H. Pan, and Y. Shao, "Design of a 3-axial force / torque sensor for arthroscopy force sensing," in *International Conference on Mechatronics and Automation*, (Beijing, China), pp. 243–248, Aug. 2011.

[3] D. Zbyszewski, P. Polygerinos, L. D. Seneviratne, and K. Althoefer, "A novel MRI compatible air-cushion tactile sensor for Minimally Invasive Surgery," in *2009 IEEE/RSJ International Conference on Intelligent Robots and Systems*, pp. 2647–2652, Oct. 2009.

[4] B. Darvish, S. Najarian, E. Shirzad, and R. Khodambash, "A novel tactile force probe for tissue stiffness classification," *American Journal of Applied Sciences*, vol. 6, pp. 512–517, Mar. 2009.

[5] M. Jia, J. W. Zu, and A. Hariri, "A new tissue resonator indenter device and reliability study," *Sensors*, vol. 11, pp. 1212–1228, Jan. 2011.

[6] S. Moromugi, S. Kumano, M. Ueda, and M. Q. Feng, "A sensor to measure hardness of human tissue," in *IEEE Sensors*, pp. 388–391, 2006.

[7] P. Schiavone, T. Boudou, E. Promayon, P. Perrier, and Y. Payan, "A light sterilizable pipette device for the in vivo estimation of human soft tissues constitutive laws," in *30th Annual International IEEE EMBS Conference*, pp. 4298–4301, 2008.

[8] R. Ahmadi, J. Dargahi, M. Packirisamy, and R. Cecere, "A new hybrid catheter-tip tactile sensor with relative hardness measuring capability for use in catheter-based heart surgery," *2010 IEEE Sensors*, pp. 1592–1595, Nov. 2010.

[9] D.-H. Kim, N. Lu, R. Ghaffari, Y.-S. Kim, S. P. Lee, L. Xu, J. Wu, R.-H. Kim, J. Song, Z. Liu, J. Viventi, B. de Graff, B. Elolampi, M. Mansour, M. J. Slepian, S. Hwang, J. D. Moss, S.-M. Won, Y. Huang, B. Litt, and J. a. Rogers, "Materials for multifunctional balloon catheters with capabilities in cardiac electrophysiological mapping and ablation therapy," *Nature Materials*, vol. 10, pp. 316–23, Apr. 2011.

[10] H. Leng and Y. Lin, "Development of a novel deformation-based tissue softness sensor," *Sensors (Peterborough, NH)*, vol. 9, no. 5, pp. 548–554, 2009.

[11] R. Ahmadi, M. Packirisamy, J. Dargahi, and R. Cecere, "Discretely loaded beam-type optical fiber tactile sensor for tissue manipulation and palpation in minimally invasive robotic surgery," *Sensors (Peterborough, NH)*, vol. 12, no. 1, pp. 22–32, 2012.

[12] T. Kawahara, Y. Miyata, K. Akayama, and M. Okajima, "Design of noncontact tumor imager for video-assisted thoracic surgery," *IEEE/ASME Transactions on*

Mechatronics, vol. 15, no. 6, pp. 838–846, 2010.

[13] A. R. Lanfranco, A. E. Castellanos, J. P. Desai, and W. C. Meyers, "Robotic surgery: a current perspective," *Annals of surgery*, vol. 239, pp. 14–21, Jan. 2004.

[14] B. M. A. Schout, A. J. M. Hendrikx, F. Scheele, B. L. H. Bemelmans, and A. J. J. A. Scherpbier, "Validation and implementation of surgical simulators: a critical review of present, past, and future," *Surgical Endoscopy*, vol. 24, no. 3, pp. 536–546, 2010.

[15] H. G. Kenngott, L. Fischer, F. Nickel, J. Rom, J. Rassweiler, and B. P. Müller-Stich, "Status of robotic assistance-a less traumatic and more accurate minimally invasive surgery?," *Langenbeck's Archives of Surgery / Deutsche Gesellschaft für Chirurgie*, vol. 397, pp. 333–41, Mar. 2012.

[16] G. Perigli, C. Cortesini, E. Qirici, D. Boni, and F. Cianchi, "Clinical benefits of minimally invasive techniques in thyroid surgery," *World Journal of Surgery*, vol. 32, pp. 45–50, Jan. 2008.

[17] C. E. Reiley, T. Akinbiyi, D. Burschka, D. C. Chang, A. M. Okamura, and D. D. Yuh, "Effects of visual force feedback on robot-assisted surgical task performance," *The Journal of Thoracic and Cardiovascular Surgery*, vol. 135, pp. 196–202, Jan. 2008.

[18] Y.-J. Shiah, F. Chang, and W.-C. Carl Tam, "Recognition of tactile relief by children and adults," *Perceptual and Motor Skills*, vol. 113, no. 3, pp. 727–38, 2011.

[19] P. Puangmali, K. Althoefer, L. D. Seneviratne, D. Murphy, and P. Dasgupta, "State-of-the-Art in force and tactile sensing for minimally invasive surgery," *IEEE Sensors Journal*, vol. 8, pp. 371–381, Apr. 2008.

[20] S. Schostek, M. O. Schurr, and G. F. Buess, "Review on aspects of artificial tactile feedback in laparoscopic surgery," *Medical Engineering & Physics*, vol. 31, pp. 887–98, Oct. 2009.

[21] M. Eltaib, "Tactile sensing technology for minimal access surgery, a review," *Mechatronics*, vol. 13, pp. 1163–1177, Dec. 2003.

[22] J. Dargahi and S. Najarian, "Human tactile perception as a standard for artificial tactile sensing, a review," *International Journal of Medical Robotics and Computer Assisted Surgery*, vol. 1, no. 1, pp. 23–35, 2004.

[23] R. Dahiya, G. Metta, M. Valle, and G. Sandini, "Tactile sensing-from humans to humanoids," *IEEE Trans. on Robotics*, vol. 26, pp. 1–20, Feb. 2010.

[24] H. Yousef, M. Boukallel, and K. Althoefer, "Tactile sensing for dexterous in-hand manipulation in robotics - A review," *Sensors and Actuators A: Physical*, vol. 167, pp. 171–187, June 2011.

[25] B.-M. Ahn, J. Kim, L. Ian, K.-H. Rha, and H.-J. Kim, "Mechanical property characterization of prostate cancer using a minimally motorized indenter in an ex vivo indentation experiment," *Urology*, vol. 76, pp. 1007–11, Oct. 2010.

[26] J. I. Lopez, I. Kang, W.-K. You, D. M. McDonald, and V. M. Weaver, "Integrative biology in situ force mapping of mammary gland transformation," *Society*, pp. 910–921, 2011.

[27] G. Tholey, J. P. Desai, and A. E. Castellanos, "Force feedback plays a significant role in minimally invasive surgery," *Annals of Surgery*, vol. 241, no. 1, pp. 102–109, 2005.

[28] C.-H. King, M. O. Culjat, M. L. Franco, C. E. Lewis, E. P. Dutson, W. S. Grundfest, and J. W. Bisley, "Tactile feedback induces reduced grasping force in robot-assisted surgery," in *IEEE Transactions on Haptics*, vol. 2, pp. 103–110, 2009.

[29] F. G. Duhaylongsod, "Minimally invasive cardiac surgery defined," *Archives of Surgery*, vol. 135, pp. 296–301, Mar. 2000.

[30] L. Walker and H. Z. Tan, "A perceptual study on haptic rendering of surface topography when both surface height and stiffness vary," in *12th International Symposium on Haptic Interfaces for Virtual Environment and Teleoperator Systems*, pp. 138–145, 2004.

[31] N. Yu, C. Hollnagel, A. Blickenstorfer, S. Kollias, and R. Riener, "Comparison of MRI-compatible mechatronic systems with hydrodynamic and pneumatic actuation," *IEEE/ASME Transactions on Mechatronics*, vol. 13, pp. 268–277, June 2008.

[32] A. B. Vallbo and R. S. Johansson, "Properties of cutaneous mechanoreceptors in the human hand related to touch sensation," *Human Neurobiology*, vol. 3, pp. 3–14, Jan. 1984.

[33] R. S. Johansson and A. B. Vallbo, "Tactile sensory coding in the glabrous skin of the human hand," *Trends in Neurosciences*, vol. 6, no. 1, pp. 27–32, 1983.

[34] E. B. Goldstein, *Sensation & Perception*, vol. 22. Wadsworth-Thomson Learn-

ing, 2004.

[35] K. O. Johnson, "The roles and functions of cutaneous mechanoreceptors," *Current Opinion in Neurobiology*, vol. 11, pp. 455–61, Aug. 2001.

[36] J. R. Phillips and K. O. Johnson, "Tactile spatial resolution. II. Neural representation of bars, edges, and gratings in monkey primary afferents," *Journal of Neurophysiology*, vol. 46, no. 6, pp. 1192–1203, 1981.

[37] R. S. Johansson, U. Landstrom, and R. M. Lundstrom, "Sensitivity to edges of mechanoreceptive afferent units innervating the glabrous skin of the human hand," *Brain Research*, vol. 244, pp. 27–32, 1982.

[38] M. A. Srinivasan, J. M. Whitehouse, and R. H. LaMotte, "Tactile detection of slip: surface microgeometry and peripheral neural codes," *Journal of Neurophysiology*, vol. 63, no. 6, pp. 1323–1332, 1990.

[39] A. Prevost, J. Scheibert, and G. Debrégeas, "Effect of fingerprints orientation on skin vibrations during tactile exploration of textured surfaces," *Communicative & Integrative Biology*, vol. 2, no. 5, pp. 422–424, 2009.

[40] B. L. Munger and C. Ide, "The enigma of sensitivity in Pacinian corpuscles: a critical review and hypothesis of mechano-electric transduction," *Neuroscience Research*, vol. 5, pp. 1–15, Oct. 1987.

[41] B. Stark, T. Carlstedt, R. Hallin, and M. Risling, "Distribution of human pacinian corpuscles in the hand, a cadaver study," *The Journal of Hand Surgery Journal of the British Society for Surgery of the Hand*, vol. 23, no. 3, pp. 370–372, 1998.

[42] F. Vega-Bermudez and K. O. Johnson, "SA1 and RA receptive fields, response variability, and population responses mapped with a probe array," *Journal of Neurophysiology*, vol. 81, no. 6, pp. 2701–2710, 1999.

[43] J. Zirjakova (Konstantinova), "Prostate post-surgical 3D imaging and data analysis," 2011.

[44] D. Mckay and G. Blake, "Optimum incision length for port insertion in laparoscopic surgery," *The Annals of The Royal College of Surgeons of England*, vol. 88, no. 1, p. 78, 2007.

[45] M. M. Bhandari A, Hemal A, "Instrumentation, sterilization, and preparation of robot," *Indian Journal of Urology*, vol. 21, pp. 83–88, 2005.

[46] R. A. Kolstad, "How well does the Chemiclave sterilize handpieces?," *Journal of the American Dental Association (1939)*, vol. 129, pp. 985–91, July 1998.

[47] J. E. Sebben and M. D. Davis, "Sterilization and care of surgical instruments and supplies," *Journal of the American Academy of Dermatology*, vol. 11, no. 3, pp. 381–392, 1984.

[48] R. J. Lederman, "Cardiovascular interventional MRI robert," *NIH Public Access*, vol. 112, no. 19, pp. 3009–3017, 2005.

[49] A. E. Sloan, M. S. Ahluwalia, J. Valerio-Pascua, S. Manjila, M. G. Torchia, S. E. Jones, J. L. Sunshine, M. Phillips, M. a. Griswold, M. Clampitt, C. Brewer, J. Jochum, M. V. McGraw, D. Diorio, G. Ditz, and G. H. Barnett, "Results of the NeuroBlate system first-in-humans phase I clinical trial for recurrent glioblastoma," *Journal of Neurosurgery*, vol. 118, pp. 1202–19, June 2013.

[50] E. Hempel, H. Fischer, L. Gumb, T. Hohn, H. Krause, U. Voges, H. Breitwieser, B. Gutmann, and J. Durke, "An MRI-compatible surgical robot for precise radiological interventions," *Computer Aided Surgery*, vol. 8, pp. 180–191, 2003.

[51] V. Seifert, M. Zimmermann, C. Trantakis, H. E. Vitzthum, K. Kühnel, A. Raabe, F. Bootz, J. P. Schneider, F. Schmidt, and J. Dietrich, "Open MRI-guided neurosurgery," *Acta Neurochirurgica*, vol. 141, pp. 455–64, Jan. 1999.

[52] A. R. Karduna, H. R. Halperin, and F. C. Yin, "Experimental and numerical analyses of indentation in finite-sized isotropic and anisotropic rubber-like materials," *Annals of Biomedical Engineering*, vol. 25, no. 6, pp. 1009–16, 1997.

[53] W. C. Hayes, L. M. Keer, G. Herrmann, and L. F. Mockros, "A mathematical analysis for indentation tests of articular cartilage," *Journal of Biomechanics*, vol. 5, pp. 541–551, 1972.

[54] E. Samur, M. Sedef, C. Basdogan, L. Avtan, and O. Duzgun, "A robotic indenter for minimally invasive characterization of soft tissues," *International Congress Series*, vol. 1281, pp. 713–718, May 2005.

[55] H. Liu, D. P. Noonan, B. J. Challacombe, P. Dasgupta, L. D. Seneviratne, and K. Althoefer, "Rolling mechanical imaging for tissue abnormality localization during minimally invasive surgery," *IEEE Trans. on Bio-medical Engineering*, vol. 57, pp. 404–14, Feb. 2010.

[56] H. Yegingil, W. Y. Shih, and W.-H. Shih, "Probing model tumor interfacial properties using piezoelectric cantilevers," *The Review of Scientific Instruments*, vol. 81, pp. 095104–9, Sept. 2010.

[57] D. O. Uribe, R. Stroop, and J. Wallaschek, "Piezoelectric self-sensing system for tactile intraoperative brain tumor delineation in neurosurgery.," in *Conference of the IEEE Engineering in Medicine and Biology Society.*, vol. 2009, pp. 737–40, Jan. 2009.

[58] P. Puangmali, H. Liu, L. D. Seneviratne, P. Dasgupta, and K. Althoefer, "Miniature 3-Axis distal force sensor for minimally invasive surgical palpation," *IEEE/ASME Trans. on Mechatronics*, vol. 17, pp. 646–656, Aug. 2011.

[59] D. Zbyszewski, H. Liu, P. Puangmali, K. Althoefer, C. S. Nunes, L. D. Seneviratne, B. Challacombe, D. Murphy, and P. Dasgupta, "Wheel/tissue force interaction: a new concept for soft tissue diagnosis during MIS.," in *Annual International Conference of the IEEE Engineering in Medicine and Biology Society*, vol. 2008, pp. 5556–9, Jan. 2008.

[60] H. Liu, J. Li, X. Song, L. D. Seneviratne, and K. Althoefer, "Rolling indentation probe for tissue abnormality identification during minimally invasive surgery," *IEEE Trans. on Robotics*, vol. 27, no. 3, pp. 450–460, 2011.

[61] E. Knoop and J. Rossiter, "Dual-mode compliant optical tactile sensor," in *IEEE International Conference on Robotics and Automation ICRA*, pp. 998–1003, 2013.

[62] K. M. Chung, Z. Liu, C. Lu, and H.-Y. Tam, "Highly sensitive compact force sensor based on microfiber Bragg grating," *IEEE Photonics Technology Letters*, vol. 24, pp. 700–702, Apr. 2012.

[63] U.-x. Tan, B. Yang, R. Gullapalli, and J. P. Desai, "Triaxial MRI-compatible fiber-optic force sensor," *IEEE Transactions on Robotics*, vol. 27, no. 1, pp. 65–

74, 2011.

[64] R. Sargeant, H. Liu, and K. Althoefer, "An MRI compatible optical multi-axis force/torque sensors robotic surgery," in *Hamlyn Symposium 2012*, pp. 79–80, 2012.

[65] I. B. Wanninayake, L. D. Seneviratne, and K. Althoefer, "Novel indentation depth measuring system for stiffness characterization in soft tissue palpation," *2012 IEEE International Conference on Robotics and Automation*, pp. 4648–4653, May 2012.

[66] V. Jalkanen, "Hand-held resonance sensor for tissue stiffness measurements-a theoretical and experimental analysis," *Measurement Science and Technology*, vol. 21, pp. 055801–9, May 2010.

[67] M. H. Araghi and S. P. Salisbury, "A feedback based dynamic instrument for measuring mechanical properties of soft tissues for minimally-invasive surgery," in *Smart Materials and Structures*, no. 22-23 October, pp. 59–69, 2009.

[68] M. Beccani, C. D. Natali, M. E. Rentschler, and P. Valdastri, "Wireless tissue palpation: proof of concept for a single degree of freedom," in *IEEE International Conference on Robotics and Automation ICRA*, pp. 703–709, 2013.

[69] P. C. Lee, J. Turnidge, and P. J. McDonald, "Fine-needle aspiration biopsy in diagnosis of soft tissue infections," *Journal of Clinical Microbiology*, vol. 22, pp. 80–3, July 1985.

[70] T. Aoki, T. Ohashi, T. Matsumoto, and M. Sato, "The pipette aspiration applied to the local stiffness measurement of soft tissues," *Annals of biomedical engi-*

neering, vol. 25, no. 3, pp. 581–7, 1997.

[71] S. Diridollou, F. Patat, F. Gens, L. Vaillant, D. Black, J. M. Lagarde, Y. Gall, and M. Berson, "In vivo model of the mechanical properties of the human skin under suction," *Skin Research and Technology*, vol. 6, pp. 214–221, Nov. 2000.

[72] M. J. Mack, "Minimally invasive cardiac surgery," *Surgical Endoscopy*, vol. 20 Suppl 2, pp. 488–492, Apr. 2006.

[73] P. Polygerinos, A. Ataollahi, T. Schaeffter, R. Razavi, L. D. Seneviratne, and K. Althoefer, "MRI-compatible intensity-modulated force sensor for cardiac catheterization procedures," *IEEE Transactions on Bio-medical Engineering*, vol. 58, pp. 721–6, Mar. 2011.

[74] M. C. Yip, S. G. Yuen, and R. D. Howe, "A robust uniaxial force sensor for minimally invasive surgery," *IEEE transactions on bio-medical engineering*, vol. 57, pp. 1008–11, May 2010.

[75] Y. Tanaka, K. Doumoto, A. Sano, and H. Fujimoto, "Active tactile sensing of stiffness and surface condition using balloon expansion," *Sensors (Peterborough, NH)*, pp. 54–50, 2009.

[76] F. M. Hendriks, D. Brokken, C. W. J. Oomens, D. L. Bader, and F. P. T. Baaijens, "The relative contributions of different skin layers to the mechanical behavior of human skin in vivo using suction experiments," *Medical Engineering & Physics*, vol. 28, pp. 259–66, Apr. 2006.

[77] M. Kalantari, M. Ramezanifard, R. Ahmadi, J. Dargahi, and J. Kovecses, "Design, fabrication, and testing of a piezoresistive hardness sensor in minimally

invasive surgery," *2010 IEEE Haptics Symposium*, pp. 431–437, Mar. 2010.

[78] P. Peng, a. S. Sezen, R. Rajamani, and a. G. Erdman, "Novel MEMS stiffness sensor for in-vivo tissue characterization measurement," in *Annual International Conference of the IEEE Engineering in Medicine and Biology Society*, vol. 2009, pp. 6640–3, Jan. 2009.

[79] J. W. Judy, "Microelectromechanical systems (MEMS): fabrication, design and applications," *Smart Materials and Structures*, vol. 10, pp. 1115–1134, 2001.

[80] A. Atieh, R. Ahmadi, M. Kalantari, J. Dargahi, and M. Packirisamy, "A piezoresistive based tactile sensor for use in minimally invasive surgery," in *2011 IEEE 37th Annual Northeast Bioengineering Conference (NEBEC)*, pp. 1–2, 2011.

[81] M. A. Qasaimeh, S. Sokhanvar, J. Dargahi, and M. Kahrizi, "A micro-tactile sensor for in situ tissue characterization in minimally invasive surgery," *Biomedical Microdevices*, vol. 10, pp. 823–37, Dec. 2008.

[82] J. Dargahi, S. Najarian, and M. A. Changizil, "A novel tactile probe with applications in biomedical robotics," in *2006 IEEE International Symposium on Industrial Electronics*, pp. 3343–3347, 2006.

[83] S. Schostek, C.-N. Ho, D. Kalanovic, and M. O. Schurr, "Artificial tactile sensing in minimally invasive surgery - a new technical approach," *Minimally Invasive Therapy*, vol. 15, pp. 296–304, Jan. 2006.

[84] M. V. Ottermo, O. Y. Stavdahl, and J. Tor A., "Palpation instrument for augmented minimally invasive surgery," *Proceedings of the 2004 IEEE/RSJ International Conference on Intelligent Robots and Systems*, pp. 3–7, 2004.

[85] J. Dargahi, S. Najarian, and R. Ramezanifard, "Graphical display of tactile sensing data with application in minimally invasive surgery," *Canadian Journal of Electrical and Computer Engineering*, vol. 32, no. 3, pp. 151–155, 2007.

[86] J. Watanabe, H. Ishikawa, X. Arouette, and N. Miki, "Surface texture and pseudo tactile sensation displayed by a MEMS-based tactile display," in *International Conference on Intelligent Robots and Systems*, vol. 7, pp. 4150–4155, 2012.

[87] F. L. H. Iii, R. K. Kramer, Q. Wan, R. D. Howe, and R. J. Wood, "Soft tactile sensor arrays for micromanipulation," in *International Conference on Intelligent Robots and Systems*, pp. 25–32, 2012.

[88] S. Sokhanvar, M. Packirisamy, and J. Dargahi, "MEMS endoscopic tactile sensor: toward in-situ," *Sensors (Peterborough, NH)*, vol. 9, no. 12, pp. 1679–1687, 2009.

[89] S. P. Abbas, S. Chauhan, and S. J. Phee, "Real-time, non-vision sensory feedback during minimally invasive surgery," in *TENCON 2009 - 2009 IEEE Region 10 Conference*, pp. 1–6, 2009.

[90] M. T. Perri, A. L. Trejos, M. D. Naish, R. V. Patel, R. A. Malthaner, and A. P. Art, "System for minimally invasive tumor localization," vol. 15, no. 6, pp. 925–931, 2010.

[91] A. Buchan, J. Bachrach, and R. S. Fearing, "Towards a minimal architecture for a printable, modular, and robust sensing skin," in *International Conference on Intelligent Robots and Systems*, pp. 33–38, 2012.

[92] M. Zillich and W. Feiten, "A versatile tactile sensor system for covering large and curved surface areas," in *International conference on Intellegent Robots and Systems*, pp. 20–24, 2012.

[93] M. W. Strohmayr, "The DLR artificial skin step I : uniting sensitivity and collision tolerance," in *IEEE International conference on Robotics and Automation ICRA*, pp. 1004–1010, 2013.

[94] A. Del Prete, S. Denei, L. Natale, F. Mastrogiovanni, F. Nori, G. Cannata, and G. Metta, "Skin spatial calibration using force/torque measurements," in *2011 IEEE/RSJ International Conference on Intelligent Robots and Systems*, pp. 3694–3700, Sept. 2011.

[95] R. Benhadj and B. Dawson, "Air jets imaging tactile sensing device for automation applications," *Robotica*, vol. 13, p. 521, Mar. 2009.

[96] M. Bianchi, J. C. Gwilliam, A. Degirmenci, and A. M. Okamura, "Characterization of an air jet haptic lump display," in *Annual International Conference of the IEEE Engineering in Medicine and Biology Society*, vol. 2011, pp. 3467–70, Jan. 2011.

[97] Y. Tanaka, Q. Yu, K. Doumoto, A. Sano, Y. Hayashi, M. Fujii, Y. Kajita, M. Mizuno, T. Wakabayashi, and H. Fujimoto, "Development of a real-time tactile sensing system for brain tumor diagnosis," *International Journal of Computer Assisted Radiology and Surgery*, vol. 5, pp. 359–67, July 2010.

[98] K. A. Nichols and A. M. Okamura, "Autonomous robotic palpation: machine learning techniques to identify hard inclusions in soft tissues," in *IEEE International conference on Robotics and Automation ICRA*, pp. 4369–4374, 2013.

[99] B. Willaert, N. Famaey, P. Verbrugghe, D. Reynaerts, and H. V. Brussel, "Design and in vivo validation of a force-measuring manipulator for MIS providing synchronized video, motion and force data," in *IEEE International Conference on Robotics and Automation ICRA*, no. 1, pp. 4842–4847, 2013.

[100] B. Ahn and J. Kim, "Measurement and characterization of soft tissue behavior with surface deformation and force response under large deformations," *Medical Image Analysis*, vol. 14, pp. 138–48, Apr. 2010.

[101] P. Boonvisut, R. Jackson, and M. C. Cenk, "Estimation of soft tissue mechanical parameters from robotic manipulation data," in *IEEE International Conference on Robotics and Automation*, pp. 4667–4674, 2012.

[102] S. Niroomandi, I. Alfaro, E. Cueto, and F. Chinesta, "Real-time deformable models of non-linear tissues by model reduction techniques," *Computer Methods and Programs in Biomedicine*, vol. 91, pp. 223–31, Sept. 2008.

[103] N. Diolaiti, S. Member, C. Melchiorri, S. Member, and S. Stramigioli, "Contact impedance estimation for robotic systems," *IEEE Trans. on Robotics*, vol. 21, no. 5, pp. 925–935, 2005.

[104] H. Eskandari, S. E. Salcudean, R. Rohling, and J. Ohayon, "Viscoelastic characterization of soft tissue from dynamic finite element models," *Physics in Medicine and Biology*, vol. 53, pp. 6569–90, Nov. 2008.

[105] D. Erickson, M. Weber, and I. Sharf, "Contact stiffness and damping estimation for robotic systems," *The International Journal of Robotics Research*, vol. 22, no. 1, pp. 41–57, 2003.

[106] Y. C. Fung, *Biomechanics: Mechanical Properties of Living Tissues*, vol. 12 of *Biomechanics / Y. C. Fung*. Springer, 1993.

[107] S. Catheline, J.-L. Gennisson, G. Delon, M. Fink, R. Sinkus, S. Abouelkaram, and J. Culioli, "Measurement of viscoelastic properties of homogeneous soft solid using transient elastography: An inverse problem approach," *The Journal of the Acoustical Society of America*, vol. 116, no. 6, p. 3734, 2004.

[108] P. Moreira, C. Liu, N. Zemiti, and P. Poignet, "Force control for robotic-assisted surgery based on viscoelastic tissue model," *BIO Web of Conferences*, vol. 1, p. 00066, Dec. 2011.

[109] M. Wiertlewski and V. Hayward, "Transducer for mechanical impedance testing over a wide frequency range through active feedback," *The Review of Scientific Instruments*, vol. 83, pp. 025001–5, Feb. 2012.

[110] O. A. J. Van der Meijden and M. P. Schijven, "The value of haptic feedback in conventional and robot-assisted minimal invasive surgery and virtual reality training: a current review," *Surgical Endoscopy*, vol. 23, no. 6, pp. 1180–1190, 2009.

[111] T. Horeman, S. P. Rodrigues, J. J. Van Den Dobbelsteen, F.-W. Jansen, and J. Dankelman, "Visual force feedback in laparoscopic training," *Surgical Endoscopy*, vol. 26, no. 1, pp. 242–8, 2011.

[112] J. Konstantinova, M. Li, V. Aminzadeh, P. Dasgupta, K. Althoefer, and T. Nanayakkara, "Force-velocity modulation strategies for soft tissue examination," in *IEEE International Conference on Intelligent Robots and Systems*, pp. 1998–2003, 2013.

[113] L. Bendtsen, R. Jensen, N. K. Jensen, and J. Olesen, "Pressure-controlled palpation: a new technique which increases the reliability of manual palpation," *Cephalalgia: an International Journal of hHeadache*, vol. 15, pp. 205–10, June 1995.

[114] L. E. Eberman and M. E. Finn, "Enhancing clinical evaluation skills: palpation as the principal skill," *Athletic Training Education Journal*, vol. 5, no. 4, pp. 170–175, 2010.

[115] N. Wang, G. J. Gerling, R. M. Childress, and M. L. Martin, "Quantifying palpation techniques in relation to performance in a clinical prostate exam," *IEEE Transactions on Information Technology in Biomedicine*, vol. 14, pp. 1088–97, July 2010.

[116] C. Volpicello, "Illustrated manual of nursing practice," *AORN*, vol. 54, no. 6, p. 1302, 1991.

[117] L. Sobin, M. Gospodarowicz, and C. Wittekind, *TNM classification of malignant tumours, 7th ed.* 2009.

[118] IARC, *Pathology and genetics of tumours of the breast and female genital organs (IARC WHO Classification of Tumours)*. World Health Organization, 2003.

[119] The International Agency for Research on Cancer, *Pathology and genetics of tumours of the urinary system and male genital organs (IARC WHO classification of tumours)*. World Health Organization, 1st ed., 2004.

[120] T. Krouskop, T. Wheeler, F. Kallel, B. Garra, and T. Hall, "Elastic moduli of breast and prostate tissue under compression," *Ultrasonic Imaging*, vol. 20,

pp. 260–274, 1998.

[121] K. Sangpradit, H. Liu, L. D. Seneviratne, and K. Althoefer, "Tissue identification using inverse finite element analysis of rolling indentation," in *IEEE International Conference on Robotics and Automation, ICRA*, pp. 1250–1255, 2009.

[122] W. A. Woodward, E. A. Strom, S. L. Tucker, M. D. McNeese, G. H. Perkins, N. R. Schechter, S. E. Singletary, R. L. Theriault, G. N. Hortobagyi, K. K. Hunt, and T. A. Buchholz, "Changes in the 2003 American Joint Committee on cancer staging for breast cancer dramatically affect stage-specific survival," *Journal of Clinical Oncology*, vol. 21, pp. 3244–8, Sept. 2003.

[123] R. W. Haines, "The mechanism of rotation at the first carpo-metacarpal joint," *Journal of anatomy*, vol. 78, pp. 44–46, 1944.

[124] K. Byl, *Metastable legged-robot locomotion*. PhD thesis, 2008.

[125] E. H. Lee and J. R. M. Radok, "Contact problem for viscoelastic bodies," *Journal of Applied Mechanics*, vol. 27, no. 3, pp. 438–444, 1960.

[126] X. Wang, L. J. Sliker, H. J. Qi, and M. E. Rentschler, "A quasi-static model of wheel-tissue interaction for surgical robotics," *Medical Engineering & Physics*, vol. 35, pp. 1368–76, Sept. 2013.

[127] M. E. Murali and K. Crabtree, "Comparison of two breast self-examination palpation techniques," *Cancer Nursing*, vol. 15, pp. 276–82, Aug. 1992.

[128] B. A. Hungerford, W. L. Gilleard, M. Moran, and C. Emmerson, "Evaluation of the ability of physical therapists to palpate intrapelvic motion with the stork test on the support side," *Physical Therapy*, vol. 87, pp. 879–887, July 2007.

[129] R. E. Goldman, A. Bajo, and N. Simaan, "Algorithms for autonomous exploration and estimation in compliant environments," *Robotica*, vol. 31, pp. 71–87, Mar. 2012.

[130] K. J. Saunders, C. A. Pilgrim, and H. S. Pennypacker, "Increased proficiency of search in breast self-examination," *Cancer*, vol. 58, pp. 2531–7, Dec. 1986.

[131] S. McDonald, D. Saslow, and M. H. Alciati, "Performance and reporting of clinical breast examination: a review of the literature," *CA Cancer Journal for Clinicians*, vol. 54, pp. 345–61, Nov. 2004.

[132] W. H. Goodson, "Clinical breast examination," *Topics in Primary Care Medicine*, vol. 164, no. 4, pp. 355–358, 1996.

Appendix A

Perception of hard inclusions embedded in the silicone

Diameter of the nodule, mm	Subject Number	Estimated Diameter of the Nodule, mm	Estimated Depth of the Nodule, mm
Empty	S1	2	3
	S2	Not perceived	Not perceived
	S3	5	10
	S4	Not perceived	Not perceived
	S5	6	10
	S6	Not perceived	Not perceived
	S7	Not perceived	Not perceived
	S8	Not perceived	Not perceived
	S9	Not perceived	Not perceived
	S10	Not perceived	Not perceived
3	S1	2	4
	S2	Not perceived	Not perceived

	S3	3	7
	S4	Not perceived	Not perceived
	S5	4	9
	S6	2	12
	S7	Not perceived	Not perceived
	S8	1	2
	S9	Not perceived	Not perceived
	S10	2	6
6	S1	7	10
	S2	6	4
	S3	8	10
	S4	5	15
	S5	10	9
	S6	8	3
	S7	12	10
	S8	1	2
	S9	2	3
	S10	4	3
9	S1	10	7
	S2	4	3
	S3	8	8
	S4	4	10
	S5	6	4
	S6	8	6
	S7	12	6

	S8	10	10
	S9	Not perceived	Not perceived
	S10	7	5
12	S1	5	5
	S2	3	7
	S3	6	6
	S4	3	15
	S5	5	6
	S6	9	6
	S7	6	8
	S8	6	6
	S9	2	6
	S10	8	4
15	S1	6	2
	S2	6	3
	S3	10	3
	S4	9	3
	S5	15	4
	S6	10	2
	S7	4	2
	S8	12	15
	S9	10	2
	S10	12	3
18	S1	9	1
	S2	6	1

	S3	20	3
	S4	10	5
	S5	12	2
	S6	12	2
	S7	8	4
	S8	25	18
	S9	10	3
	S10	20	2